DEVELOPMENT OF TARGETED POLYMERIC NANOPARTICLES FOR
CHEMOTHERAPEUTICS DELIVERY TO HEAD AND NECK SQUAMOUS
CELL CARCINOMA

By
MR. Chaiyakarn PORNPITCHANARONG

A Thesis Submitted in Partial Fulfillment of the Requirements
for Doctor of Philosophy (PHARMACEUTICAL TECHNOLOGY)
Department of PHARMACEUTICAL TECHNOLOGY
Graduate School, Silpakorn University
Academic Year 2021
Copyright of Silpakorn University

การพัฒนาพอลิเมอริกนาโนพาทิเคิลสำหรับการนำส่งยาเคมีบำบัดสู่เป้าหมายเซลล์มะเร็ง
ศีรษะและลำคอ

โดย
นายไชยกาญจน์ พรพิชณรงค์

DEVELOPMENT OF TARGETED POLYMERIC NANOPARTICLES FOR CHEMOTHERAPEUTICS DELIVERY TO HEAD AND NECK SQUAMOUS CELL CARCINOMA

By

MR. Chaiyakarn PORNPITCHANARONG

A Thesis Submitted in Partial Fulfillment of the Requirements
for Doctor of Philosophy (PHARMACEUTICAL TECHNOLOGY)
Department of PHARMACEUTICAL TECHNOLOGY
Graduate School, Silpakorn University
Academic Year 2021
Copyright of Silpakorn University

Title   Development of targeted polymeric nanoparticles for chemotherapeutics delivery to head and neck squamous cell carcinoma
By   Chaiyakarn PORNPITCHANARONG
Field of Study (PHARMACEUTICAL TECHNOLOGY)
Advisor   Professor TANASAIT NGAWHIRUNPAT , Ph.D.

Graduate School Silpakorn University in Partial Fulfillment of the Requirements for the Doctor of Philosophy

---Dean of graduate school
(Associate Professor Jurairat Nunthanid, Ph.D.)

Approved by

---Chair person
(Associate Professor Theerasak Rojanarata , Ph.D.)

---Advisor
(Professor TANASAIT NGAWHIRUNPAT , Ph.D.)

---Co advisor
(Associate Professor Prasopchai Patrojanasophon , Ph.D.)

---Co advisor
(Professor Praneet Opanasopit , Ph.D.)

---External Examiner
(Associate Professor Chuda Chittasupho , Ph.D.)

60353805 : Major (PHARMACEUTICAL TECHNOLOGY)
Keyword : POLYMERIC NANOPARTICLES, HEAD AND NECK CANCER, TARGETED DRUG DELIVERY, N-VINYL PYRROLIDONE, ACRYLIC ACID, CHITOSAN, HYALURONIC ACID, CATECHOL

MR. CHAIYAKARN PORNPITCHANARONG : DEVELOPMENT OF TARGETED POLYMERIC NANOPARTICLES FOR CHEMOTHERAPEUTICS DELIVERY TO HEAD AND NECK SQUAMOUS CELL CARCINOMA THESIS ADVISOR : PROFESSOR TANASAIT NGAWHIRUNPAT, Ph.D.

The purpose of this study was to develop polymeric nanoparticles (NPs) loaded with chemotherapeutic agents using different NPs preparation methods to target head and neck squamous carcinoma cells (HNSCC) by passive targeting and local delivery approaches. For passive targeting, the bottom-up approach was used to prepare polymeric NPs from N-vinylpyrrolidone (NVP) and acrylic acid (AA). Surfactant-free emulsion polymerization was performed to construct NPs of the two monomers using an azo initiator (V50) and bisacrylamide crosslinker. NPs were synthesized using two different methods to obtain the NPs with different structural arrangement. Cisplatin (CDDP) was bounded to the NPs using adsorption method. The characteristics of the NPs and CDDP-bounded NPs were characterized on particle size, surface charge, morphology, drug loading, and CDDP release. Furthermore, the cytotoxic effect, cellular accumulation of CDDP-bounded NPs and cell death mechanism were analyzed. Besides, mucoadhesive catechol-bearing nanoparticles (Cat-NPs) for local drug delivery of doxorubicin (DOX) to HNSCC were formulated through the top-down approach. Chitosan (CS) and hyaluronic acid (HA) were functionalized with catechol (Cat) moiety and employed in the preparation of Cat-NPs. The Cat-NPs were prepared using ionic gelation between catechol-succinyl CS (SCScat) and catechol-functionalized HA (HAcat) and loaded with DOX by physical adsorption. The physicochemical characteristics, mucoadhesive capability, drug loading, and DOX release were evaluated. Apart from that, cytotoxicity, cellular uptake, and apoptosis assay on HN22 cell HNSCC cell line were examined. The NVP/AA NPs obtained from both methods were relatively spherical, and presented a negative surface charge with the hydrodynamic diameter of 135-185 nm. CDDP was coordinated bounded on the NPs as proved by FT-IR analysis. The CDDP-bounded NPs presented promising drug loading capacity and %loading efficiency of 4 mmol/g and 12–18%, respectively. The release profile was sustained for 7 days with around 47–83% CDDP released which depended on the pH and amount of chloride ion in the release medium. The blank NPs were not toxic to the human gingival fibroblast and CDDP-bounded NPs had IC50 slightly above 20 μg/mL towards a head and neck cancer cell line. A higher percentage of early apoptosis and cellular accumulation was presented in CDDP-bounded NPs compared to free CDDP which concluded that the formulated systems presented a slower but less inflammatory anticancer effect. The findings showed potential anticancer of the CDDP-bounded NVP/AA NPs for systemic delivery for HNSCC. For localized delivery, mucoadhesive Cat-NPs were successfully developed. The spherical Cat-NPs had a particle size of around 160 nm with negative surface charge. The Cat-NPs presented superior *ex vivo* mucoadhesion compared to non-functionalized NPs on porcine cheek mucous tissue. The DOX loading capacity was considerably high (250 μg/mg) and the release of DOX was sustained for 24 h. The anticancer of DOX-loaded Cat-NPs (DOX-NPs) towards HN22 HNSCC cell line was promising represented by a very low IC50. The cellular uptake of DOX-NPs was significantly higher than free DOX and the apoptosis induction was also superior. The findings pointed out that the developed Cat-NPs were a probable candidate for local administration of DOX. Above all, the novel polymeric NPs developed for passive targeting and local delivery of chemotherapeutic drugs may be potential carriers for delivery of the chemotherapeutics and produce the effective killing activity against HNSCC.

ACKNOWLEDGEMENTS

Chaiyakarn PORNPITCHANARONG

TABLE OF CONTENTS

Page

LIST OF TABLES

LIST OF FIGURES

Page

LIST OF TABLES
LIST OF ABBREVIATIONS

DMSO	Dimethyl sulfoxide
DOX	Doxorubicin
e.g.	exempli gratia (Latin); for example,
et. al	And others
etc.	et cetera (Latin); and other things/ and so forth
EPR	Enhanced permeability and retention
FTIR	Fourier-transformed infrared spectroscopy
g	Gram
h	Hour
^{1}H-NMR	Proton nuclear magnetic resonance spectroscopy
HA	Hyaluronic acid
HAcat	Catechol-functionalized hyaluronic acid
HNSCC	Head and neck squamous cell carcinomas
IC50	The half maximal inhibitory concentration
L	Liter
M	Molar
mAb	Monoclonal antibody
MBA	*N,N'*-methylenebisacrylamide
mg	Milligram
min	Minute
mL	Milliliter
mM	Millimolar
mm	Millimeter
mmol	Millimole
mV	Millivolt
N_2	Nitrogen
nm	Nanometer
NPs	Nanoparticles
NVP	*N*-vinylpyrrolidone
PEG	Polyethylene glycol
Pt	Platinum
ppm	Part per million

rpm	Round per minute
SCS	Succinyl chitosan
SCScat	Catechol-functionalized succinyl chitosan
V50	2,2'-azobis(2-methylpropionamidine) dihydrochloride
WO_{50}	Wash Out_{50}
wt%	Percent weight by weight

CHAPTER 1

INTRODUCTION

1.1   STATEMENTS AND SIGNIFICANCE OF THE PROBLEMS

Cancer is a significant leading cause of death in the world today [1]. Particularly, the head and neck squamous cell carcinomas (HNSCC), which refer to cancer occurring along the mucosal surfaces of the digestive tract and the upper airway, are marked as one of the major cancers that occurred in men and elder people [2-4]. The prognosis of the disease is considered poor where only slightly more than half of the patients survive after a 5-years diagnosis [5]. Despite having various treatment approaches including radiotherapy, surgery, chemotherapy, immunotherapy, targeted therapy, and a combination of the treatment modes, HNSCC have been found to be a critical cause of death [6]. Major challenges in achieving a successful HNSCC treatment are low response rate, drug resistance, relapse, and toxicity of the conventional standard treatments [7].

HNSCC are commonly treated by surgery, radiation, and chemotherapy. Chemotherapeutic agents can be introduced as a single therapy or in a combination with other treatment modules as an adjuvant or neoadjuvant therapy to achieve complete removal of the cancer cells. [8, 9]. Cisplatin (CDDP) , or cis-diamminedichloroplatinum (II), is a platinum-based chemotherapeutic agent that is well-known and commonly used against various types of cancer including brain cancers, lung, testes, ovarian, and head and neck solid tumors [10]. Chiefly in the HNSCC treament, CDDP plays an important role as a chemotherapeutic drug to be combined with radiotherapy to establish a complete cure of the disease [11]. CDDP is a non-cell cycle-specific alkylating antineoplastic agent which performs its action by crosslinking the purine base at the N7 position to interrupt DNA and protein synthesis. After the alkylation, DNA replication stops leading to the induction of apoptotic death of cancer cells [6]. When water molecules replaced the chloride atoms of CDDP in a solvent-assisted pathway (aquation) , an aquated form of positively

charged CDDP is created. At this state, CDDP exhibits its activity [12, 13]. Although the metal-based compound is highly reactive and effective against the cancer cells, CDDP can be strongly toxic to the normal tissue upon unlocalized delivery and could lead to serious side effects and further drug resistance due to low cellular drug accumulation [14]. Doxorubicin (DOX) is a potent anthracycline anticancer agent with the capability to cure different types of cancers. The drug intercalates the DNA strands and disrupts topoisomerase-II mediated DNA repair. Apart from that, DOX generates free radicals which would damage cellular membranes, proteins, and DNA. Nevertheless, unlocalizable drug administration techniques could bring about serious systemic adverse effects such as severe nausea, vomiting, alopecia, and cardiotoxicity [15, 16].

Nanoparticles (NPs) are defined as an ultrafine structure having a size ranging between 1-100 nm. NPs have been widely used in the biomedical field through many aspects including drug carriers [17]. They are most easily captivated by the cells upon having optimal physicochemical and biological properties considering their enormous surface area [18, 19]. Various types of NPs have been developed to effectively deliver chemotherapeutic agents to the target cells e.g., nano-constructed polypeptide and polypeptide micelles with the smart pH-sensitive property that have shown the synergistic anti-cancer effect of multiple anticancer drugs [20-22]. Furthermore, polymeric NPs referred to the NPs constructed from polymers with a size range from 10-1000 nm. They have been shown great potential among novel drug delivery materials because of having adaptable and promising characteristics such as amendable properties, extensive drug loading, controllable drug release, biodegradability, and biocompatibility [23, 24]. Polymeric NPs are auspicious as drug carriers for the treatment of cancers because of their ability to be deposited in the cancer cells by the enhanced permeability and retention (EPR) effect of the abnormal tumor's vasculature [25]. Also, polymeric NPs have tuneable characteristic; for example, carboxylic acid group can be decorated onto the polymerized NPs for the delivery of CDDP using a coordinate covalent bond. A number of nano-structured preparations have been developed for the delivery of CDDP and DOX such as inorganic NPs (silica, iron oxide, gold NPs), organic NPs (liposomes, micelles, polymeric NPs), or hybrid NPs (carbon nanotubes) [26-34].

Strategies of drug delivery to the head and neck cancer cells can be classified into local and systemic deliveries. Local delivery of chemotherapeutics to the mucosa allows the specific administration of the drug at the affected tumor area. The administration mode enables the anticancer agent to extensively remain at the cancer site compared to the systemic circulation. Hence, the method is advantageous in minimizing the toxicity of the cytotoxic drug on the normal tissues. Additionally, the locally given anticancer drugs to the tumor would bring about a safer and more convenient treatment owing to the frequent turnover of the mucosal surfaces. The renewing of the mucosa allows a more tolerable treatment in the long-term administration. [35-37]. On the contrary, anticancer drugs given through the systemic approach are also beneficial by facilitating the passive and active drug targeting strategies. Passive drug targeting is related to the drug accumulation in the tumors via passive diffusion through leaky vasculature due to the EPR effect. Delivery of a drug by NPs allows the distribution and accumulation of the drug in the tumor site while avoiding the systemic clearance from the reticuloentocytothelial system (RES) . Therefore, these carriers enhance the therapeutic efficiency by significantly increasing the amount of drug at the target cells and lowering the adverse effects [38].

Polymeric NPs can be prepared using two main techniques consisting of top-down and bottom-up methods. The bottom-up approach is the polymerization of monomers and crosslinkers to create the structure of networked colloidal solid nanoparticles. To allow the control of structural characteristics, modifications of functional groups, physicochemical attributes, and targetability, the synthesis of novel polymeric NPs is preferable [39]. For preformed polymers, the top-down methods are favored. In this approach, NPs are created by different techniques including nanoprecipitation, dialysis, emulsification, and ionotropic gelation. Ionotropic gelation method is employed to prepare polymeric nanoparticles through ionic interactions between charged polymers or a charged polymer and electrolyte with counterions. The particle size of the particles is then reduced using physical or mechanical interventions [40, 41].

Mucoadhesive drug delivery has received great interest among researchers these days because it allows the delivery of an active pharmaceutical compound to a certain location by contacting and consolidating to a mucosal surface by various

interfacial adhesion interactions [42, 43]. Polymers, e.g. polysaccharides and celluloses that are equipped with mucoadhesive capabilities can adhere to the mucosal membrane through weak interactions such as physical entanglement, van der Waals forces, hydrogen bond, hydrophobic bond, ionic interaction, etc. [44]. Besides, polymer functionalization enabled the creation of a newer generation of mucoadhesive polymers and provided the ability of these functionalized materials to form a covalent bond with the mucin glycoprotein which is a rather strong and permanent interaction. The polymers that contained thiols, acrylate, maleimide, and catechols in the molecule showed empowered mucoadhesive properties by forming a covalent bond through the nucleophilic addition mechanisms. [45-47]. Interestingly, catechols were found as a hidden adhesion mechanism underwater of mussels and were further studied to be a multi-mode mucoadhesive functional group that can attach to the thiols and amines in the glycoprotein [48]. Apart from that, drug delivery systems acquiring catechol-modified polymers were proven to improve the mucoadhesive properties of the novel formulations including microcapsules, hydrogels, and NPs [49-51].

In this study, we aimed to develop polymeric NPs as a targeted drug delivery carrier of anticancer drugs for head and neck cancer. The NPs were generated using different preparation methods including bottom-up NPs synthesis and top-down ionotropic gelation. The NPs were expected to reach the cancer cells through the different targeting strategies. The hydrophilic biocompatible monomers and polymers were employed for the formation of NPs. The synthesized NPs and polymers were evaluated for their structural attributes, physicochemical properties, and targeting performances. Anticancer agents (CDDP and DOX) were then incorporated into the NPs. Subsequently, the drug content, release profiles, biocompatibility, and *in vitro* anticancer effect of the drug-loaded NPs were examined.

1.2   OBJECTIVES

1.2.1. To synthesize and prepare new polymeric nanoparticles (NPs) with specific functional groups for targeted delivery of anticancer drugs to head and neck cancer cells.

1.2.2. To evaluate the physicochemical properties, drug loading, and release characteristics of the drug-loaded NPs.

1.2.3. To evaluate the *in vitro* cellular uptake and anticancer effect of drug-loaded NPs in a head and neck cancer cell line.

1.3   HYPOTHESIS

1.3.1. The hydrophilic NPs of *N*-vinylpyrrolidone (NVP) and acrylic acid (AA) can be successfully synthesized by surfactant-free emulsion polymerization with promising characteristics as a nano-drug carrier.

1.3.2. The NPs of catechol-functionalized succinyl chitosan/hyaluronic acid can be successfully prepared and possessed good attributes.

1.3.3. Anticancer agents (CDDP and DOX)-loaded NPs can be delivered to the head and neck cancer cells using different targeting strategies and perform the efficient deposition and killing potential against head and neck cancer cells.
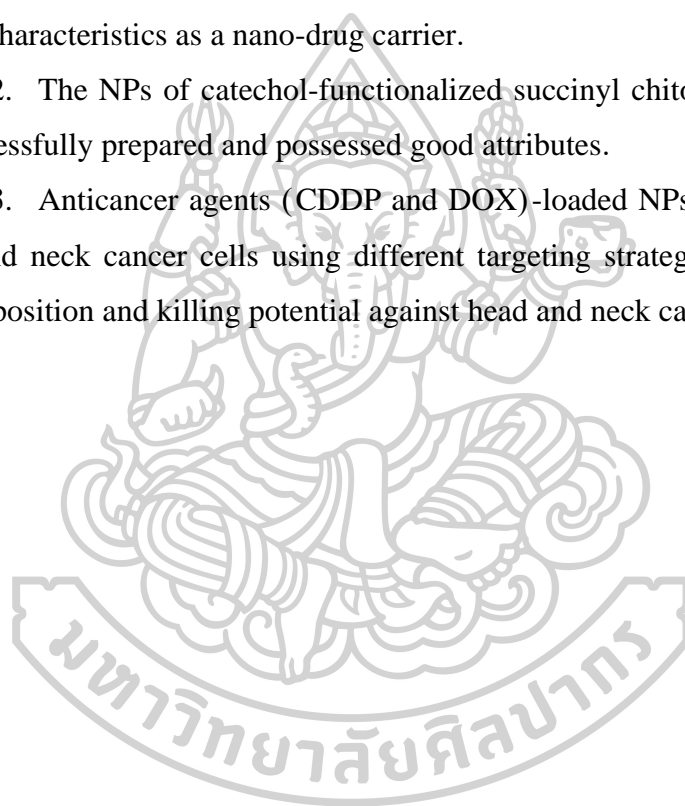
CHAPTER 2

LITERATURE REVIEW

2.1   Head and neck squamous cell carcinoma

      2.1.1   Definition and etiology

      2.1.2   Management of head and neck squamous cell carcinoma

2.2   Chemotherapeutics in head and neck squamous cell carcinoma

      2.2.1   Cytotoxic drugs

      2.2.2   Molecularly targeted compounds

      2.2.3   Checkpoint inhibitor immunotherapy

2.3   Drug targeting strategies

      2.3.1   Systemic targeting

            2.3.1.1   Passive targeting

            2.3.1.2   Active targeting

            2.3.1.3   Stimuli-sensitive nanocarrier

      2.3.2   Local targeting

2.4   Nanoparticles

      2.4.1   Definition and classification

      2.4.2   Inorganic nanoparticles

      2.4.3   Polymer-based nanoparticles

      2.4.4   Lipid-based nanoparticles

2.5   Polymeric nanoparticles

      2.5.1   Definition

      2.5.2   Preparation of polymeric nanoparticles

            2.5.2.1   Top-down approach

            2.5.2.2   Bottom-up approach

2.6   Mucoadhesive drug delivery

      2.6.1   Definition and mechanism

      2.6.2   First-generation mucoadhesive polymers

2.1   Head and neck squamous cell carcinomas

2.1.1   Definition and etiology

Head and neck squamous cell carcinomas (HNSCC) are cancers dominantly affecting the squamous cells of the mucosal linings head and neck areas [9]. Its severity is considered significant as HNSCC was reported as the sixth most common cancer in the world. The term includes the disease occurring in the oral cavity, sinonasal cavity, nasopharynx, salivary glands, hypopharynx, and larynx. This type of cancer is caused by heavy tobacco use and alcohol consumption, whist other related risk factors including age, gender, diet, hygiene, and career are also noticeable. HNSCC are more common among men aged over 40 years old; moreover, consumption of betel nuts, areca nut, or having solvents-related occupations can increase the risk of developing head and neck cancer. Another cause of HNCSS is human papilloma virus (HPV) infection, dominantly the type 16 HPV. It was recently found that HPV has an impact on the increasing incidence of HNSCC cases, especially among young patients [52-54]. Common symptoms such as swelling, pain, red or white patches, and difficulty of speaking, swallowing, and breathing are the signs of HNSCC that could lead to later stages of the cancer. The prognosis of the diseases varies by the cause and severity. Moreover, the 5-year survival rate of head and neck cancer reduces from 70% to less than 50% with higher staging. Locally affected cancer can lead to an advanced stage by metastasizing to the lymph nodes and spread through the lymphatic system. It also could cause serious and undesirable effects once invade to the bones, cartilages, and muscles [55-57].

Oral cancer is a major type of head and neck cancers with the main cause of the disease is attributed to exogenous factors e.g., tobacco and alcohol [58, 59]. Also, it was reported that cigarette pack-year value is a direct determination factor for the risk of oral cancer development. Cigarettes contain toxic polycyclic hydrocarbons, nitrosamines, and other carcinogenic molecules. Alcohol has been reported to increase the chance of oral cancer development in nonsmoking patients. Importantly, both tobacco and alcohol play a synergistic role in the development of oral squamous cell carcinoma. Other factors such as oral hygrines, diets, and irritant exposure also have a correlation to the cause of oral cancer [55]. Premalignant lesions determining the disease and could lead to more severe malignancies consist of erythroplakia,

leukoplakia, oral lichen planus, and submucosal fibrosis. The most common lesion is erythroplakia which is the red sore patch occurring in the oral cavity; whereas, the occurrence can be ruled out from other causes. Leukoplakia refers to the white patch lesions that are known to be resulted from tobacco or alcohol consumption which cannot be pointed out to other conditions [60-62].

The impact of HNSCC affects the patient's quality of life in various aspects including physical, psychological, and financial sides. Hence, the advancement in disease diagnosis and treatment can improve the effects on the patients [63].

2.1.2   Management of head and neck squamous cell carcinoma

Cancers presented in the head and neck areas are mostly curable with a high success rate upon early detection. The goal of HNSCC treatment is primarily to eliminate the cancer while the functions of surrounding tissues and organs are preserved. The diagnosed stage of cancer prognoses the patients' survival rates and the treatment modules. Primary tumors with relatively small size and non-nodal involvement are classified as stage I or stage II cancers. Once have a larger size, invade into the underlined tissues, and/or metastasize to the nearby nodes, the tumors are categorized as stage III or IV cancers. The options for the treatment of head and neck cancers consist of radiation, surgery, chemotherapy, and targeted therapy. These mentioned approaches may be used as a single-modality treatment or a combined modality according to the stage, area, and pathologic finding of the disease [64-66].

2.1.2.1 Localized disease (early stage)

Nearly half of the HNSCC patients are diagnosed at the earlier stage of the disease. Stages I and II head and neck cancers are generally treated with surgery or radiation as a single module to achieve a complete cure of the disease. Apparently, the overall survival rate in stages I and II head and neck cancer patients are ranged from 70% to 90%. After the treatment interventions, attentive inspections and follow-up are required to identify possible recurrence and management of treatment plan for the secondary tumors.

Head and neck cancers are greatly influenced by the use of alcohol and tobacco; hence, reduction of alcohol consumption and smoking are highly suggested in the prevention of secondary tumors. Other common HNSCC interventions include the use of radiotherapy and surgery where both treatment modes provide similar success and survival rates, so the treatment method is chosen considering the affected area, limitations, treatment accessibility, expected outcome, and risk assessment. Notably, cancers occurring in the oral cavity are commonly treated by surgery with a higher cure rate and less toxic upon the patients than treating with radiation therapy [67-70].

Different surgical techniques are applied to excise the primary tumor depending on the potential to access the target site. Traditional skin incision surgery is used for the treatment of thyroid and salivary gland cancers which need wide excision. Apart from that, less invasive technologies of transoral laser microsurgery (TOLM) and transoral robotic surgery (TORS) have been applied for the removal of the larynx/hypopharynx, and oropharyngeal cancers, respectively, to improve the transoral approach and patient preferences. Functional outcomes improvement together with the reduction of morbidity can be achieved using these advanced techniques as compared to the traditional surgery, especially in the earlier stages of oral cancers that are mostly curable by the transoral surgical method [71, 72].

Radiotherapy techniques of an external beam or internal radiotherapy (brachytherapy) are used for definitive cancer treatment. Nevertheless, the cure from radiation approaches will need 3-dimensions conformal techniques; for example, image-guided radiation therapy (IGRT) and intensity-modulated radiation therapy (IMRT) to achieve successful treatment outcomes and stand as HNSCC standard care [73].

2.1.2.2 Locoregionally advanced disease

Combination therapy is generally needed for the treatment of advanced-stages III and IV locoregionally HNSCC. These later stages propose an extensive risk of further distant metastasis and recurrences at the locally affected area. The use of multiple modalities of surgery, radiation therapy, with or without concurrent chemotherapy provides a significant improvement of disease control. The

multiple treatment approaches could be either a combination of surgery, radiation, and chemotherapy by giving together with or after one another; for example, primary surgery plus concurrent chemotherapy, post-operative radiation, or chemoradiation, neoadjuvant chemotherapy before surgery or radiation interventions, concurrent chemotherapy and radiation without surgery, or induction chemotherapy followed by radiation without surgery. The selection of treatment methods and sequencing is decided in accordance with the affected site, tumor size, disease severity, patients' factors and preferences, and possibly the expected outcomes on functional and safety aspects [74, 75].

2.1.2.3 Metastatic disease

The metastatic and recurrent HNSCC usually have a poor prognosis. The disease is treated with systemic therapy for severe and advanced head and neck cancer. Different factors are considered in the selection of the treatment procedure including clinical status, patients' safety and compliances, comorbidities, treatment history, and pathologies. Chemotherapy, immunotherapy, and targeted therapy are accounted for the choices for systemic treatment; whereas, the options could be given in a single or combination therapy [70, 76].

2.2 Chemotherapeutics in head and neck squamous cell carcinoma

Chemotherapeutic drugs may be given to head and neck cancer patients at different stages of the disease, especially for the locally advanced HNSCC, metastasis, and recurrent cancer. The term chemotherapeutics refers to both the use of a cytotoxic agent and targeted drugs; whereas, the introduction of the cytotoxic drug into the treatment regimen can be classified into different approaches considering the affected site, staging, severity, comorbidity, preference, and patient's tolerability to the management plan. The strategies to initiate chemotherapeutics in the treatment include a single modality, adjuvant chemoradiation, induction chemotherapy, concurrent chemotherapy, and sequential treatment as presented in Table 2.1 and 2.2 according to the staging and tumor origin, respectively [74, 75, 77, 78].

Table 1 Roles of chemotherapeutics in the treatment of head and neck cancer as classified by the cancer staging

Staging	Treatment options
Early-stage, stage I & II (localized disease)	• Primary surgery • Definitive radiation therapy
Stage III & IV (locoregionally advanced disease)	• Surgery then radiotherapy • Surgery then chemoradiotherapy • Chemotherapy then surgery ± radiotherapy • Chemoradiotherapy • Chemotherapy then chemoradiotherapy
Metastatic disease	• Palliative chemotherapy • Immunotherapy • Supportive care

Table 2 Roles of chemotherapeutics in the treatment head and neck cancer as classified by the cancer origin

Origin	Treatment options	Remark
Oral cavity	• Surgery	Stage I or II
	• Radiotherapy ± chemotherapy	Locoregional recurrence
Oropharynx, hypopharynx, and larynx	• TORS • TOLM • Chemoradiotherapy	Organ preservation modules
Neck	• Definitive radiation therapy ± chemoradiotherapy	

2.2.1   Cytotoxic drugs

2.2.1.1   Methotrexate

Methotrexate (MTX) is the first and one of the most commonly used chemotherapeutic agents in the late stages of HNSCC [79]. MTX is classified as an antifolate antimetabolite; the structure of MTX is presented in Figure 2.1. The cells uptake the drug via human reduced folate carriers (SLC19A1). Its metabolite, MTX-polyglutamate, inhibits the dihydrofolate reductase enzyme that is used to convert dihydrofolate to the folic acid active form of tetrahydrofolate which is essential for the synthesis of DNA and RNA nucleotides. The metabolite also prevents de novo purine synthesis of both purine and thymidylate synthase. Above all, the synthesis of DNA is prohibited. The drug is useful as a combination with other drugs for the treatment of HNSCC with concurrent radiotherapy. Also, it can be used as a single agent in HNSCC palliative care where the overall survival benefit is similar to drug combination with less toxicity [80, 81].
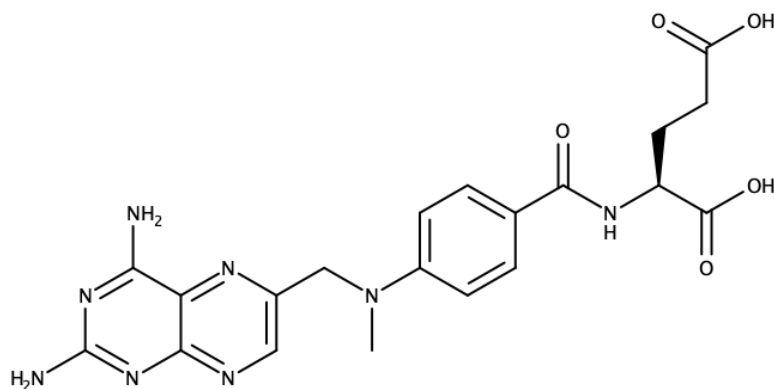
Figure 1 Chemical structure of methotrexate

2.2.1.2   Platinum-based analogs

Platinum-based chemotherapeutic agents present their activities to the cancer cells by crosslinking at DNA purine base, interrupt the DNA repair process, causing DNA damage, and induce apoptotic cell death as a consequence [82]. Member of the family includes cisplatin (CDDP), carboplatin, oxaliplatin, satraplatin, etc., as shown in Figure 2.2. CDDP is the first and most widely used platinum analog for the treatment of HNSCC. The agent can be used in the loco-regional stage of HNSCC as

definitive concurrent chemoradiotherapy. Also, the drug showed a desirable response rate and overall survival rate in the late stages of HNSCC when given with radiation therapy [83, 84]. Carboplatin (with 5-fluorouracil (5-FU)) has been reported to be superior to CDDP when it is used as induction chemotherapy for untreated advanced head and neck cancer patients with similar effectiveness but less toxicity than CDDP [85]. In recent years, satraplatin has become a promising alternative to CDDP due to its properties of having a less toxic effect, absence of CDDP cross-resistance, high efficacy against non-responsive cancers which are nonresponsive to formerly treated platinum-based analog. Moreover, this class is known to have a radiosensitizing effect which improved the treatment efficiency when combined with the chemoradiotherapy approach [86]. The toxicity of platinum analogs includes nausea and vomiting, diarrhea, mucositis, anaphylaxis, cytopenias, ototoxicity, cardiotoxicity, hepatotoxicity. Cisplatin has a sting relationship towards nephrotoxicity, myelosuppression for carboplatin, and oxaliplatin is dominant on neurotoxicity [87].
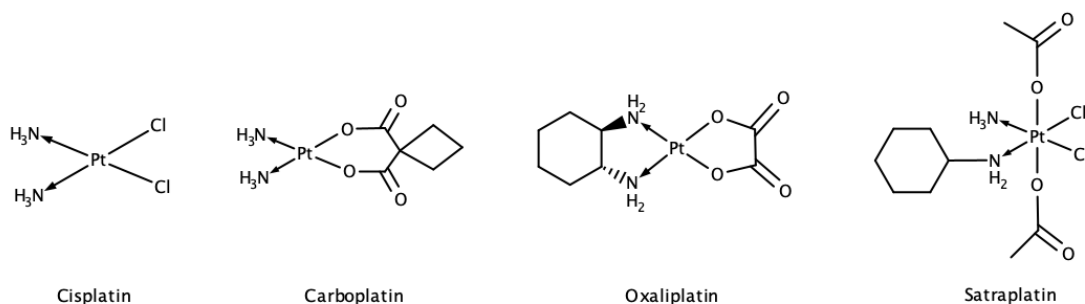
Figure 2 Chemical structures of platinum-based chemotherapeutic agents

2.2.1.3 5-fluorouracil

5-Fluorouracil (5-FU) is an antimetabolite chemotherapeutic compound that has a structure similar to DNA and RNA pyrimidine base (Figure 2.3). The drug acts by inhibiting the production of deoxythymidine monophosphate (dTMP) which is crucial for DNA replication and repair. Once dTMP is not produced, the metabolism of the nucleoside is interfered with 5-FU can also incorporate into DNA and RNA causing the cytotoxic effect and lead to the cell death [88, 89]. The role of 5-FU in the treatment is usually in the locally advanced stage, recurrent, or metastasis HNSCC as a combination with other cytotoxic drugs e.g., platinum-based analogs and cetuximab

with concurrent radiation therapy [90]. The drug had benefits in reducing tumor progression, ameliorate the response rate and helped prolonged survival when given with platinum-based agent and cetuximab [91, 92]. The adverse effects of 5-FU are nausea and vomiting, alopecia, myelosuppression, neutropenia, cardiotoxicity, neurotoxicity, etc. [89]
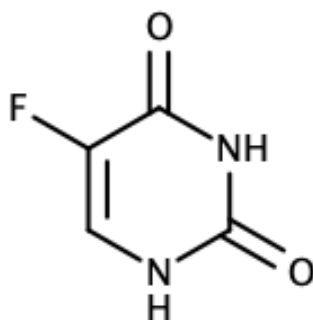
Figure 3 Chemical structure of 5-FU

2.2.1.4   Taxanes

Taxanes are naturally derived diterpenes from the plant in the Taxus genus (yew tree) where the most well-known, paclitaxel, was originally obtained from the pacific yew. Taxanes are mitotic inhibitors with the mechanism that promotes polymerization of tubulin and forms a stable microtubule. The stabilized microtubules lose their ability in cell division which disrupt the mitotic steps leading to cells death. Paclitaxel-bounded human albumin nanoparticles are currently available for the treatment of tongue cancer, and also used to sensitize radiologic response and improve the curative response and survival rate [93, 94]. Paclitaxel and docetaxel (Figure 2.4) are used in the treatment of locally advanced and metastatic HNSCC as an induction, concurrent, or palliative care [95]. Studies have investigated that taxanes may be beneficial to replace 5-FU in the regimen combined with cetuximab and cisplatin for presenting less toxic effects [96]. However, the toxicity of taxanes considering peripheral neuropathy, arthralgias, myalgias, myelosuppression, and skin changes would affect the patients' quality of life [97].
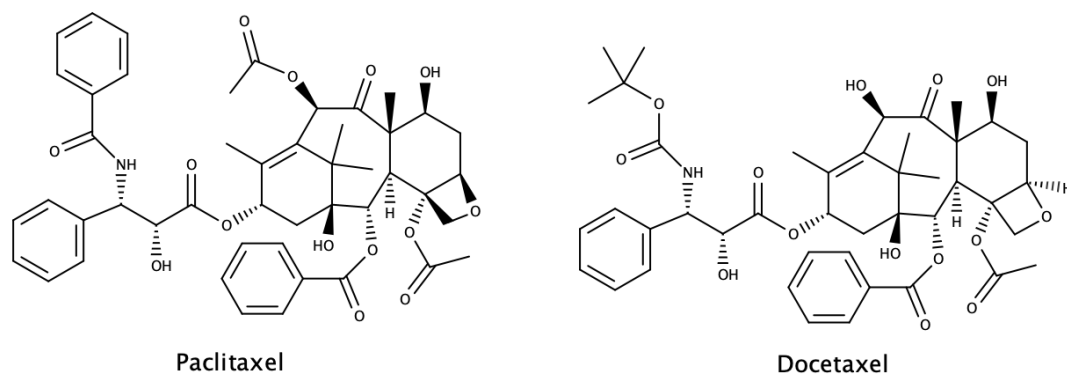
Figure 4 Chemical structure of taxanes

2.2.1.5 Doxorubicin

Doxorubicin (DOX; as shown in Figure 2.5) is a broad-spectrum anticancer agent in the class of anthracyclines. Its mechanism of action is to intercalate between DNA base pairs and interrupt RNA and DNA synthesis. DOX can also inhibit the topoisomerase II enzyme leading to the damage of DNA and inducing cellular apoptosis. Moreover, it is proposed to generate reactive oxygen species and damage cell membrane, DNA, and proteins [15]. The use of DOX in the treatment of HNSCC are a second-line or alternative of other mentioned agents and in the regimen for salivary gland cancer in a combination with cyclophosphamide and CDDP [98]. Also, it had been proven to be beneficial in recurrent and metastasis HNSCC once it was given with gemcitabine [99]. In addition, numerous novel studies investigated the effectiveness of DOX against HNSCC using various nano-formulations for instance, liposomes, polymeric hydrogels, nano-ferritins, etc. Not only these developed formulations could improve the treatment efficacy but they also led to better tolerability with reduced dosing and side effects or even solving drug-resistance issues [100-102]. Adverse effects of DOX are alopecia, severe nausea and vomiting, and most importantly, cardiotoxicity [15].
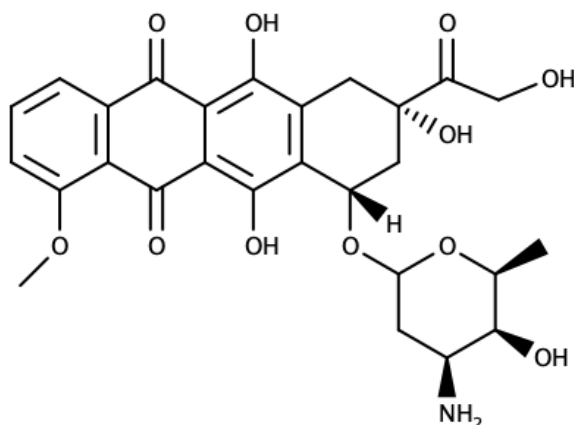
Figure 5 Chemical structure of DOX

2.2.1.6 Pan-Phosphoinositide 3-kinase inhibitors

The phosphoinositide 3-kinase (PI3K) signaling pathway has a very crucial role in HNSCC for being responsible for cell proliferation, cell growth, metabolism, and cell survival. The enzyme is a member of lipid kinase integrals that mediate intracellular signaling upon external stimuli [103]. The inhibition of PI3K and its PI3K/Akt/mTOR pathway has recently gained interest in the treatment of HNSCC due to the pathway's significance in tumorigenesis, metastasis, and drug resistance. The most important PI3K inhibitor under clinical studies for HNSCC treatment is the orally administered buparlisib (Figure 2.6). The drug showed promising efficacy in the treatment of locally advanced, recurrent, and metastatic HNSCC when combined with cetuximab, CDDP, erlotinib, or radiation therapy [104, 105].
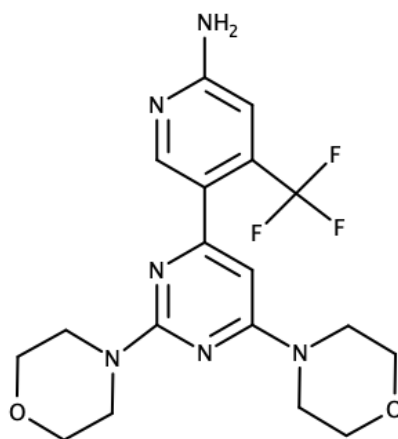
Figure 6 Chemical structure of buparlisib

2.2.2   Molecularly targeted compounds

The first approved monoclonal antibody (mAb) for the treatment of HNSCC is cetuximab which is currently recommended to be used in combination with platinum-based chemotherapy for recurrent or metastatic HNSCC considering cancer initiated in the oral cavity. Cetuximab is classified as an immunoglobulin G1 chimeric monoclonal antibody that binds to the extracellular domain of the human epidermal growth factor receptor (EGFR) with high affinity. With higher affinity than the endogenous ligand, cetuximab inhibits ligand binding and preventing ligand-mediated EGFR pathway activation. Apart from that, cetuximab induces the downregulation of EGFR and activates antibody-dependent cell-mediated cytotoxicity. The mAb showed a better response rate of HNSCC when it was given with radiotherapy with or without other chemotherapeutic agents for locally advanced HNSCC including recurrent, and metastatic disease [106-108]. Another anti-EGFR mAb undergoing clinical studies is nimotuzumab which has proven the effectiveness against advanced HNSCC when combined with low dose CDDP and radiotherapy [109]. Bevacizumab, a humanized IgG1 VEGF inhibitor, is under clinical study for HNSCC treatment. Its combination with chemotherapy or erlotinib showed improved efficacy considering response rate and overall survival [110].

2.2.3   Checkpoint inhibitor immunotherapy

Immune checkpoints are the regulator of the human immune system. They play an important role in self-monitoring and preventing the immune from attacking the cells aimlessly and prevent autoimmunity [111]. HNSCC develops dysfunctional immune checkpoints or prevents recognition of the immune cells allowing the cancer cells to tolerate and evade immunologic response. An important immune checkpoint that downregulates the immune response is Programmed cell Death 1 (PD-1). The signaling of the PD-1 regulated pathway is dependent on the attachment to its ligands PD-L1 and PD-L2 that are upregulated on head and neck cancers as well as other solid tumors. The inhibition of PD-1 or its ligands allows the immune to properly manage the cancer cells by restoring dysfunctional immune cells and recover tumor-specific immunity leading to the elimination of cancer [112, 113]. The most studied

PD-1 inhibitors for HNSCC are pembrolizumab and nivolumab which are humanized mAb studied for the treatment of recurrent and metastasis HNSCC where the former has been approved and guided to be used for untreated metastatic or unresectable recurrent HNSCC as monotherapy and the latter is recommended with patients whose disease had progressed on platinum-based chemotherapy. Meanwhile, the PD-L1 inhibitor, durvalumab, is under clinical trial [79, 114].

2.3 Drug targeting strategies

Adverse effects of chemotherapy have been the greatest obstacle to achieve a successful cancer treatment including HNSCC. It is known that the toxicity of chemotherapeutic agents limits the administration dose concerning the patient's tolerability to the side effects [36]. Moreover, problems on insufficient drug quantity at the affected cancer area and lead to cytotoxic drug resistance. Several strategies are proposed with intensive and extensive studies to modulate drug pharmacokinetics and biodistribution. The use of nano-formulations enables the localization of chemotherapeutic agents at the tumor site with the aid of different strategies classified as systemic targeting approach and locally targeting drug delivery [37, 115] as presented in Figure 2.7. There are three main types of systemic drug targeting which are passive, active, and stimuli-sensitive drug targeting where each provides an opportunity to target the tumor area through the tumor microenvironment and cancer cell presentation [116].

2.3.1 Systemic targeting

2.3.1.1 Passive targeting

In the passive targeting approach, the nanocarriers passively extravasate and accumulate within the tumor microenvironment due to the EPR effect of the tumor. The EPR effect is resulted from the angiogenesis of disorganized and highly perforated vessels which are generated by the fast-growing tumor [117]. The irregularity of the vasculature allows macromolecules and nano-formulations to penetrate well compared to normal healthy tissues. Moreover, the developed tumor has a dysfunctional lymphatic drainage system which allows the nanocarrier to retain in the tumor interstitium. The delivery of the nano-colloidal system is beneficial to

target and enhance drug accumulation within the tumor; however, an optimal nanoscale formulation is required. RES plays an important role in eliminating particulate system through the mononuclear phagocyte system (MPS) which can capture the nanoparticles (NPs) depending on their size and surface properties and sent them to the RES organs (mainly liver and spleen) for elimination. Therefore, the properties of the formulated nano-system must be tuned to avoid RES capture or renal filtration while the extravasation through the EPR effect is not diminished [117, 118]. The preferred particle size allowing the particle to enter the leaky vasculature of the tumor is between 100–600 nm. Considering the surface properties, NPs are suggested to have a hydrophilic outer surface which would facilitate the evasion of macrophage capture. Methods to improve hydrophilicity of the particle are conjugation or coating with polyethylene glycol (PEG) and formulation of NPs using co-block polymer of hydrophilic and hydrophobic units. The appropriate particle size and surface characteristics would prolong the plasma circulation time of the nano-formulation whilst entering the leaked vessel through the ERP effect and avoid RES removal [116].

2.3.1.2　　　Active targeting

Drug delivery system comprises of drug and carrier in which a non-decorated nanocarrier system provides a passive targeting delivery. The attachment or decoration of a specific ligand- or receptor-mediated compound on the nanocarrier surface may improve targeting specificity and selectivity of the delivery system, thus enhancing drug accumulation at the tumor site and minimize the drug at the unaffected regions. Active targeting approach can be categorized into two types based on surface modification which are ligand-mediated active targeting and receptor-mediated targeting [116, 119].

Ligand-mediated active targeting refers to the carriers having a surface decoration with mAbs, integrins, peptides, and aptamers. These biological ligands can specifically bind to the receptors presented on the surface of cancer cells and assist cellular uptake of drug-incorporated NPs leading to improved efficacy. It was conveyed that higher ligand density per unit of nanocarriers is advantageous for encouraging high cellular communication compared to a single ligand. Means for

conjugating these ligands onto the carriers include physical adsorption and chemical conjugation after the preparation of drug carrier or pre-conjugation of a ligand with the carrier component e.g. polymer prior to the formulation [116, 119, 120].

Antibodies are proteins with very large sizes which are highly specific towards the target site. They have not only been proven to be beneficial for active targeting purposes, but also have potent therapeutic effects. Different mAbs were conjugated on the various nano-formulations including lipid-based, inorganic-based, and polymer-based NPs, and showed superior targeting and anticancer activities to the non-decorated systems [116, 121]. Examples of antibody-mediated active targeting are the use of cetuximab, an anti-EGFR mAb, conjugated with nanodiamonds for cytotoxic effect against human liver hepatocellular carcinoma or pegylated liposome conjugated trastuzumab as an anti-HER2 antibody for breast cancer targeting [122, 123].

Peptides, integrins, and aptamers are important ligand for active targeting in cancer therapy. Due to the ease of production, small molecular size, stability, and simple conjugation method, peptides became advantageous for cancer targeting. These molecules can be densely conjugated on nanocarriers providing a smaller particle size compared to mAb-conjugated nanocarriers. They have been used in drug delivery platforms for targeting various receptors presented on cancer cells; for example, interleukin-4 receptors expressed on tumor endothelial cells [124]. Integrins are overexpressed on tumor neovasculature presenting as small peptide molecules. Different ligands are bonded to the nanocarriers for integrin binding including the RGD (arginine, glycine, aspartic acid) peptide sequence, peptidomimetic compounds, and other peptide sequences. These conjugations facilitate cancer recognition and cellular responses to cancers. Aptamers are short-chain nucleic acid compound or DNA or RNA oligonucleotide which selectively binds to the antigen presented on cancer cell surfaces. The molecules are small and easily fabricated. In addition, they are promising for targeting and therapeutic purposes. Aptamers can be conjugated to nanocarriers for cancer treatment without a chemotherapeutic drug or they can be combined with an anticancer compound for precise and effective delivery of the drug [116, 119].

Receptor-mediated active targeting is used in some nano-formulations such as those coupled with folic acid for folate receptor targeting or transferrin for binding to

transferrin receptors. Folate receptors are commonly overexpressed in solid tumors since folates are required for DNA synthesis in tumor cells. The binding of folic acid to the receptor induces endocytosis of the folic acid-conjugated NPs and enhances the cytosolic accumulation of the nanocarrier [119, 120]. Also, folic acid conjugation does not only be advantageous for drug targeting, but it is also useful for phototherapy, imaging, and diagnosis. Folic acid was used in many nano-formulations providing improved cellular uptake, increased cytotoxic effect of the chemotherapeutic agents, and reduced undesired effects. Transferrin is a type of glycoprotein accountable for iron-binding and iron transport within the cells. The transferrin receptors are also overexpressed in many malignant tumors which can be employed for cancer targeting. The benefit of targeting to transferrin receptor is the ability to overcome multidrug resistance proteins and p-glycoprotein. The conjugation of transferrin to the drug delivery systems allows optimization of pharmacokinetics of the drug and prolonged contact of the chemotherapeutic drug to cancer cells. Nevertheless, transferrin receptors can be saturated by endogenous plasma transferrin, so the use of mAbs and specific site administration would help to improve transferrin receptor targeting [116].
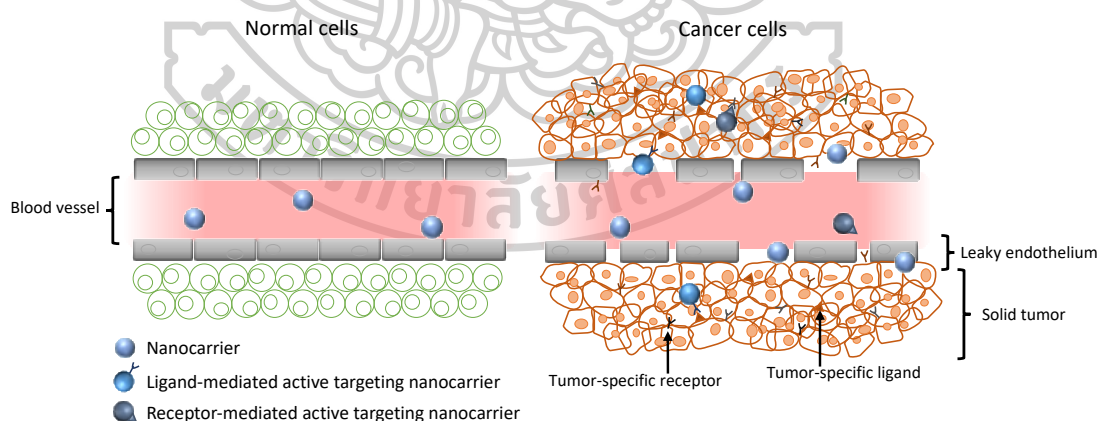
Figure 7 Presentation of the tumor microenvironment and nanocarrier targeting

2.3.1.3 Stimuli-sensitive nanocarrier

Stimuli-sensitive nanocarriers are designed to provide a release or an action of the therapeutic agent once they are stimulated by a stimulus. Intrinsic physiological conditions or pathological factors of tumor and tumor microenvironment e.g., pH,

enzyme, redox potential, peroxides, and hypoxia are useful for drug targeting. In addition, various novel systems have been formulated to respond to external stimuli, for example, heat, light, ultrasound, and magnetic fields. The stimulation of such factors facilitates the specific delivery of chemotherapeutics, controlled drug release, drug activation, drug accumulation in cancer cells, and alteration of the physicochemical properties. The purposes of a stimuli-sensitive nanocarrier are ranged from therapeutics, diagnostics, imaging, and also theranostics [125].

2.3.2 Local targeting

The precise delivery of cytotoxic agents to the tumor site could be enabled by local administration of chemotherapeutics to the oral cavity. The administration approach allows the medicine to remain in the affected area for a longer period with a higher quantity than compared to systemic delivery. Site-specific delivery can also be obtained by intratumoral or topical application. Local targeting may improve the treatment efficacy of the cytotoxic drug and reduce the toxicity to normal tissues. Furthermore, because of the high turnover rate of the oral mucous membrane, local delivery of antineoplastic drugs against oral cancer would allow safer and more convenient drug use [35]. Studies on local delivery of anticancer compounds to oral cancer have been published; for example, aerosols have been examined for the local delivery of paclitaxel in the treatment of lung cancer, chitosan NPs containing ellagic acid showed promising efficacy towards oral cancer cells, and 5-FU-loaded buccal tablets for locoregional chemotherapy of HNSCC have also been developed. To date, numerous formulations have been developed for local delivery of anticancer agents to the cancer cells, including tablets, gels, NPs, polymeric films, rods, and wafers [35, 121, 126].

Mucosal permeability is a major barrier for successful topical application on the mucosal epithelial membrane. There are several methods for drugs and drug delivery systems to penetrate across the barrier. Firstly, the nano-formulations can penetrate by passive diffusion which is accounting for the paracellular and transcellular routes. Secondly, endocytosis pathway allows the cell to take up the drug-loaded nanocarriers. Lastly, a certain carrier can be bounded and enable the uptake of the nanocarriers through the carrier-mediated transport pathway. These

options are dependent on the properties of the nanocarriers which determine the pathway of cellular uptake. Surprisingly, tumors and malignant lesions in the oral cavity have higher membrane permeability allowing the drugs and carriers to transport easily to the cells. The alteration promotes drug accumulation at the affected site and provides improved treatment efficacy. The mentioned delivery pathways permit the drug to enter the target cells passively; meanwhile, the active targeting approach can also be applied to the local delivery where the nanocarriers are functionalized with targeting ligands can bind to a specific tumor receptor after penetrating through the mucosal surface [121, 126].

2.4 Nanoparticles

2.4.1 Definition and classification

Nanotechnology has gained interest among researchers in the medical field aiming to develop for treatment, imaging, diagnosis, targeting, and most importantly for more efficient and safer drug delivery [127]. The term NPs referred to particles having a size less than 100 nm. However, in the biomedical field, the developed nanomaterials are accepted in the range of the nano-scale. NPs have unique characteristics which are high surface-to-volume ratio, tunable surface functionalization, having the ability to adsorb different compounds, and enabling controlled/sustained release of the drug from drug delivery systems. The advantages of NPs in cancer therapy are the ability to passively target tumors via the EPR effect, improved drug solubility, bioavailability, slow physiological clearance, and specific target delivery [115]. Moreover, the use of NPs in drug delivery allows the reduction of the dose of active compounds required to reach therapeutic effect leading to reduced adverse effects and toxicity of the delivering compounds. The types of NPs can be classified into inorganic NPs, polymer-based NPs, and lipid-based NPs as shown n Figure 2.8 based on the type of materials used to form NPs which offer the unique characteristics of the NPs [128].
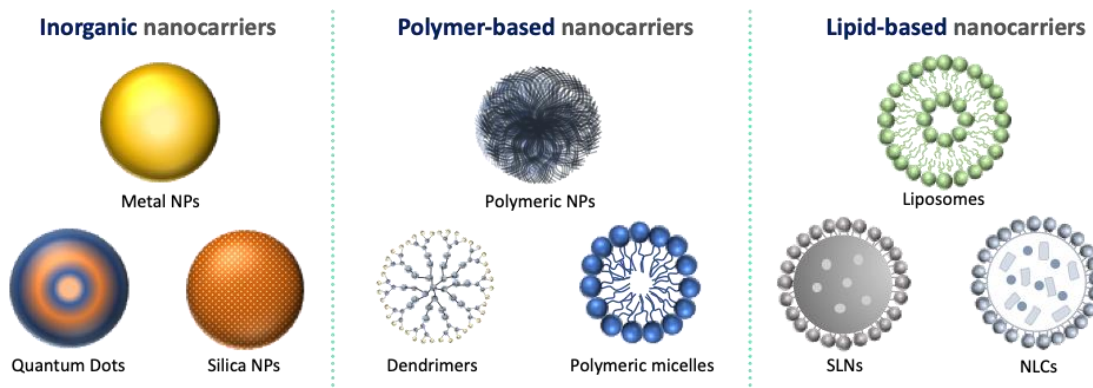
Figure 8 Classification of nanoparticles for drug delivery

2.4.2 Inorganic nanoparticles

Different inorganic NPs have been widely studied and possessed advantages in drug delivery and especially in diagnostic and imaging purposes. Common inorganic NPs include gold NPs (AuNPs), silver NPs, carbon nanotubes, quantum dots, magnetic NPs, silica, and titanium oxide NPs. These NPs are easily fabricated and have very small sizes and a high surface-to-volume ratio [129]. Metal NPs have a distinctive attribute that is tunable of optoelectronic properties. They present different colors due to their surface plasmon resonance (SPR) characteristics that enabled the change of AuNPs color upon the change in particle size. The modification of inorganic NPs usually on their surfaces using different chemical conjugation or pre-formulated functionalization. However, the drawbacks of these compounds are poor biodegradability and biocompatibility [129, 130]. Examples of inorganic NPs in the biomedical application include gadolinium-conjugated TiO_2-DNA oligonucleotide NPs which can be applied as MRI contrast agents with superior detection sensitivity compared to the free contrast agent and the use of EGFR targeting antibody-conjugated AuNPs for anticancer effect of HNSCC. The latter formulation also benefited in hyperthermia, treatment with heat above 40ºC, by the use of SPR property which can convert the SPR band to heat [131, 132].

2.4.3 Polymer-based nanoparticles

Polymer-based NPs are the nanocarriers that are fabricated from polymers or synthesized from monomers as the main components. The members of the class are

polymeric NPs, polymeric micelles, and dendrimers in which each type of polymer-based NPs has its unique structural arrangements [127].

The properties of polymeric NPs are varied by the type of polymer used in the preparation process. The flexibility of polymers allowed modification and functionalization of the NPs which tunes the characteristics of the NPs. The structure of polymer-based NPs can be divided into two types which are nanosphere where the NPs are solid polymers with drugs adsorbed or entrapped within the polymer matrix and nanocapsules in which the NPs have a spacious core for incorporation of a drug compound [133]. More importantly, polymeric NPs can rely on the physiological EPR effect caused by the tumor growth for drug delivery and they are usually biocompatible and biodegradable [127, 128, 134]. Different attempts have been made on the use of polymeric NPs for cancer therapy. Recently, a research study reported the incorporation of paclitaxel into polymeric NPs of alpha-tocopheryl succinate targeting HNSCC. The results of paclitaxel-loaded NPs were found to improve the antitumor effect and apoptosis induction of the drug in a mouse xenograft model. Furthermore, the NPs formulation improved the safety profile of the drug and significantly suppressed the angiogenesis markers [135].

Dendrimers are three-dimensional branched polymeric NPs that are also versatile and beneficial in drug delivery. These NPs contain multiple functional groups allowing the numerous compounds to be attached to their surface. Dendrimers can be used in delivering therapeutic compounds, diagnostic agents, and imaging agents while maintaining biocompatible properties [128].

Micelles are self-arranged NPs from compounds that have hydrophilic head groups and a hydrophobic tail, whereas, polymeric micelles are constructed from amphiphilic copolymers self-assembled to form a hydrophobic core and hydrophilic shell when the concentration higher than a critical micelle concentration. The core of polymeric micelles is useful in encapsulating hydrophobic drugs and provide delivery of the poorly soluble compound to the target site. The hydrophilic head presenting at the outer shell is responsible for enhancing drug stability, avoiding RES uptake, and extend the circulation time of the nano-formulation [36, 115].

2.4.4   Lipid-based nanoparticles

The lipid-based NPs have gained much attention in the development of anticancer medications. Common lipid NPs are liposomes, solid lipid NPs (SLN), and nanostructured lipid carriers (NLC). These NPs can be valuable in the delivery of both hydrophobic and hydrophilic molecules, exhibiting very low to no toxicity, providing controlled drug transport and release, and prolonging the circulation of drugs in the bloodstream leading to a longer systemic half-life. However, the surface of lipid-based NPs should be tuned to improve hydrophilicity through conjugation with polyethylene glycol (PEG) to reduce elimination by the immune system. The advantages of using lipid-based NPs are the ease of preparation, having a low cost of production, high drug loading capacity, biocompatibility, biodegradability, and good temporal and thermal stability [136].

Liposomes are phospholipid bilayers arranged to form a particle-structured colloidal system. They can be categorized as small unilamellar vesicles (less than 100 nm), large unilamellar vesicles (100–1000 nm), and multilamellar vesicles (having multiple bilayers). The carrier consisted of a spacious core allowing the entrapment of hydrophilic drugs inside the core, while hydrophobic drugs are captured between the lipid bilayers. Tremendous efforts have been made to develop liposomes as carriers for anticancer agents aiming to transport the compounds through passive, active, and also stimuli-sensitive strategies. A study developed DOX-loaded glycol-modified chitosan-coated pH-responsive liposomes which protonated at tumor acidic environment and promoted cellular uptake of DOX into the cancer cells. The development of pH-responsive liposomes showed significant improvement of anticancer efficacy in the HT1080 fibrosarcoma cell line [137]. Also, oxaliplatin incorporated-liposome conjugated cetuximab showed improved drug targeting and efficacy via active target to EGFR expressed colorectal cancer [138].

SLNs are lipid colloidal system prepared from a solid lipid at ambient and body temperature. The components of SLNs are triglycerides, smaller glycerides, or complex glycerides with fatty acids and stabilized surfactants or polymers. These particles usually have a size between 50–100 nm and could encapsulate hydrophobic and hydrophilic compounds within the solid lipid matrix. The pros of SLNs are good physical stability, controllable drug release, protection sensitive compounds from the

environment, enabling site-specific delivery, high permeability through membranes, and very low toxicity. In contrast, the limitations of SLNs are low drug loading capacity and release ability due to the crystallization upon storage [136]. A research article reported that the developed docetaxel-loaded SLNs had a great anticancer effect on breast cancer cells and also prevented cancer metastasis [139].

NLCs are derived form of SLNs which not only contains solid lipid but are made from mixed liquid and solid lipids; for example, ethyl oleate, glyceryl tricaprylate, glyceryl dioleate, and isopropyl myristate. NLCs surmounted the limitations of SLNs by providing higher drug loading capacity and preventing drug crystallization during the storage as they contain liquid lipids in the formulation. The particle size of NLCs is similar to or slightly bigger than SLNs because of the liquid components (between 10–1000 nm). Promisingly, the NLCs allow the transportation of both hydrophilic and lipophilic agents; moreover, the surface of NLCs can be modulated to allow special properties like drug targeting and persuading controlled drug delivery. NLCs have also been used in the delivery of chemotherapeutics to cancer cells [136]. A published article presented the co-delivery of CDDP and paclitaxel in folic acid-conjugated NLCs. The particle was prepared from COMPRITOL®-888 ATO, Cremophor ELP, and olive oil as lipid phase and CTAB combined with polysorbate-80 as surfactants. The drugs were loaded inside the lipid structure and coated with folic acid-conjugated PEG DSPE. The study revealed that the formulated NLCs could improve the delivery of the drugs with enhanced *in vitro* and *in vivo* efficacy towards head and neck cancers [140].

2.5 Polymeric nanoparticles

2.5.1 Definition

Polymeric NPs are defined as sub-micron solid colloidal particles that are made up of polymers or synthesized from monomers and have particle sizes ranged between 10–1000 nm. The NPs comprised of active pharmaceutical ingredients encapsulated within or adsorbed into the particles using physical adsorption, interactions, or chemically bonded to the polymeric surface [141]. There are two types of polymeric NPs depending on the NPs structures which are nanospheres, where the particles act as matrix systems with drug dispersion in the matrix, and

nanocapsules in which the NPs create vesicles for drug residence coated with a polymer layer [133]. The advantages of polymeric NPs are tunable properties, controlled release, protection of drug molecules, allowance of specific targeting, delivery, and retention, facilitating improvements in the therapeutic index, low drug toxicity, biocompatibility and biodegradability [142]. Furthermore, polymeric NPs can be applied in various aspects including, therapeutic, diagnostics, imaging, and theranostics [143].

2.5.2 Preparation of polymeric nanoparticles

Polymeric NPs can be prepared from natural polymers, semi-synthetic polymers, or synthetic polymers, also they can be designed to have unique characteristics by synthesizing from functional monomers [144]. Whereas, the characteristics of the polymeric NPs can be justified according to the designed purposes and applications [142]. To obtain the desired properties, the appropriate mode of NPs preparation plays a crucial role. Approaches to formulate NPs can be classified into two methods which are the top-down approach and bottom-up approach. The former method creates NPs from pre-formed polymer chains, while the bottom-up strategy builds up the NPs from monomer units [145].

2.5.2.1 Top-down approach

In the top-down approach, the polymeric NPs are prepared from the dispersion of the preformed polymer in a solvent. The polymers can be naturally derived, semi-synthetic, or synthetic polymers. Also, the polymers can be functionalized to create polymers with the desired properties or designed functional groups. This strategy can further be categorized into one-step procedure method, two-step procedure method, and ionic gelation of hydrophilic polymers [142, 143].

The one-step procedures include nanoprecipitation and dialysis methods (Figure 2.9). Nanoprecipitation is a widely used method as it is a simple process, convenient, and time-saving. In this method, the polymers are dissolved in a proper solvent usually organic, then the polymer solution is added to an anti-solvent (aqueous phase) which can be optionally prepared with surfactants. The polymer would self-assemble to form NPs upon the addition to the opposite phase and stable after the evaporation of the organic solvent [143]. Dong et. al (2004) prepared

methoxy-PEG-polylactide NPs loaded with paclitaxel using nanoprecipitation method. The polymer and the anticancer drug were dissolved in acetonitrile and prior to being added into the Pluronic®-F68 solution in water. Acetonitrile was removed by overnight stirring to create the drug-loaded NPs that were collected after filtration and centrifugation. The obtained NPs from this method had well-defined sizes with narrow distribution [146]. For the dialysis method, the processes are similar to that of nanoprecipitation. In this method, the polymers are dissolved in water-miscible solvents, for example, dimethylsulfoxide (DMSO), dimethylformamide (DMF), dimethylacetamide, or *N*-methyl pyrrolidone. The polymer solution is added into the dialysis bag and dialyzed against water. The solvent exchange across the membrane will create NPs inside the bag and be collected after solvent removal. A study by Akagi et. al (2005) prepared polymeric NPs from poly(γ-glutamic acid using dialysis method. The polymer was dissolved in different solvents and dialyzed for 3 days. The size and size distribution of the NPs varied based on the solvent used [147].
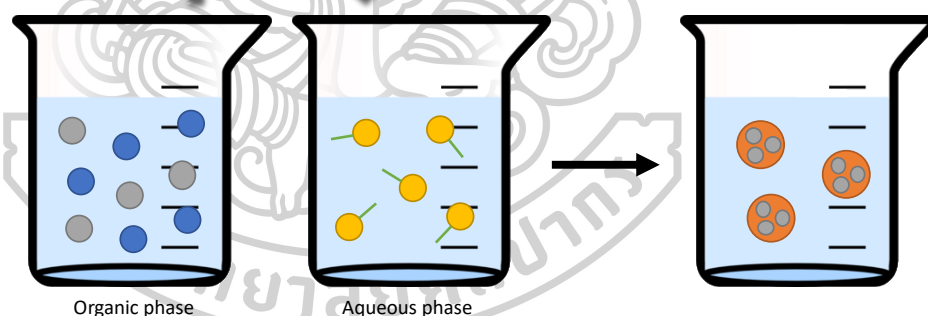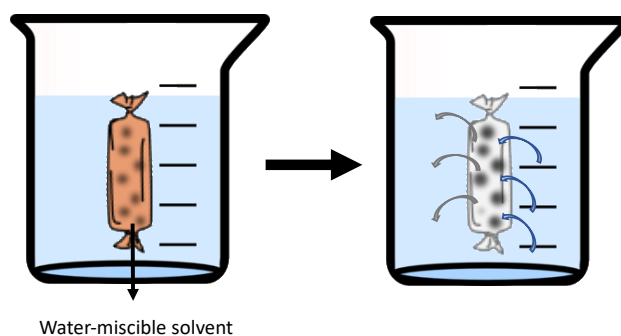
Figure 9 Top-down approach for polymeric NPs preparation (One-step procedures)

The two-step approach consists of emulsification-solvent evaporation, diffusion, and salting-out methods (Figure 2.10). These methods used the same principle on forming an emulsion of the polymer through a mixture of aqueous and organic phases. The NPs are formed using ultrasonication or homogenization prior to solvent removal or NPs collection [143]. The emulsification-solvent evaporation method uses water-immiscible solvents to dissolve the polymers with or without the drug and added to the aqueous phase contained stabilizers. After applying the physical force, the organic solvents are removed via evaporation to form NPs in water. This method was used in a study preparing polylactic-co-glycolic acid (PLGA) NPs loaded with DOX. The preparation process precisely followed the aforementioned method and collected particles of less than 300 nm with narrow size distribution [148]. In the emulsification-solvent diffusion, the organic phase is usually partially water-miscible. The mixture of the two phases was given mechanical/physical force to generate emulsion, then an extensive volume of water was added to promote the diffusion of solvent from the droplet creating colloidal particles. In 2011, Jain et. al produced PLGA NPs loaded with tamoxifen. The polymer was dissolved in ethyl acetate along with the drug and added mixed with water phase containing different stabilizers. The particles produced had particle sizes less than 170 nm with very narrow size variations [149]. For the emulsification-solvent salting out procedure, water-miscible organic solvents are used to dissolve the polymer. Meanwhile, the aqueous phase is prepared with stabilizers and salting-out out agents (commonly calcium chloride, magnesium chloride, and magnesium acetate). The salting-out agents reduce water miscibility of organic solvent which will then create an emulsion of polymer in the immiscible solvent. Again, a large amount of water is added to reverse the salting-out effect and stimulate precipitation of the polymer matrix [150].

Emulsification – Solvent evaporation

Emulsification – Solvent diffusion

Emulsification – Solvent salting out
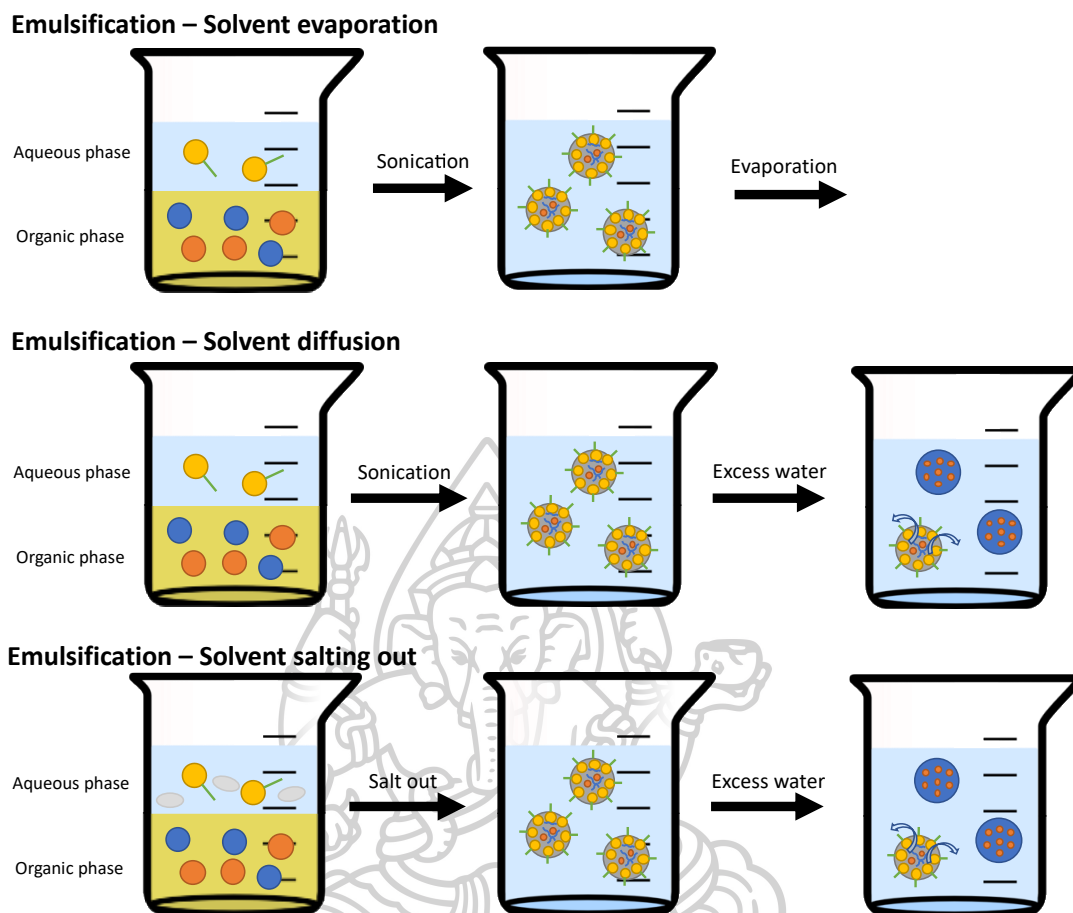
Figure 10 Top-down approach for polymeric NPs preparation (two-step procedures)

Ionic gelation of hydrophilic polymers is one of the most common techniques used to prepare polymeric NPs due to its ease of preparation and use of non-toxic solvent. The method (Figure 2.11) requires one or more polymers, and the particles are formed using ionic interaction between the two components. For single polymer NPs, the polymer is dissolved in an aqueous phase and dropped into a counter ion, for example, chitosan NPs were prepared by dissolving the polymer in acidic water and the solution of tripolyphosphate in water was dropped in the chitosan solution. The NPs were formed via ionic interaction between the positively charged chitosan from its amine groups and the negative ions of polyphosphate. The two polymer NPs follow the same concept where polymers with the opposite charges were separately dissolved and slowly mixed to form NPs [142, 151].

Ionic gelation
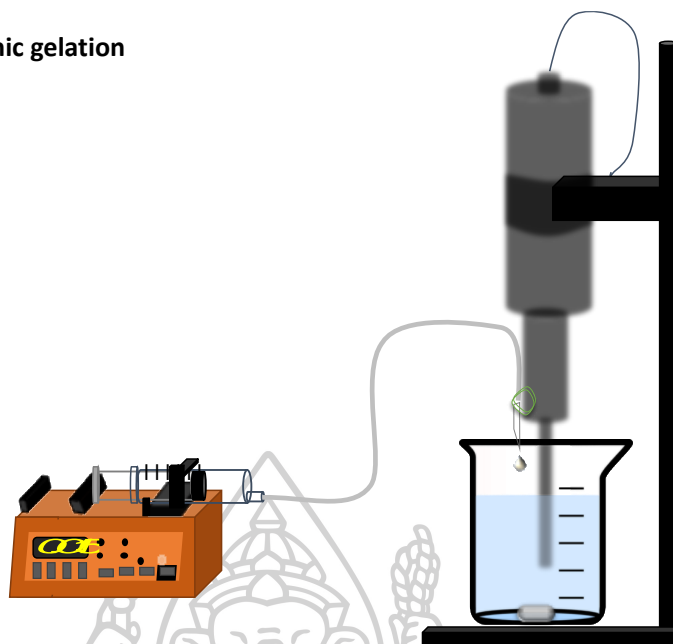
Figure 11 Top-down approach for polymeric NPs preparation (ionic gelation of hydrophilic polymers)

2.5.2.2 Bottom-up approach

To formulate NPs with particularly desired properties or with a specific functional group in the structure, the NPs can be generated by the polymerization of monomers. The selection of appropriate monomers and polymerization methods can produce NPs of certain characteristics. The components for NPs generation include monomers, initiators, and cross-linkers. The bottom-up methods used to create NPs are emulsion polymerization, interfacial polymerization, and controlled/living free-radical polymerization [142, 143].

Emulsion polymerization (Figure 2.12) is the simplest readily scalable polymerization method. The method can further be divided into two types which are conventional emulsion polymerization and surfactant-free emulsion polymerization. The conventional method commonly uses water as the continuous phase where droplets of monomers in the organic phase are added. Thereafter, the monomer swollen nucleation process occurs in the micellar-surfactant prepared in the water phase. The decomposed initiator began to initiate polymer chain growth within the monomer-swollen micelle that occurred in the water phase [152, 153]. An example of the method can be referred to an article preparing poly (*N*-vinyl carbazole) NPs. In

this article, monomer of *N*-vinylcabazole was prepared in toluene, while the water phase was prepared with a surfactant, sodium dodecyl sulfate, and 1 wt% V-50 initiator at a 70ºC inert atmosphere. The NPs were spherical with nano-scale size and low size distribution under an electron microscope observation [154]. The surfactant-free emulsion polymerization reaction follows the same principle of conventional emulsion polymerization with a difference where there was no surfactant involved. The polymerization process begins in the droplet of the organic phase slowly added to the continuous phase of the initiator in water. NPs from PEGylated methacrylate and 2-hydroxyethyl methacrylate-functionalized ε-caprolactone was reported to be created using potassium sulfate as the initiator. The NPs were less than 120 nm and were used as carriers of paclitaxel for anticancer effect [155].

Interfacial polymerization involves more than one monomer dissolving individually in continuous and dispersed phases. The polymerization process (polycondensation, polyaddition, or radical polymerization) occurs at the interfacial surface of the two phases. The method enables the formation of nanocapsules when aprotic solvents are used [152]. The controlled/living radical polymerization overcomes the limitation of conventional radical polymerization and allows control of particle size and size distribution, also NPs function and architecture [142].
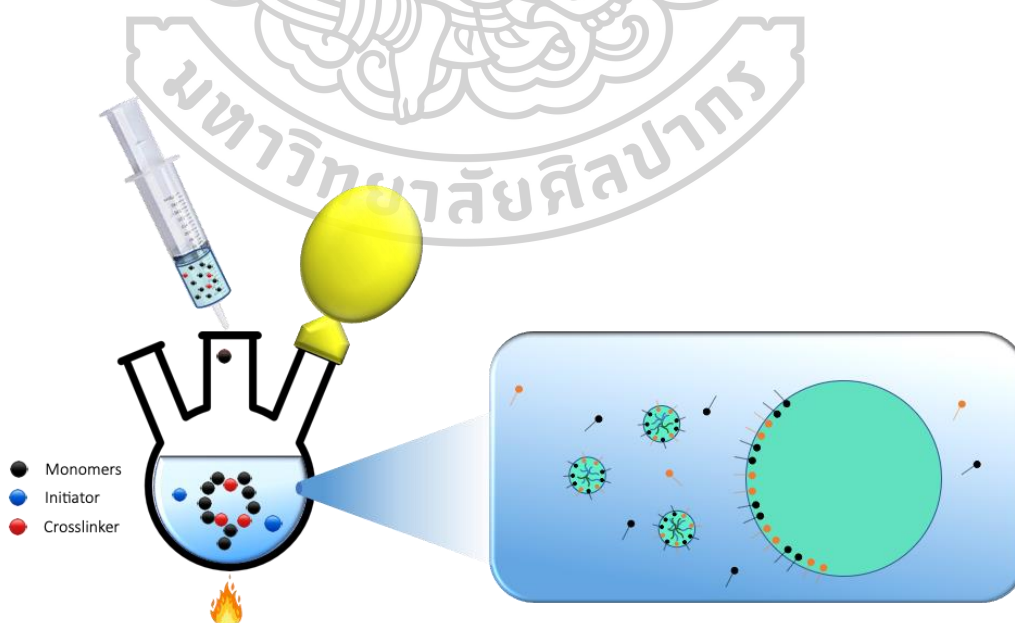
Figure 12 Emulsion polymerization

2.6   Mucoadhesive drug delivery

2.6.1   Definition and mechanism

Adhesion is a term that refers to the state where two surfaces are attached with an interfacial force. More specifically as members of the term, bioadhesion is used to describe when the phenomenon occurred between an adhesive material and a biological surface; whereas, mucoadhesion defines the adhering to the mucosal membrane for an extended period supported by a force or bond between the surfaces [156].

Decades ago, mucoadhesion phenomena in a drug delivery were brought up for its capability to extend the residence time of the active pharmaceutical agent at the site of action or absorption. The system concept is the incorporation of drug molecules to a mucoadhesive formulation. Once administered, the preparation will adhere to the mucosal surface and release the drug to provide therapeutic efficacy. Mucoadhesive drug delivery systems can be maintained at the delivery site, hence, increase the drug bioavailability. Some mucoadhesive materials may be used for particular site targeting, giving controlled drug delivery, avoiding first-pass metabolism, and protecting the active ingredient from the either enzymatic or acidic environment [157, 158].

Mucoadhesive drug delivery has been formulated as tablets, films, hydrogels, liposomes, and other micro- and nano-formulations; where these systems are composed of mucoadhesive polymers to perform the adhesion process with the mucous linings. The formulations were designed to be administered via certain routes aiming for local and systemic effect [157, 159]. The delivery system facilitates the treatment with a higher drug concentration at the absorption site, increases intimate contact of the preparation at the mucosal membrane, and improves drug bioavailability. The mucoadhesion process, therefore, diminishes the limitations of drug localization and adsorption [158].

Mucus is the viscous hydrated gel coving the lining membranes of the body cavities such as gastrointestinal, respiratory tract, vaginal, eyes, and other mucosal surfaces [160]. It is made up of main water, mucins, inorganic salts, enzymes, lipids, and biological residues [161]. Mucin glycoproteins, employing 2–5% of the mucus weight, are the major component responsible for gel-like viscoelastic and adhesive

properties of the mucus for their crosslinking and entangling structure [162, 163]. The glycoproteins expressed in the mucus are made up of amino acids serine, threonine, and proline joined to the oligosaccharides mostly through *O*-linkage; however, the main structure that plays an important role in forming the three-dimensional hydrogel network is the cysteine-rich subdomain that links the mucin monomers to oligomers [164, 165]. Mucin glycoproteins can form interaction with mucoadhesive materials through different bond formations. Notably, the cysteine subdomain acts a crucial function in forming strong bindings with novel mucoadhesive polymers [166].

The fundamental process of mucoadhesion comprises two steps as shown in Figure 2.13. First, the contact stage in which the polymer approaches the moist surface of the mucous membrane and gets wet or swells spreading along the mucosal area. Then later in the consolidation stage, the polymer form physical or chemical bonds with the mucus compositions through either weak bond of van der Waals' force, electrostatic interactions, hydrogen bonds, or the strong covalent bond [157].
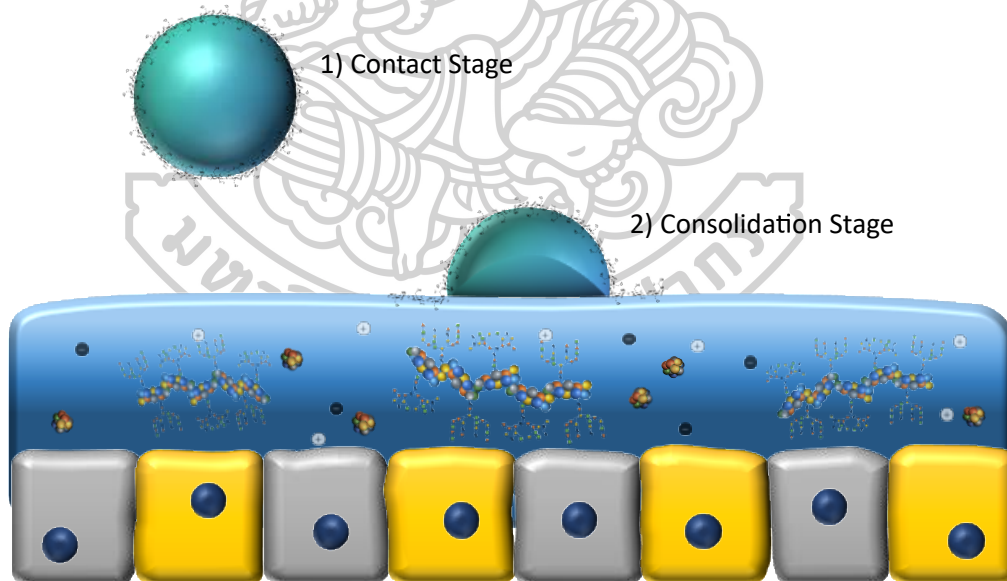
Figure 13 Mucoadhesive mechanism

2.6.2   First-generation mucoadhesive polymers

The first generation mucoadhesive polymers referred to the polymers that adhere to the mucosal membrane using non-covalent interactions e.g., physical

entanglement, ionic interactions, van der Waal forces, and hydrogen bond. This generation binds to the mucous membrane or mucin glycoprotein non-specifically. The first-generation mucoadhesive polymers can be naturally derived or synthetic macromolecule which possessed extensive functional groups that can create intermolecular interactions, for example, hydroxyl, carboxylic acid, and amine. These polymers can be divided into three classes according to the ionic status which are cationic, anionic, and non-ionic polymers [157, 158].

Chitosan (CS) is the most obvious cationic mucoadhesive polymer which is widely used in the biomedical and pharmaceutical fields. Positively charged chitosan can adhere to the mucous membrane by forming ionic interaction with the negatively charged sialic acid of the mucin glycoprotein. Studies on mucoadhesive drug delivery systems developed chitosan mucoadhesive formulation to prolong residence time at the desired area [162]. Research work demonstrated the mucoadhesive properties of chitosan through mucin adsorption efficiency of the chitosan/tripolyphosphate NPs by colorimetric analysis [151].

Anionic polymers are polymers that present negatively charged status at the physiological condition. Examples of these polymers are alginate, carboxymethyl cellulose (CMC), and polyacrylic acid. This class of polymers adheres to the mucous membrane using physical and weak chemical interactions such as polymer viscosity, polymer entanglement, and hydrogen bond. An article reported the mucoadhesive properties of sodium alginate and CMC by rheological analysis. It was concluded that the enhanced viscosity was due to the mucin-polymer adhesion force from physical chain entanglement and intermolecular non-covalent interactions [167].

Non-ionic mucoadhesive polymers; for instance, methylcellulose (MC), hydroxypropylmethylcellulose (HPMC), hydroxyethylcellulose (HEC), possess weaker mucoadhesive properties relative to the charged polymers. A recent study published the use of HPMC/PLGA NPs as mucoadhesive carriers for sitagliptin. The optimal prepared NPs showed prolonged residence time of the drug in the gastrointestinal tract leading to extended drug release profile and improved treatment efficacy of the orally administered drug delivery system [168].

2.6.3   Second-generation mucoadhesive polymers

The second-generation mucoadhesive polymers improve the properties of the first-generation mucoadhesive polymers by increased adhesion specificity. These polymers are functionalized to adhere to the mucosal layer through the formation of a covalent bond with the mucin glycoprotein. The target of these novel polymers is the cysteine-rich domain in the structure of mucin glycoprotein. The molecular structure of cysteine consisted of a thiol group in the side chain which is reactive to form covalent bonds via different mechanisms including, oxidation, disulfide formation, disulfide exchange reaction, Michael-type reaction, Schiff base reaction, etc. The formation of covalent bond enabled the second generation mucoadhesive polymers to adhere to the mucous membrane more specifically with stronger adhesion leading to prolonged residence time of the formulation at the target area [157, 158]. The development of novel functionalized polymer promotes the efficacy of the drug delivery system in terms of residence time and specificity. The organic functional groups that have been studied to improve the mucoadhesive properties of polymers are lectins, thiols, acrylates, catechols, and maleimides [169].

Lectins are glycotargeting proteins that recognize the carbohydrate recognition domain on the glycosylated surface resulting in lectins specifically binds to the sugar moiety of the cell surface while being capable to resist enzymatic degradation [170]. There are two ways to apply lectin targeting in the mucoadhesive drug delivery system. Firstly, lectins can be attached to a material to recognize the sugar or carbohydrate on the cell surface, or secondly, the ligands that are specific to lectin adhesion can be conjugated to the material to improve mucoadhesive specificity [171]. A study reported that lectin-conjugated NP enhanced the adhesion of NPs on the inflamed epithelial surface through sugar-lectin interaction. The lectin-mediated adhesion promotes the accumulation of the nano-formulation and increases the therapeutic efficacy of the mucoadhesive preparation [172].

Thiomers or thiolated polymers (Figure 2.14) are defined as polymers that have been functionalized with the thiol (–SH) moiety to improve mucoadhesion. Thiomers adhere to the mucous membrane by forming a disulfide bond with the thiols of the cysteine-rich domain in the mucin glycoprotein. In relative to the first-generation mucoadhesive polymers, thiolated polymers showed superior

mucoadhesive properties and provided longer adhesion time due to the covalent bond formation, which is a permanent and stronger adhesive interaction. The oxidation reaction creates a disulfide bridge linking the polymer to the mucosal membrane [166, 173]. Several articles have mentioned the benefit of thiomers on different drug delivery systems accounting for liposomes, NPs, micelles, etc. [174] Mahmood et. al (2003) published a study on thiolated micelles which was found to improve the mucoadhesive capacity on the intestinal mucosa and vaginal mucosa by 56.1-fold and 28.6-fold compared to non-functionalized micelle, respectively. The measurement was observed by the change of viscosity of the modified polymer. In addition, an advanced class of thiolated polymer has been studied [175]. Pre-activated thiolated polymers increase the sensitivity, stability, and mucoadhesion capability from the conventional thiomers. Usually, the thiolated polymers are pre-activated with 2-mercaptonicotinic acid. The modification created a pre-formed disulfide bond in the polymer which can reactively exchange with the thiols of the cysteine-rich domain upon reaching the glycoprotein leading to a faster disulfide bond formation and prevention of intra- and intermolecular oxidation of the thiol groups in the polymer which deducts the mucoadhesion of thiomers [176]. Pre-activated thiolated glycogen has been reported to improve the adhesion of thiolated and non-thiolated glycogen by 20-fold and 45-fold, respectively [177].
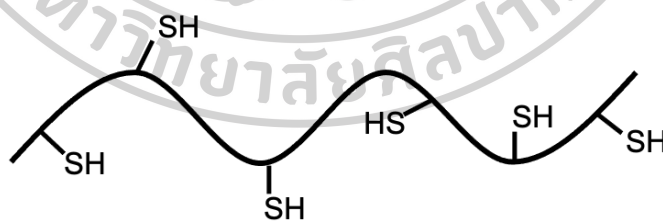
Figure 14 Chemical structure of a thiolated polymer

Acrylates is composed of carboxylic acid and vinyl groups. Polymer functionalization using the carboxylic part can bring about an acrylate functionalized macromolecule which is ready to adhere to the mucous membranes as illustrated in Figure 2.15. The acrylates form a covalent bond with the mucin glycoprotein using the Michael adhesion mechanism, whereas, lone pair electron transfer of thiols attack

the partially positive carbon of the vinyl group to create the adhesion bond [169]. Studies on acrylate mucoadhesive materials are the formation of acrylate functionalized micelles and acrylate-modified NPs. The first example revealed that the critical micelle concentrations of the acrylate micelles and non-functionalized micelle were similar, but the former exhibited better mucoadhesion analyzed using viscosity [178]. The second example showed that acrylate-grafted NPs create additional mucoadhesive mode from the positively charged polymer. By that, the polymeric NPs could adhere to the mucus with ionic interaction using its amine group and the ionized carboxylate of the sialic acid while acrylates helped to attach with protein thiols with a covalent bond. This formulation promotes the delivery of pilocarpine on the conjunctival tissue [179].
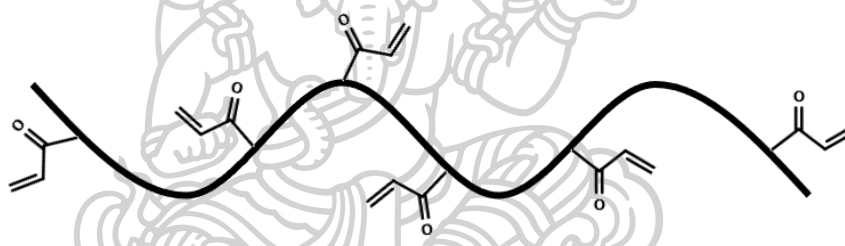
Figure 15 Chemical structure of acrylate polymers

Catechols has gained a lot of interest in recent years' research. The functional group was discovered as the hidden mechanism of sea mussels that is used to adhere to the surface under the sea. Thus, this functional group could impressively tolerate fluid wash-off [180]. The structure of catechol is an aromatic ring with hydroxyl groups at the meta- and para- position from the α-carbon position Figure 2.16. Once the catechol is conjugated on the polymer backbone, the moiety can adhere to the mucus using non-covalent interactions and covalent bonds which can be formed by the oxidation process, Michael adhesion mechanism, and Schiff base reaction. These covalent bond formations are also linked to the mucin glycoprotein at the cysteine domain. Owing to different adhesion mechanisms, the catechol-bearing polymeric materials can adhere well to different surfaces [48, 180]. Attempts on adding catechol group to the biocompatible and biodegradable polymers have shown to be successful

including catechol-modified chitosan. As mentioned, chitosan non-selectively bind to the mucosal membrane using weaker bond like ionic interaction, but the modification with catechol improves mucoadhesion. A study developed a catechol-functionalized chitosan-based hydrogel that is cross-linked with genipin as a carrier of lidocaine. The result illustrated that the hydrogel of modified chitosan had a higher density than the chitosan hydrogel leading to higher resistance to washing off and prolonging drug release. *Ex vivo* experiment showed that the catechol-functionalized formulation could adhere to the mucosal tissue for over 6 hours, while the unmodified hydrogel only stayed on the tissue for 1.5 h. More importantly, the findings were related to the *in vivo* examination [181].
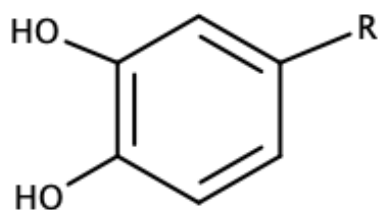
Figure 16 Chemical structure of catechol

Another proven mucoadhesive functional group is maleimide which has the structure as shown in Figure 2.17. This functional group can form a covalent bond with thiols on the glycoprotein using a 1,4–addition reaction. The double-bond inside the five-membered ring of maleimide is reactive due to the ring strain that the moiety is ready to form a bond to the thiol without catalyst. The thioether bond is specifically formed at the physiological condition which attracts the development of maleimide-containing material for transmucosal delivery. The delivery of active pharmaceutical ingredients using maleimides was proven to be efficient, reactive, stable, and maintain polymer safety profile [169]. Maleimide functionalized mucoadhesive liposomes were developed for drug delivery to the urinary bladder. It was found that maleimide-functionalized liposomes showed a longer retention time on the bladder tissue compared to the PEGylated liposome, and non-functionalized liposomes for their capability to form covalent bonds with the mucosal component [182].
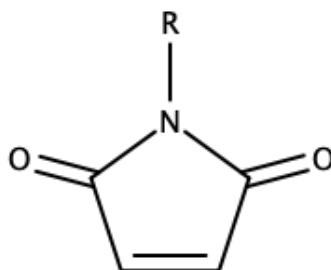
Figure 17 Chemical structure of maleimide

2.7   *N*-vinylpyrrolidone

N-vinylpyrrolidone (NVP) is a monomer of a widely used polymer, polyvinylpyrrolidone. The monomer is hydrophilic, biocompatible, nontoxic, stable, and inert. Also, NVP is commonly used as particle dispersant and helps to prevent particle aggregation due to its steric hindrance structure (Figure 2.18). NVP can be applied to polymer and copolymer preparation in different aspects and be used in many industries considering foods, cosmetics, textile, printing inks, pharmaceuticals, and biomedical fields owing to its versatility [183]. The structure of NVP consisted of a pyrrolidone ring connected to a vinyl group which is initiated and propagate in the polymerization reaction. Focusing on its use in the pharmaceutical and biomedical applications, NVP can be utilized to develop functional and advanced materials through the preparation of homopolymers, co-copolymers cross-linked polymers [184]. An example of NPs prepared from NVP is the preparation of amphiphilic poly-*N*-vinylpyrrolidone NPs as the carriers for indomethacin. The NPs were synthesized using NVP and mercaptoacetic acid through free-radical polymerization with azobisisobutyronitrile (AIBN) as the initiator. Then, functionalized PVP chains were attached to hydrophobic moiety with coupling reaction and create amphiphilic NPs via dialysis and solvent evaporation method [185]. Another study also prepared and investigated the properties of NPs from amphiphilic poly-*N*-vinyl-2-pyrrolidone with hydrophobic octadecyl mercaptan and AIBN initiator. The NPs were obtained after emulsion-free radical polymerization and solvent evaporation. The synthesized NPs

were less than 350 nm in size and were able to carry poorly water-soluble fluorescent dye [186].
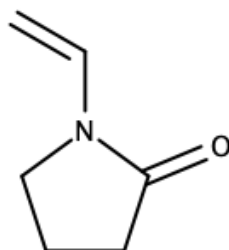
Figure 18 Chemical structure of NVP

2.8 Acrylic acid

Acrylic acid (AA) is a monomer of synthetic polyacrylic acid which is used in different drug delivery platforms. The structure of AA shown in Figure 2.19 is comprised of a carboxylic acid group that is versatile for functionalization and a vinyl group that can be used in polymerizations or conjugations. As mentioned, AA is used to create homopolymer and copolymers that can be used in different industries, including paints, coatings, plastics, polishes, adhesive, medical products, and pharmaceutical fields. The monomer has promising characteristics of biocompatible and biodegradable which gathered the interest for drug delivery [187, 188]. The application of AA in biomedical research is the development of chitosan cross-linked poly(acrylic acid) hydrogel. Functionalized chitosan was acquired as the crosslinker in the polymerization of AA with an ammonium persulfate initiator. The system was found to be pH-responsive with swelling behavior changes at different crosslinking amounts. Also, the hydrogel of poly(acrylic acid) and chitosan could control the delivery of active pharmaceutical compounds [189].
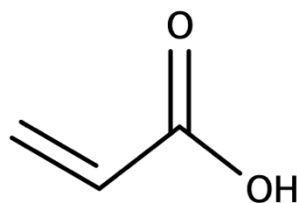
Figure 19 Chemical structure of AA

2.9   Chitosan

CS is a naturally derived polymer and is known as deacetylated chitin. The compounds are extracted from shells of crustaceans such as crabs, lobsters, crayfish, shrimps, etc. The chemical structure of CS contains proportableucosamine units and the *N*-acetyl glucosamine units linked with the β-(1,4)-linkage (Figure 2.20); therefore, CS is considered a cationic polymer with properties varied according to its molecular weight and degree of acetylation [190-192]. The polymer is used in food, chemical, cosmetics medical, biochemical, and biomedical engineering industries. Considering its biocompatibility and biodegradability, CS has become a polysaccharide that is widely used for biomedical purposes. CS itself possesses unique characteristics, for example, having antibacterial activity, mucoadhesive properties, antioxidant activity, and antitumor activity [193, 194]. The limitation of CS is commonly referred to the poor water solubility profile and the need to be solubilized in an acidic environment. Additionally, derivatization of CS allowed the attributes of the polymer to be tuned for specific purposes such as improving solubility, drug targeting ability, and enhance mucoadhesive properties [190, 193]. An example of CS in biomedical research is the conjugation of RDG peptides onto CS-NPs loaded with raloxifene for targeting breast cancer. The CS-based NPs showed great anticancer activity while being highly biocompatible. Also, the carrier showed pH-responsive behavior, a specific targeting approach, selectively suppresses angiogenesis, and tumor growth [195].
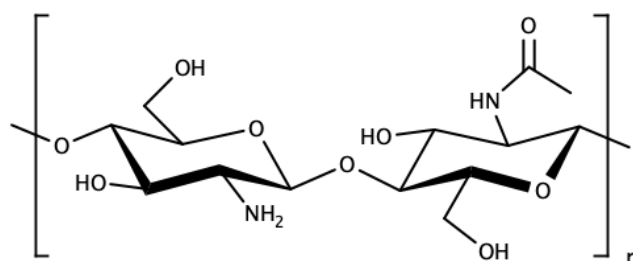
Figure 20 Chemical structure of CS

2.10 Hyaluronic acid

Hyaluronic acid (HA) is a mucopolysaccharide composed of glucuronic acid linked *N*-acetylglucosamine through the β-(1,3)-glucuronidic linkage (Figure 2.21). The polymer is known to have various biological effects commonly anti-inflammatory, anti-aging, skin regeneration effect, wound healing and benefits tissue engineering [196]. The glucuronic acid subunit of HA contains carboxylic acid with pK_a of 3–4 which can be mostly deprotonated at the physiological condition creating an anionic polymer [197]. Apart from that, several functional groups on the structure (carboxylic acid, hydroxyls, acetamido) are versatile for functionalization and producing derivatives of HA that benefit drug delivery. HA is biocompatible, biodegradable, nontoxic, highly viscoelastic, and promotes cell adhesion especially on CD44 receptors expressed on cancer cells. HA has been incorporated in different carrier systems for therapeutics, diagnostics, and imaging [197, 198]. A study investigated HA hydrogel formed by oxidized HA and crosslinking HA as a drug carrier and therapeutic agent for tendinopathy. The hydrogel was able to provide a sustained drug release profile and showed biodegradability properties after the injection while enabling the justification of the symptoms both *in vitro* and *in vivo* models [199]. Another study revealed that HA-coated camptothecin nanocrystals were successfully prepared using nanoprecipitation method. The carrier improved the water solubility of the hydrophobic drug, had high drug loading capacity, prolonged the release of camptothecin through pH-responsive means, improved drug stability, and was able to target CD44 overexpressed on the cancer cells [200].
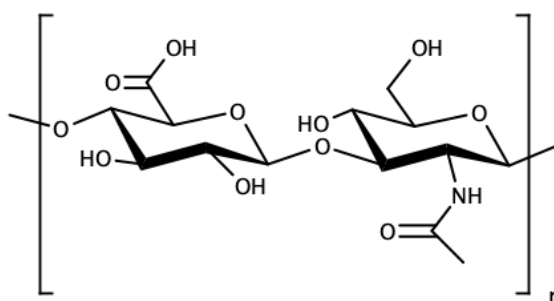
Figure 21 Chemical structure of HA

CHAPTER 3

MATERIALS AND METHODS

3.1   Materials

3.2   Equipment

3.3   Methods

    3.3.1 Development of coordination bond-forming *N*-vinylpyrrolidone/acrylic
acid nanoparticles (NVP/AA NPs) for cisplatin (CDDP) delivery

        3.3.1.1   Synthesis of NVP/AA NPs

        3.3.1.2   Characterizations and evaluations

            3.3.1.2.1 ^{1}H-nuclear magnetic resonance spectroscopy (^{1}H-NMR)

            3.3.1.2.2   Fourier-transformed infrared spectroscopy (FTIR)

            3.3.1.2.3   Particle size, size distribution, zeta potential

            3.3.1.2.4   Morphology

            3.3.1.2.5   COOH content

            3.3.1.2.6   Drug loading

            3.3.1.2.7   Drug content determination

            3.3.1.2.8   Drug release

            3.3.1.2.9   *In vitro* biocompatibility and cytotoxicity

            3.3.1.2.10 Cell death mechanism

            3.3.1.2.11 *In vitro* intracellular accumulation

    3.3.2   Development of mucoadhesive NPs for localized delivery of
doxorubicin (DOX)

        3.3.2.1   Synthesis of catechol-functionalized succinyl chitosan
(SCScat)

        3.3.2.2   Synthesis of catechol-functionalized hyaluronic acid (HAcat)

        3.3.2.3   The synthesized polymer characterizations

            3.3.2.3.1 ^{1}H-NMR

3.1   Materials

2,2′-azobis(2-methylpropionamidine) dihydrochloride (V50; Sigma Aldrich, St. Louis, MO, USA)

Accutase® (Sigma Aldrich, St. Louis, MO, USA)

Acrylic acid (AA; Sigma Aldrich, St. Louis, MO, USA)

Annexin V Alexa Fluor^{TM} 647 (Invitrogen, Carlsbad, CA, USA).

Annexin V binding buffer (Invitrogen, Carlsbad, CA, USA)

Chitosan (MW =11 kDa, 95 % degree of deacetylation) OilZac Technologies Co., Ltd. (Bangkok, Thailand)

Chloroform (Merck & Co., Darmstadt, Germany)

Cisplatin (CDDP; Sigma Aldrich, St. Louis, MO, USA)

Deuterium oxide (D$_2$O) was bought from Cambridge Isotope Laboratories (Tewksbury, MA, USA)

Dimethyl sulfoxide (DMSO; Merck & Co., Darmstadt, Germany)

Dopamine hydrochloride (Sigma Aldrich, St. Louis, MO, USA)

Doxorubicin hydrochloride (DOX; Sigma Aldrich, St. Louis, MO, USA)

Dulbecco's modified Eagle's medium (DMEM; Gibco BRL, Rockville, MD, USA)

Fetal bovine serum (FBS; Gibco BRL, Rockville, MD, USA)

Fluorescein sodium salt (Sigma Aldrich, St. Louis, MO, USA)

Glacial acetic acid (Merck & Co., Darmstadt, Germany)

Hyaluronic acid (MW =1550 kDa) P.C. Drug Center (Bangkok, Thailand)

HN22 cell line (Faculty of Dentistry, Naresuan University, Phitsanulok, Thailand)

Hoechst 33342 (Invitrogen, Carlsbad, CA, USA)

Human gingival fibroblast cells (HGF; Faculty of Dentistry, Naresuan University, Phitsanulok, Thailand)

Hydrochloric acid (Merck & Co., Darmstadt, Germany)

L-glutamine (Gibco BRL, Rockville, MD, USA)

Methylthiazolyldiphenyltetrazolium bromide (MTT; Sigma Aldrich, St. Louis, MO, USA)

N-(3-dimethylaminopropyl)-*N'*-ethylcarbodiimide hydrochloride (EDAC) (Sigma Aldrich, St. Louis, MO, USA)

N-hydroxysuccinimide (NHS; Sigma Aldrich, St. Louis, MO, USA)

N-vinylpyrrolidinone (NVP; Sigma Aldrich, St. Louis, MO, USA)

N,N'-methylenebisacrylamide (MBA; Sigma Aldrich, St. Louis, MO, USA)

N,N'-dimethylformamide (DMF) (Sigma Aldrich, St. Louis, MO, USA)

Nitric acid (Merck & Co., Darmstadt, Germany)

Non-essential amino acids (Gibco BRL, Rockville, MD, USA)

Penicillin-streptomycin (Gibco BRL, Rockville, MD, USA)

Porcine mucosal membrane (A slaughterhouse, Nakhon Pathom, Thailand)

Potassium dihydrogen phosphate (Merck & Co., Darmstadt, Germany)

Potassium phosphate (Merck & Co., Darmstadt, Germany)

Sodium chloride (Sigma Aldrich, St. Louis, MO, USA)

Sodium hydrogen phosphate (Merck & Co., Darmstadt, Germany)

succinic anhydride (Sigma Aldrich, St. Louis, MO, USA)

SYTOX™ Green nucleic acid stain (Invitrogen, Carlsbad, CA, USA)

Trypsin–EDTA (Gibco BRL, Rockville, MD, USA)

3.2 Equipment

Analytical balance

Attenuated Total Reflectance Fourier transformed infrared spectrophotometer (ATR-FTIR)

Automated cell counter (TC20™, BIO-RAD, CA, USA)

Automatic autoclave (LS-2D, Scientific promotion. Co., Ltd.)

Bath sonicator

CO_2 incubator

Flow cytometer (BD FACS Canto™ flow cytometer (BD Bioscience, CA, USA))

Freeze dryer (FreeZone2.5, LABCONCO, USA)

Incubator shaker

Inductive coupled plasma – Mass spectroscopy (ICP-MS; Agilent Technologies, 1100 series, Santa Clara, CA, USA)

Inverted fluorescence microscope (Nikon® TE2000-U, Japan)

Inverted microscope (Nikon® T-DH, Japan)

Laboratory centrifuge (Sorvall® BiofugeStratos)

Magnetic stirrer

Micropipettes (Eppendorf Research™ plus single-channel pipettes)

Microplate fluorometer (Fluoskan Ascent™, Thermo Scientific, MA, USA)

Multimode microplate reader (VICTOR Nivo™, Perkin Elmer, MA, USA)

Nitrogen gas tank

Oil bath

pH meter (HORIBA compact pH meter B-212)

Probe sonicator (Sonic VibraCell™)

Reflux condenser

Scanning electron microscope (Tescan Mira 3, Czech Republic)

Stereoscope with fluorescent detection (Leica M60, Wetzlar, Germany)

Syringe pump (NE-1000 Programmable Single Syringe Pump, KF Technologies)

Top load balance (Sartorius® CP2202S)

Transmission electron microscope (Philips® Model TECNAI 20)

Tube rotator

Vortex mixer

Zetasizer NanoZS (Malvern Instruments, Malvern, UK)

3.3   Methods

3.3.1   Development of coordination bond-forming *N*-vinylpyrrolidone/acrylic acid nanoparticles for CDDP delivery

3.3.1.1 Synthesis of NVP/AA NPs

The synthesis of *N*-vinylpyrrolidone/acrylic acid nanoparticles (NVP/AA NPs) was performed employing two different methods as follows:

3.3.1.1.1 Method 1

The NPs synthesized using method 1 (M_1-NPs) were acquired from a one-step surfactant-free emulsion polymerization. In search for the optimal condition, the ratio of NVP:AA was varied as 1:1, 1:3, and 1:5. Roughly, deionized water (50 mL) was placed in a round-bottom flask and heated in an oil bath to 65–70 °C. Then, 0.1 wt% of the free radical initiator (2,2'-azobis(2-methylpropionamidine) dihydrochloride, V50) was added. Nitrogen gas was purged to the solution which was vigorously stirred to keep the atmosphere inert. Meanwhile, AA, NVP, and the crosslinker (*N,N'*-methylenebisacrylamide, MBA, 10 wt%) were dispersed in chloroform (5 mL). The organic phase mixture was then gently added to the heated V50 solution. the polymerization reaction was carried out for 18 h before the resultant NPs dispersion was filled in a dialysis bag (molecular weight cut-off 3500 Da) and dialyzed against deionized water for 3 days before being freeze-dried.

3.3.1.1.2 Method 2

The core-shell structured NPs (M_2-NPs) were synthesized via two-steps polymerization. In the synthesis process, NVP, MBA crosslinker (10 wt%), and V50 initiator (0.2 wt%) were employed in the surfactant-free emulsion polymerization reaction to obtain polyvinylpyrrolidone (PVP) NPs. Thereafter, the prepared PVP NPs were further polymerized with AA. Briefly, V50 free radical initiator (0.2 wt%) was heated in deionized water (200 mL) at 65–70 °C. The environment was controlled using nitrogen flush for at least 20 min. Then, the organic phase was prepared by mixing NVP (5.8 mmol, 2.50 g) and MBA (10 wt%) in chloroform (5 mL). The mixture was gradually dropped to the initiator solution. Then, the polymerization reaction was allowed to perform for 18 h in the controlled atmosphere. Then, the unreacted substrates were removed via dialysis in deionized water which was replaced every 6 h for 3 days. Lyophilization was carried out to obtain the PVP NPs. Subsequently, to synthesize the core-shell structured NPs, AA (2.5 g), PVP NPs (0.25 g), and MBA (10 wt%) were mixed in the organic solvent (chloroform) prior to addition into a round bottom flask containing heated deionized

water (65–70 °C) an V50 (0.2 wt%). The reaction was continued at 65–70 °C for 18 h before the purification and freeze-drying procedures.

3.3.1.2 Characterizations and evaluations

3.3.1.2.1 ^{1}H-nuclear magnetic resonance spectroscopy (^{1}H-NMR)

The molecular attribute of the resultant NPs was analyzed using ^{1}H-nuclear magnetic resonance spectroscopy (^{1}H-NMR) spectroscopy. Each sample was dissolved in deuterium oxide (D_2O). ^{1}H-NMR spectra were collected with NMR 300 MHz (AVANCE III HD, Bruker) spectrometer at 298 K. All chemical shifts (δ) were recorded and reported in parts per million (ppm), using the chemical shift of solvent as references (D_2O: $\delta = 4.80$ ppm).

3.3.1.2.2 Fourier-transformed infrared spectroscopy

The chemical structures of the synthesized NPs, the CDDP-loaded NPs, and the physical mixture of CDDP and the blank NPs were confirmed by Fourier-transformed infrared spectroscopy (FTIR) using a Perkin Elmer spectrum 100 infrared spectrophotometer with the wavenumber ranged from 400 to 4000 cm^{-1}.

3.3.1.2.3 Carboxylic acid content determination

The amount of the carboxylic acid moiety contained in the synthesized NVP/AA NPs was determined by salt splitting titration. Roughly, the proton of COOH was altered to sodium carboxylate salt (COO^-Na^+) by immersing the NPs in 0.01 M NaOH (25 mL) overnight with energetic stirring. The excessed NaOH was further back titrated with standardized 0.01 M HCl while the endpoint was indicated by the change of pink to colorless phenolphthalein. The content of the carboxylic acid group was then calculated by the following equation.

$$\text{COOH content (mmol/g)} = \frac{(V_{VR} - V_{HCl}) \times C_{HCl}}{\text{NPs weight (g)}}$$

Where V_{VR} is the volumetric relation of standardized HCl (0.01 M) and NaOH (0.01 M),

V_{HCl} is the volume of titrant used, and

C_{HCl} is the standardized concentration of HCl.

3.3.1.2.4 Particle size, size distribution, zeta potential

The particle size, polydispersity index (PDI), and zeta potential of the NVP/AA NPs were determined by dynamic light scattering (DLS) technique using a Malvern Zetasizer Nano ZS (Malvern, UK). Samples were diluted 1:99 with ultrapure water and disaggregated with a Vibra Cell™ VCX134BP probe sonicator equipped with a 3 mm tip (Sonics, CT, USA). The test solutions were then transferred to a 1-mL polystyrene latex zeta cell for the measurement. Moreover, each sample was dispersed in different media (PBS, cell culture medium with and without serum), and stored for 14 days at 37 °C. The size measurement before and after the 14 days of storage was conducted in triplicate.

3.3.1.2.5   Morphology

3.3.1.2.5.1   *Transmission electron microscope*

The morphological characteristics of the NPs were scrutinized under a transmission electron microscope (TEM, JEOL JEM-1400, Tokyo, Japan) at an accelerated voltage of 80 kV. The sample was prepared in purified water, stirred overnight, and sonicated for 1 h. Uranyl acetate (1%) was used to stain the NPs to enhance visualization on the copper grid.

3.3.1.2.5.2   *Scanning electron microscope*

The morphology and surface characteristics of the NPs were observed using a scanning electron microscope (SEM, Tescan Mira 3,

Czech Republic). The lyophilized NPs were fixed on a metal stub using an adhesive tape and sputter-coated with a thin layer of gold prior to the investigation.

3.3.1.2.6 Drug loading

CDDP was loaded into the NPs using the adsorption method, CDDP and the NPs were accurately weighed and separately dissolved in ultrapure water pH 8.0–8.5 before being mixed at different weight ratios of NPs:CDDP (1:1, 1:2.5, 1:5, and 1:10). The mixtures were shaken overnight for complete coordination bonding. The unbonded drug was removed by dialysis (molecular weight cut-off 6000-8000 Da) against 6 cycles of deionized water (30 min/cycle) before being freeze-dried.

3.3.1.2.7 Drug content determination

The drug content in the NPs was determined by digesting the NPs components to obtain the platinum (Pt(II)) residues for the quantification. To the accurately weighted CDDP-loaded NPs, concentrated nitric acid (1 mL) was added and heated at 90°C for 1 h. After that, the digested solutions were diluted with ultrapure water and quantified using inductively coupled plasma-mass spectrometry (ICP-MS, Agilent 1100 series, Santa Clara, CA, USA). The analysis was performed using argon carrier gas 0.86 L/min, make-up gas 0.2 L/min, with Mira-Mist (PEEK) nebulizer at 0.1 rpm connected to a mass spectrometer set with a mass ranged between 2–208 AMU. The atomic absorption of ^{195}Pt isotope determined the amount of Pt(II) which correlated to the content of CDDP coordinately bounded to the NVP/AA NPs. The drug loading capacity (LC) and % loading efficiency (%LE) were calculated using the following equations.

$$LC \ (\mu g/mg) = \frac{\text{The amount of drug found}}{\text{The weight of drug-loaded NPs}}$$

$$\%LE = \frac{\text{The amount of drug found}}{\text{Total amount of drug initially added}} \times 100$$

3.3.1.2.8 Drug release

CDDP released from the NVP/AA NPs was examined using 10 mM phosphate buffer saline with 150 mM NaCl at various pH (5, 6.5, and 7.4) as the release medium. The CDDP-loaded NPs (equivalent to 2 mg CDDP) dissolved in the release medium (1 mL) were filled in a dialysis bag (molecular weight cut-off 6000–8000 Da). The bags were soaked in the release medium (10 mL) and constantly shaken at 150 rpm under a temperature-controlled (37±0.5 $^{\circ}$C) atmosphere. The release medium was sampled at each predetermined time up to 7 days for the quantification of CDDP content; whereas, the same volume of fresh release medium was then added to maintain sink condition. The cumulative release of CDDP from the NVP/AA NPs in each medium can be investigated using ICP-MS after the samples were digested by concentrated nitric acid.

3.3.1.2.9 *In vitro* biocompatibility and cytotoxicity using MTT assay

MTT assay was performed to evaluate the cytotoxicity of CDDP, blank NPs, and CDDP-loaded NPs on human gingival fibroblast (HGF) cells and head and neck cancer cells (HN22). HGF cells were cultivated in DMEM with FBS (10%), non-essential amino acids (1%), L-glutamine (1%), and penicillin-streptomycin (1%). HN22 cells were cultured in DMEM with FBS (10%), L-glutamine (1%), and penicillin-streptomycin-amphotericin B (1%). Each cell line was counted and seeded into 96-well plates to contain about 10,000 cells/well. The cells were incubated in an incubator maintained at 5% CO_2 and 37 $^{\circ}$C until confluence. CDDP, blank NPs, and CDDP-loaded NPs were prepared at various concentrations in the serum-free DMEM before being added (100 µL) into each well. The cells were then placed in the incubator for 24 h. After that, the media were taken out before the cells were rinsed with sterile PBS. DMEM with serum (100 µL) was then added to each well with 0.5 mg/mL MTT solution (25 µL) and incubate for another 3 h. After the removal of the MTT solution, DMSO (100 µL) was added to dissolve the formazan crystals in the cells. The cell viability was measured at 550 nm with a VICTOR Nivo^{TM} multimode microplate reader (Perkin Elmer, MA, USA) . The

percentage of relative cell viability in relation to the untreated control cells was calculated by the following equation.

$$\%\text{Relative cell viability} = \frac{\text{OD}_{550,\ \text{sample}} - \text{OD}_{550,\ \text{blank}}}{\text{OD}_{550,\ \text{control}} - \text{OD}_{550,\ \text{blank}}} \times 100$$

3.3.1.2.10 Cell death mechanism

The apoptotic induction cell death mechanism of the HN22 cell after being treated with CDDP-loaded NPs compared to free CDDP solution was examined using the double staining technique. The treated cells were stained with membrane-permeable and impermeable fluorescence stain and investigated under a fluorescence detector-equipped inverted microscope and flow cytometer. In brief, the HN22 cells were cultured in a 96-well plate (10,000 cells/well) and incubated in a controlled atmosphere for 24 h. Then, free CDDP and CDDP-loaded NPs prepared in the culture medium at the concentration of their IC50 value were added to each well (100 µL) and further incubated for 24 h. At the specified period, 10 µg/mL of Hoechst 33342 (10 µL) and propidium iodide (PI) at the final concentration of 5 µg/mL was added for cell staining and incubate for another 20 min prior to the evaluation. The cell death pathway analysis of the free CDDP compared to CDDP-loaded NPs was also examined by flow cytometry. The technique assists to analyze the stage of cell death through fluorescence staining detection. By that, the head and neck cancer cells were cultivated in complete DMEM and seeded in a 6-well plate. The cells were grown in an CO_2 incubator until confluence. Then, free CDDP and CDDP-loaded NPs at the IC50 value were dissolved in a serum-free medium and placed in the well to treat the cells. After 24-h incubation, the treated solution was discarded, and cells were cleansed with serum-free DMEM twice before Accutase® was added to detach the cells. Complete medium was used to stop the detachment. All solutions were stored together in a 15-mL conical tube. After each step, the cells were centrifuged (4°C, 1000 rpm, 3 min) to remove the solutions. The cells were rinsed once with 1x PBS and twice with a complete medium. An aliquot (100 µL) was taken to be mixed with Muse® Annexin V & a dead cell assay kit (Millipore, Billerica, MA, USA) at the ratio of 1:1. The mixture was gently made homogenous and incubated in the dark for

20 min. Muse® cell analyzer was acquired to analyze the cell suspension and reported as percentages of viable cells, apoptotic cells, and dead cells.

3.3.1.2.11 *In vitro* intracellular accumulation

The uptake of CDDP from the free drug solution and CDDP-loaded NPs in the HN22 cell was evaluated. The cell line was cultured in a 25-cm^2 cell culture flask (50,000 cells) and stored in an incubator controlling 95% air with 5% CO$_2$ at 37°C until 70% confluence. The test samples were prepared in FBS-free DMEM to a concentration equivalent to 50 μM. After the culture medium was removed, the sample solution (5 mL) was added and left in the incubator for 4, 8, and 24 h. At the determined time, the solutions were discharged and cells were cleansed with PBS (2 mL) twice. The HN22 cells were detached using Accutase® and centrifuge to collect the cell pellet. The cells were resuspended with sterile water, and the number of live cells was counted by an automated cell counter with trypan blue staining (TC20^{TM}, BIO-RAD, CA, USA). The collected cells were freeze-dried and digested with concentrated nitric acid to be analyzed using ICP-MS as the method mentioned in section 3.3.1.2.7. The amount of CDP in the HN22 cell was calculated using the following equation.

$$\text{Pt(II)/1000 cells} = \frac{\text{CDDP concentration}}{\text{Lived cell per mL}} \times 1000$$

3.3.2 Development of mucoadhesive NPs for localized delivery of doxorubicin

3.3.2.1 Synthesis of catechol-functionalized succinyl chitosan (SCScat) using succinylation and carbodiimide coupling reaction.

Catechol-functionalized succinyl chitosan (SCScat) was synthesized using two reactions which are succinylation and carbodiimide coupling reaction. Firstly, chitosan was grafted with the succinyl groups at the primary amine of the deacetylated glucosamine unit and the primary alcohols. Chitosan (8.28 mmoles) was dissolved in a solvent mixture of 1 %v/v acetic acid (50 mL), DMF (10 mL), and

DMSO (10 mL) contained in a round-bottomed flask. The system was vigorously stirred and connected to a reflux condenser, and heated to 100 °C. The environment was controlled with a nitrogen flush. Thereafter, succinic anhydride (44.97 moles) was introduced to the reaction and the reaction was continued for 24 h in an inert environment. The resulted succinyl chitosan (SCS) was dialyzed in deionized water for at least 3 days using a dialysis tube (molecular weight cut-off 3500 Da) and freeze-dried to collect the dried polymer. SCS was characterized for its molecular structure to confirm the successful synthesis. Catechol groups were decorated on the synthesized SCS using a carbodiimide reaction with dopamine HCl. The SCS polymer (1.0048 g) containing carboxylic acid groups was dissolved using 1 % v/v acetic acid (80 mL). Then, EDAC as the coupling agent and NHS as the catalyst was added at an amount equivalent to dopamine HCl by mole (5.15 moles). The mixture was stirred at ambient temperature for 2 h. In the end, dopamine HCl which was prepared in deionized water (20 mL) was gradually added to the SCS solution. The pH of the system was adjusted to 4.5–5.0. The reaction was continued for 18 h before the purification process via dialysis in PBS pH 4.5–5.0 for 4 cycles of 6 h and in acidic water (pH 5.0–6.0) for 12 h. SCScat was acquired after lyophilization.

3.3.2.2 Synthesis of catechol-functionalized hyaluronic acid using carbodiimide coupling reaction

Catechol-functionalized hyaluronic acid (HAcat) was synthesized by conjugating the catechol group from dopamine to the HA backbone. The ratio between HA and dopamine was varied from 1:1, 1:2, and 1:3 by weight to observe the alteration of the degree of substitution (DS). Briefly, HA (0.5 wt%) was prepared in a round-bottomed flask containing deionized water (100 mL). The coupling agent (EDAC) and catalyst (NHS) at a molar ratio equivalent to dopamine HCl were then added. The reaction was purged with nitrogen under constant stirring for 20 min. After that, dopamine HCl was accurately weighed and added to the HA solution. The reaction was controlled at the pH of 4.5–5.5 at an ambient temperature with nitrogen purge and light protection to prevent catechol oxidation for 18 h. The purification step was performed by dialysis in PBS with 1 mM HCl (pH 4.5–5.5). The dialysis medium

was changed every 6 h for 4 cycles. The last dialysis medium was changed to deionized water (pH 4. 5–5. 5) . The solution was lyophilized to collect the dried HAcat. Percentage yield of synthesis was then calculated.

3.3.2.3 Polymer characterizations
3.3.2.3.1 ^{1}H-NMR

The molecular structure of the synthesized polymers was investigated by ^{1}H-NMR spectroscopy following the method mentioned in section 3.3.1.2.1. The DS of the catechol groups on the HA chain was computed according to the following equation by the integration of the signals representing catechol moiety on the ^{1}H-NMR spectra in relation to protons of the acetamide methyl group in the HA structure.

$$DS = \frac{\text{Integration of catechol signals / no. of proton}}{\text{Integration of HA acetamide signal / no. of the proton}}$$

3.3.2.3.2   ATR-FTIR

The structural characteristics of the synthesized polymers were evaluated with an attenuated total reflection Fourier transform infrared spectroscopy (ATR FT-IR, Nicolet iS5, Thermo Fisher Scientific, MA, USA) equipped iD7 ATR accessory. The dried polymer was placed over the monolithic diamond crystal, and the pressure device was lowered to ensure results consistency. The spectra of wavenumber 400 to 4000 cm^{-1} were then recorded.

3.3.2.4 NPs preparation, drug loading, and evaluations
3.3.2.4.1   NPs preparation

Ionotropic gelation was performed to prepare the SCScat/HAcat mucoadhesive NPs. Roughly, SCScat solution was prepared in 1.5 % v/v acetic acid (20 mL) to the concentration of 0.025–0.050 % w/v. On the other hand, HAcat was solubilized in deionized water (20 mL) to the concentration of 0.025–0.050 % w/v. SCScat was continuously stirred using a magnetic stirrer, while HAcat was filled in a

glass syringe (diameter 11.50 cm) and fitted to a syringe pump (NE-1000 Programmable Single Syringe Pump, KF Technologies). The HAcat solution was gradually pumped at a fixed rate of 0.15 mL/min to the SCScat solution. A probe sonicator (Vibra cell^{TM} VCX134BP with 6 mm tip, Sonics, CT, USA) was used to reduce the particle size during the addition of HAcat to SCScat and 30 min after complete addition. The NPs preparation was optimized by varying the ratio of SCScat to HAcat with respect to the polymer weight to 1:1, 1:2, and 2:1. The mucoadhesive NPs were obtained after lyophilization.

3.3.2.4.2   Particle size, size distribution, zeta potential

The particle size, size distribution, and surface charge of the NPs were investigated as previously described in section 3.3.1.2.4.

3.3.2.4.3   Morphology

The morphology of the NPs was scrutinized under TEM as previously described in section 3.3.1.2.5.1.

3.3.2.4.5   *Ex vivo* mucoadhesion

The mucoadhesive properties of the prepared mucoadhesive NPs were examined using the flow-through method with fluorescence detection. The technique was used to determine the amount and time of mucoadhesive materials that remained on the mucosal membrane after being washed off. Porcine buccal mucosal membrane was freshly obtained from an abattoir in Nakhon Pathom, Thailand. The mucosa was stored in a 0.9% NaCl solution at 37 ^{o}C and used on the same day. Prior to the examination, the membrane was sliced and cut into 10×10 mm size and glued to a glass slide. A fluorescent compound was adsorbed into the mucoadhesive NPs along with dextran and unmodified NPs which were used as a negative and positive control, respectively. The adsorption was performed by mixing each sample (1 mg) with fluorescein sodium (0.5 mg) solution in deionized water (1 mL) overnight using

a microcentrifuge tube rotator. The image of the blank mucous membrane was captured as a background using a stereomicroscope (Leica M60, Wetzlar, Germany) equipped with a fluorescence detector, and the green fluorescence intensity (GFI) was quantified with the LAS X software version 3.6. All the camera and image settings were fixed throughout the examination with the magnifying power controlled at 10×. The fluorescent samples were pipetted (20 µL) on the porcine buccal membrane and washed at a rate of 1 mL/min with artificial saliva fluid (8 g NaCl, 2.38 g Na_2HPO_4, and 0.19 g KH_2PO_4 in 1 L of deionized water with pH adjusted to 6.8 with *ortho*-phosphoric acid). At each defined timepoint (0, 5, 10, 20, 30, 40, 50, 60 min), the washing was paused and the membranes were taken out for imaging and detection of GFI. The percentage of the sample that remained on the membrane was computed according to the following equation. Apart from that, the Wash Out$_{50}$ (WO$_{50}$) values of each remaining profile was calculated as a comparable representation value of the mucoadhesive properties. The WO$_{50}$ was calculated by extrapolating the exponential and linear regression of the experimented sample remaining profiles.

$$\%\text{Remaining} = \frac{\text{GFI}_{\text{time}} - \text{GFI}_{\text{blank}}}{\text{GFI}_0 - \text{GFI}_{\text{blank}}} \times 100$$

3.3.2.4.6　Drug loading

Adsorption method was conducted for loading of DOX into NPs. The NPs (10 mg) and DOX were weighted at different weight ratios and dispersed in ultrapure water (10 mL). The mixture was shaken overnight with a tube rotator. The excess drug was then removed by centrifugation for 5 min at 14,000 rpm. The supernatant was taken out and the precipitate was rapidly washed twice with ultrapure water. The drug-loaded NPs were collected after lyophilization.

3.3.2.4.7　Drug content determination

The content of DOX was quantified by dispersing the NPs (1 mg) in ultrapure water (1 mL). The drug was separated from the NPs by agitation

using a vortex mixer and the addition of 2% HCl to break the NPs. A microplate fluorometer (Fluoskan Ascent™, Thermo Scientific, MA, USA) with $\lambda_{ex} = 485$ and $\lambda_{em} = 538$ nm was acquired in the determination of the DOX content. The drug loading capacity (LC) and % loading efficiency (% LE) were calculated using the equations described in section 3.3.1.2.7.

3.3.2.4.8 Drug release

The drug release characteristics of DOX from DOX solution and the DOX-loaded NPs (DOX-NPs) were investigated using dialysis method. Artificial saliva fluid was employed as the release medium. Each sample was weighed to contain an amount equal to 1 mg of DOX and dispersed in the artificial saliva (1 mL). The samples were then transferred to the dialysis membrane (molecular weight cut-off 6000–8000 Da) and immersed in the release medium (15 mL). The system was shaken at a rate of 25 rpm and the environment was controlled at 37 ± 0.5 °C. At the specified time, the artificial saliva (1 mL) was collected with the same volume of fresh release medium replaced. The release of DOX at each time period was determined by a microplate fluorometer with the set parameters mentioned in section 3.3.2.4.7.

3.3.2.4.9 *In vitro* biocompatibility and cytotoxicity using MTT assay

In vitro biocompatibility and cytotoxicity studies were performed using MTT assay as previously mentioned in section 3.3.1.2.9. The tested concentrations of the blank NPs were ranged between 0.1–2500 µg/mL, while the DOX-NPs were prepared at drug concentrations of 0.5–200 µg/mL.

3.3.2.4.10 *In vitro* cellular uptake

The ability of DOX-NPs to be taken up by the HN22 cell line compared with free DOX solution was evaluated by the flow cytometry analysis.

Precisely, the HN22 cells cultured in a complete DMEM were seeded in a 24-well plate to contain 50,000 cells/ well and incubated (95% air, 5% CO_2, 37° C) until confluence. The sample solutions (equivalent to 3 µM of DOX, 1.5 mL) were prepared in the culture medium without serum and treated with the cells for 4, 8, and 24 h in an incubator. After each time period, the sample solutions were removed and cells were cleansed with 1× PBS and trypsinized with 0.25% trypsin-EDTA. The cell suspensions were gently mixed to homogeneous and instantly fixed using 4% formaldehyde. The prepared cell suspension was kept at 4°C until the investigation. A flow cytometer (BD FACS Canto^{TM}, BD Bioscience, CA, USA) was used to determine the mean fluorescent intensity (MFI) of DOX in each cell for 10,000 events.

3.3.2.4.11 Cell death mechanism

The cell death pathway of HN22 cells after being treated with DOX-NPs compared to the free drug was observed using a double staining method and scrutinized under an inverted microscope with fluorescence detection. In a 96-well plate, the cancer cell line was cultivated and seeded to 10,000 cells/ well and incubated to the confluence at a controlled environment. The formulated samples (DOX-NPs and free DOX equivalent to 3 µM of DOX) were then added to the cells before additional 24-h incubation. The cells were then stained with 10 μg/ mL of Hoechst 33342 (10 µL) and 0.5 μM of SYTOX^{TM} green nucleic acid stain (5 µL) for 15–30 min prior to the observation to distinguish the cell death mechanism under an inverted fluorescence microscope.

To further analyze the apoptotic induction of the DOX-NPs compared to free drug, the cell death mechanism by double staining assay was also evaluated using flow cytometry. The assay distinguishes the stages of cell death by the staining with the fluorescent compounds. Briefly, the HN22 cells cultured in a DMEM with serum were propagated in a 6-well plate at 100,000 cells/well density. The plates were placed in an incubator controlling 95% air, 5% CO_2, and 37 °C overnight. Then, the cells were treated with 3 μM of DOX from either free DOX solution or DOX-NPs dispersed in serum-free DMEM. The HN22 cells were further

incubated for 24 h. At the determined time, the sample solutions were collected and the cells were rinsed twice with DMEM without serum, trypsinized with 0.25% trypsin-EDTA, and washed with $1\times$ PBS (all solutions were collected in the same tube). After that, the test samples were prepared as follows: The DOX-NPs and DOX test solution was prepared by adding $1\times$ annexin binding buffer to rinse the cell pellets twice. After that, annexin binding buffer (500 µL) was added to the cell suspensions and kept in the dark for 15 min. A hundred microliter of the suspensions were then added with annexin V, Alexa Fluor^{TM} 647 conjugate (5 µL), and 0.5 µM SYTOX^{TM} green (5 µL), and incubated again in the dark for 15 min. Finally, the binding buffer (400 µL) was added to the sample and mixed before analysis with a flow cytometer.

3.3.3   Statistical analysis

The experiments were completed in triplicate and numerical data were reported as mean $\pm$ standard deviation (SD) . Statistics of analysis of variance (ANOVA), post-hoc, F-test, and independent t-test under the confidence interval of 95% were analyzed with Microsoft$^{®}$ Excel 2018; where $p < 0.05$, a significant difference is declared.
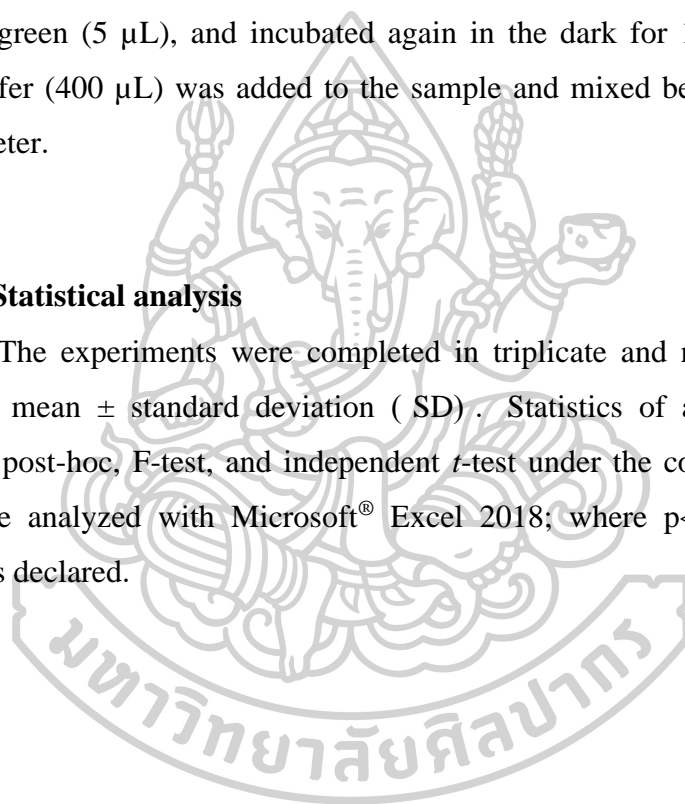
CHAPTER 4

RESULTS AND DISCUSSION

4.1 Development of coordination bond-forming NVP/AA NPs for CDDP delivery

    4.1.1   Synthesis of NVP/AA NPs

    4.1.2   Characterizations and evaluations

        4.1.2.1   COOH Content

        4.1.2.2   Particle size, size distribution, zeta potential and morphology

        4.1.2.3   Drug loading and drug content

        4.1.2.4   Drug release

        4.1.2.5   *In vitro* biocompatibility

        4.1.2.6   *In vitro* cytotoxicity and cell death mechanism

        4.1.2.7   *In vitro* intracellular accumulation

4.2 Development of mucoadhesive NPs for localized delivery of DOX

    4.2.1   Synthesis of catechol-functionalized hyaluronic acid (HAcat)

    4.2.2   NPs characterizations

        4.2.2.1   Particle size, size distribution, zeta potential, and morphology

        4.2.2.2   *Ex vivo* mucoadhesion

        4.2.2.3   Drug loading

        4.2.2.4   Drug release

        4.2.2.5   *In vitro* biocompatibility and cytotoxicity

        4.2.2.6   *In vitro* cellular uptake

        4.2.2.7   Cell death mechanism

4.1 Development of coordination bond-forming NVP/AA NPs for CDDP delivery

      4.1.1   Synthesis of NVP/AA NPs

              Method 1: Co-polymerization of hydrophilic monomers, NVP and AA was employed in the synthesis of M_1-NPs. The synthesis reaction is displayed in Figure 4.1a. The synthesis was performed at different weight ratios of NVP:AA (1:1, 1:3, and 1:5), and the %yields of each resulted NPs are shown in Table 4.1. It was found that the ratio which provided the highest yield was 1:3 which could be an optimal condition for the synthesis of M_1-NPs. Hence, the NVP:AA ratio of 1:3 was chosen for further investigation [201]. From the molecular analysis using ^{1}H-NMR, the spectra of the monomers and M_1-NPs in relative to the solvent (D$_2$O, δ = 4.80) are shown in Figure 4.2. The spectra showed that the signals at 5.95–6.37 ppm which belonged to the protons of the vinyl groups from the AA monomers (Figure 4.2a) and the peaks at 4.62–4.67 and 6.93 ppm of NVP vinyl groups (Figure 4.2b) disappeared in the spectrum of the NPs (Figure 4.2c) representing complete polymerization of the NVP and AA. The synthesized NPs presented multiple signals ranging between 1.36–2.74 ppm region. The protons of NVP rings are witnessed with multiplet, triplet, and triplet signals at 2.11, 2.54, and 3.60 ppm, respectively which were shifted to the upfield region due to the shielding effect of the structure of the NPs after the polymerization. The signal at 4.93 ppm is referred to the protons located on the polymer chain where the pyrrolidone ring is presented. Moreover, the structure of the synthesized M_1-NPs was confirmed with FT-IR spectroscopy and the spectrum is illustrated in Figure 4.3. The asymmetric C–H stretching of the polymerized chain is displayed at 2958 cm^{-1}. From the NVP structure, the cyclic amide (O=C–N) bands and C–N bonds are shown at 1654 and 1115 cm^{-1}, respectively. The AA incorporated in the NPs is represented by the peaks of C=O stretching (strong) at 1720 cm^{-1}, O–H stretching (broad) at 3385 cm^{-1}; moreover, the bands of C–O stretching, carboxylate group (COO-), and O–H out of plane bending are shown at 1174, 1449, and 647 cm^{-1}, respectively. The presence of the acrylamide crosslinker is confirmed by a significant peak of secondary amine at 1541 cm^{-1}. So, the findings assured the complete synthesis of the M_1-NPs.
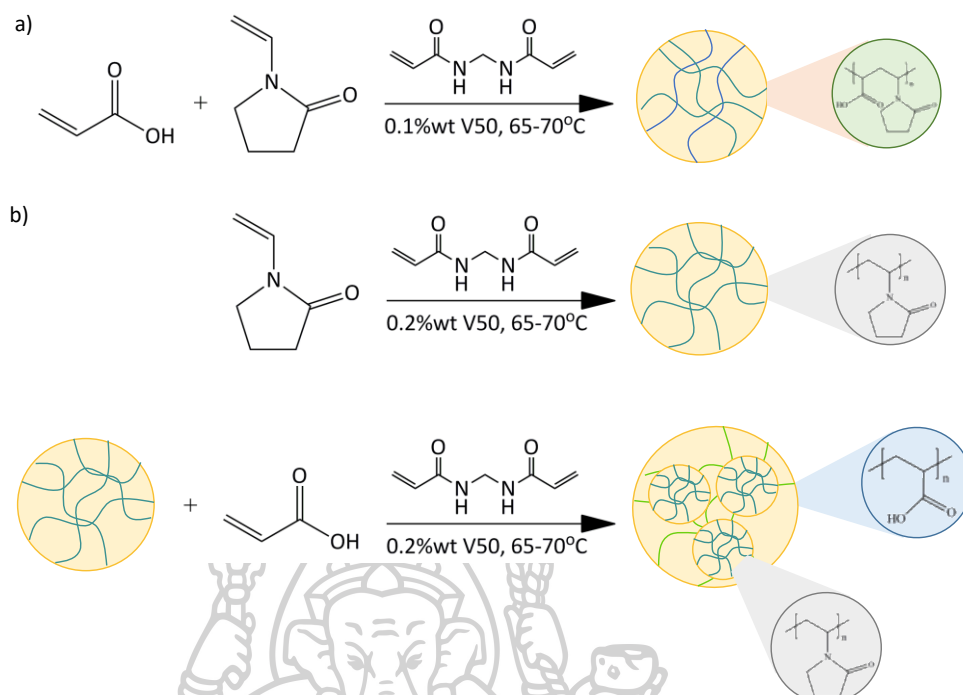
Figure 22 Synthesis scheme of NVP/AA NPs a) M_1-NPs and b) M_2-NPs.

Method 2: **The M_2-NPs made of NVP and AA were synthesized using** two polymerization steps as displayed in the synthesis scheme disclosed in Figure 4.1b. The core-shell particles were created by synthesizing the core PVP NPs and further polymerized with AA as the coating shell. MBA crosslinker was employed in both synthesis reactions to form the network structure. The synthesized M_2-NPs was characterized for the molecular attributes using ^{1}H-NMR and FT-IR spectroscopy. The ^{1}H-NMR spectrum of the M_2-NPs is displayed in Figure 4.2d. The spectrum of the NPs confirmed the polymerization of the NVP and AA as it can be seen by the disappearance of the splitting pattern of the vinyl groups. Besides, the multiplets of the polymerized backbone are presented at 1.77–2.76 ppm. From the shielding effect of the complex network, the pyrrolidone protons were shifted to the upfield region of the spectrum. Also, the functional characteristics analyzed with FT-IR spectroscopy presented the spectrum related to the structure of M_1-NPs (Figure 4.3d) with similar bands observed. Yet, the bands of the pyrrolidone ring were found to have lower sensitivity compared to the bands of the AA functional group. The sharp peak of the hydrogen bond at 3448 cm^{-1} and lower intensity of the band at 1720

cm^{-1} represented the 5-membered cyclic amide bond. Finally, the secondary amine bending of the crosslinker can also be found at the wavenumber of 1541 cm^{-1}.
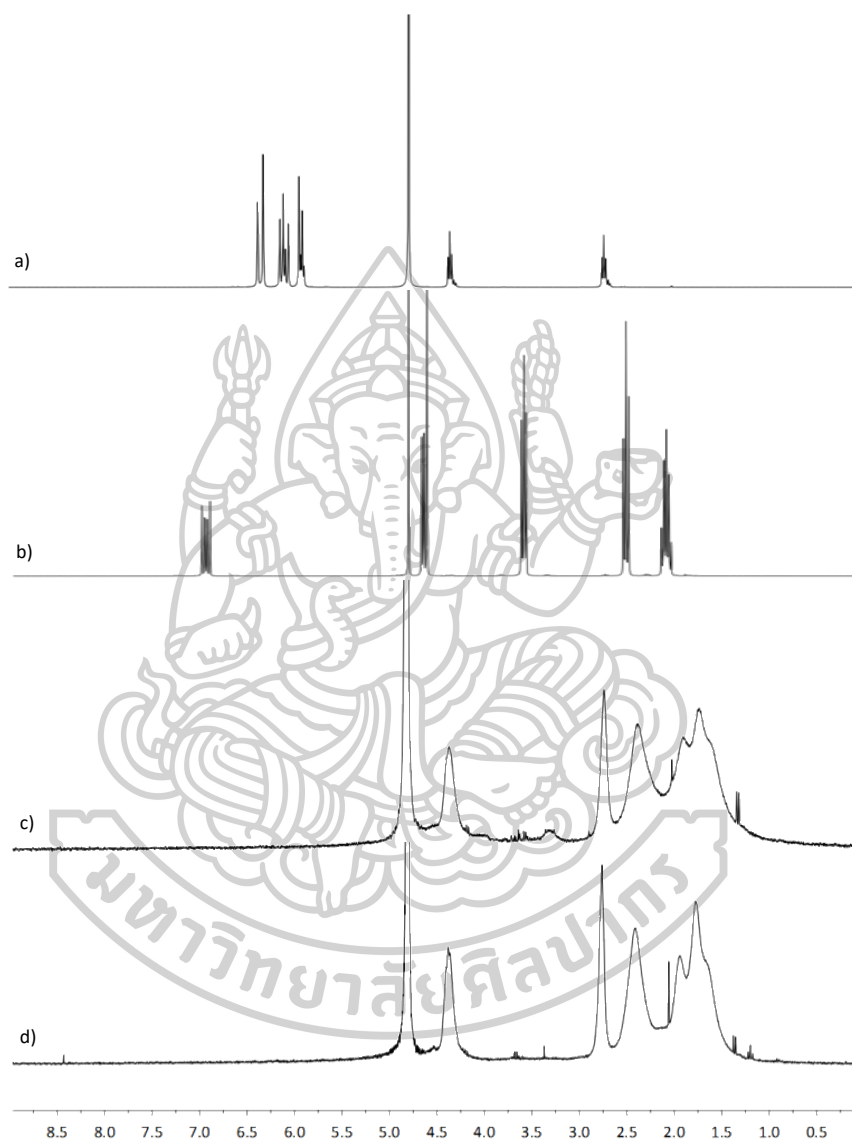
Figure 23 ^{1}H-spectra of a*)* AA, b*)* NVP, c*)* the synthesized M$_1$-NPs, and d*)* the synthesized M$_2$-NPs.
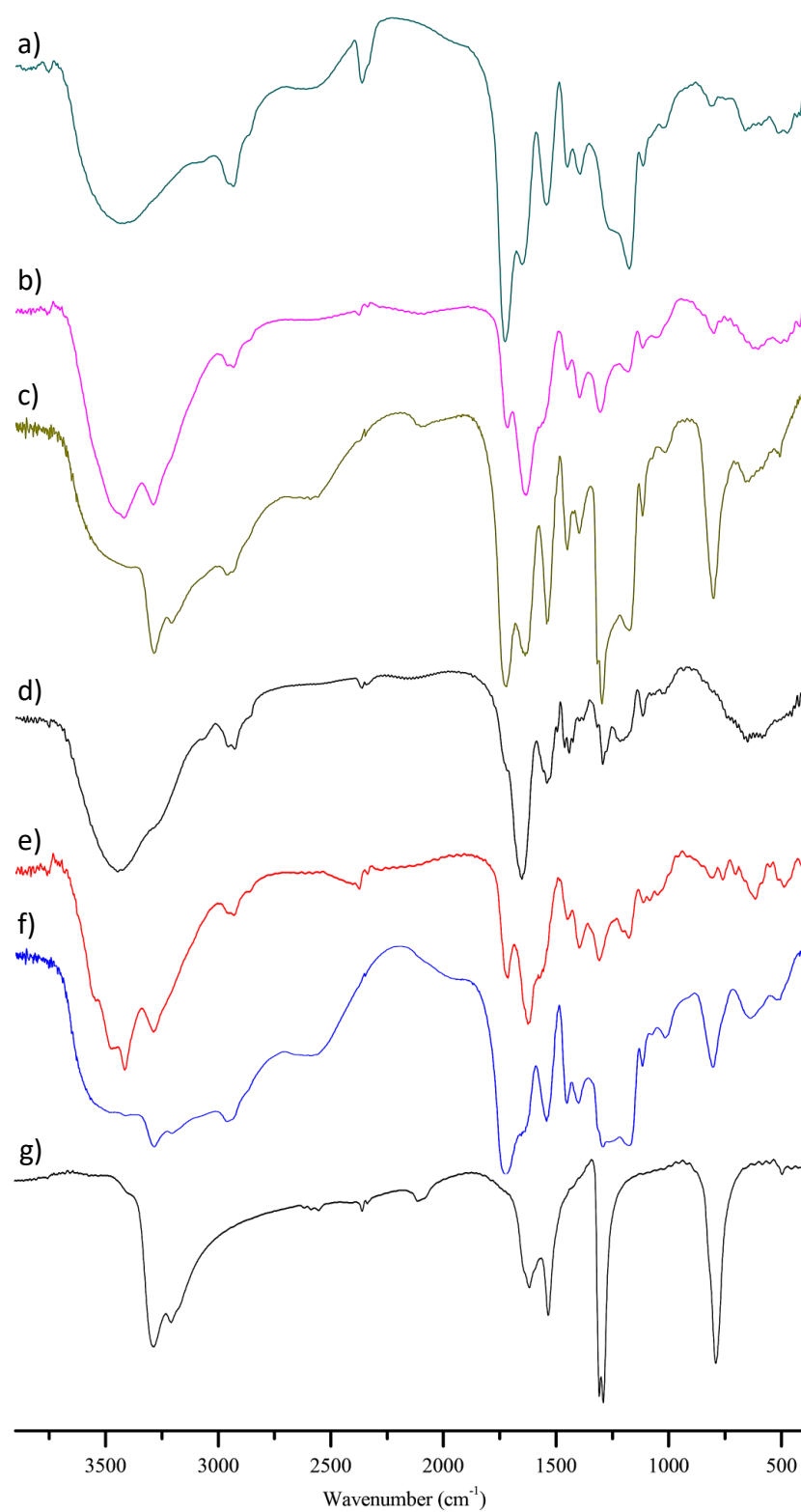
Figure 24 FT-IR spectra of a) M_1-NPs, b) CDDP-bounded M_1-NPs, c) Physical mixture of CDDP and M_1-NPs, d) M_2-NPs, e) CDDP-bounded M_2-NPs, f) Physical Mixture of CDDP and M_2-NPs, and g) Free CDDP.

4.1.2 Characterizations and evaluations

4.1.2.1 COOH Content

The amount of carboxylic group presented on the NPs is shown in Table 4.1. It was noted that the M_1-NPs with the ratio of NVP:AA of 1:3 showed the highest content of carboxylic groups than at other ratios ($p < 0.05$). The result showed that at this synthesis condition, AA could suitably be incorporated into the NPs. Furthermore, the carboxylic acid group content on the M_2-NPs was similar to that of the M_1-NPs at the optimal ratio. A great amount of the COOH group on the NPs is favorable for the coordination bond formation with CDDP.

Table 3 Physical properties of the synthesized NPs

Formulation (NVP:AA ratio)	Blank NPs					CDDP-loaded NPs		
	% yield	Particle size (nm)	PDI	Zeta potential (mV)	COOH content (mmol/g)	Particle size (nm)	PDI	Zeta potential (mV)
M_1-NPs (1:1)	24.0	173.6±18.4	0.4±0.0	-8.5±0.2	4.3±0.6	-	-	-
M_1-NPs (1:3)	42.3	155.7±4.1	0.3±0.1	-19.5±0.2	7.3±0.4	212.4±9.6	0.4±0.1	-7.4±0.2
M_1-NPs (1:5)	28.7	183.7±2.4	0.2±0.0	-2.7±0.2	5.1±0.2	-	-	-
M_2-NPs (1:10)	39.0	136.2±4.3	0.4±0.0	-26.3±0.6	7.7±0.2	177.8±10.1	0.3±0.0	-7.6±0.0

4.1.2.2 Particle size, size distribution, zeta potential and morphology

The analysis of particle size and ζ-potential of the synthesized NPs was performed using dynamic light scattering (DLS) technique. Also, the morphology was observed using SEM and TEM. The results are presented in Table 4.2 and Figure 4.4. The synthesis method provided particles with hydrodynamic size ranged in the nanoscale for all ratios of NVP:AA for M_1-NPs. The particle sizes were not correlated to the ratio of NVP:AA as the sizes obtained from the same synthesis method were not significantly different ($p > 0.05$). On the contrary, the particles synthesized with different synthetic routes presented significantly smaller sizes. The M_2-NPs sizes were somewhat less than the size of M_1-NPs, but the polydispersity indexes (PDI) of the M_2-NPs were larger. The greater size

distribution of M_2-NPs may be resulted from the high surface area and the hydrophilic nature of the component that caused partial aggregation even though sonication and stirring processes have been performed before the size measurement [202]. After the drug loading, the particle size was found to increase compared with the blank NPs which may be resulted from the coordination bond formed between CDDP and the carboxylic groups on the NPs. The finding is correlated with a study from Raj et. al which described that after CDDP was loaded onto a Cassava starch acetate–PEG/gelatin nanocomposites by coordination bond, the particle sizes of the particles increased [203]. Moreover, the findings complied with the micrographs from the TEM and SEM investigations which showed that the synthesized particles were in the nanoscale and had a relatively spherical shape. Nevertheless, the aggregation of the NPs can still be observed under the microscope which could be the reason for the high PDI value. According to the ζ-potential analysis, the negative surface charge was shown for all particles which was due to the carboxylic acid group of AA presented on the NPs. Interestingly, the M_2-NPs presented a greater value of ζ-potential than the M_1-NPs. This may be because the M_2-NPs structure presented the carboxylic acid functional group at the outer surface as the shell of the NPs; whereas, some of the AA in the M_1-NPs were incorporated within the network. Adding more AA to the synthesis may not be appropriate since the reaction with the NVP:AA ratio of 1:5 to showed less negative surface charge. Considering the % yield, the particle size, ζ-potential, and the carboxylic acid group content, it can be concluded that the M_1-NPs with the ratio of NVP: AA of 1: 3 and the M_2-NPs were suitable for further examinations. To further examine the stability of the NPs in a different media, the particle size, PDI, and ζ-potential were tested in a different media (PBS, cell culture medium with and without serum) after 14-day storage. According to the investigations, Table 4.2 shows that both M_1-NPs and M_2-NPs were found to be appropriately stable in all medium tested. The result showed that the size, PDI, and ζ-potential barely changes but are in the characters that are suitable for tumor passive targeting delivery [204]. Hence, the alterations of the particle size and ζ-potential found could be due to the medium properties in term of viscosity, ionic status, and charged ions contained in the medium.

Table 4 Particle size of NVP/AA NPs in various media over time

Formulation	Medium	Day 0			Day 14		
		Particle size (nm)	PDI	Zeta potential (mV)	Particle size (nm)	PDI	Zeta potential (mV)
M_1-NPs	PBS	152.2 ± 1.7	0.4 ± 0.0	-25.2 ± 3.3	130.4 ± 7.4	0.3 ± 0.0	-15.1 ± 0.7
	DMEM (without serum)	127.5 ± 0.6	0.3 ± 0.0	-21.3 ± 1.2	122.8 ± 1.1	0.2 ± 0.0	-21.0 ± 0.9
	DMEM (with serum)	115.2 ± 1.1	0.5 ± 0.0	-20.3 ± 0.5	120.7 ± 0.8	0.4 ± 0.0	-17.2 ± 1.2
M_2-NPs	PBS	168.8 ± 15.3	0.2 ± 0.0	-17.3 ± 0.2	131.9 ± 6.6	0.2 ± 0.0	-11.1 ± 0.6
	DMEM (without serum)	130.6 ± 7.6	0.2 ± 0.0	-11.3 ± 0.9	204.2 ± 11.0	0.3 ± 0.0	-21.3 ± 1.2
	DMEM (with serum)	146.8 ± 19.6	0.2 ± 0.0	-18.4 ± 0.6	147.4 ± 4.1	0.2 ± 0.0	-12.1 ± 0.9
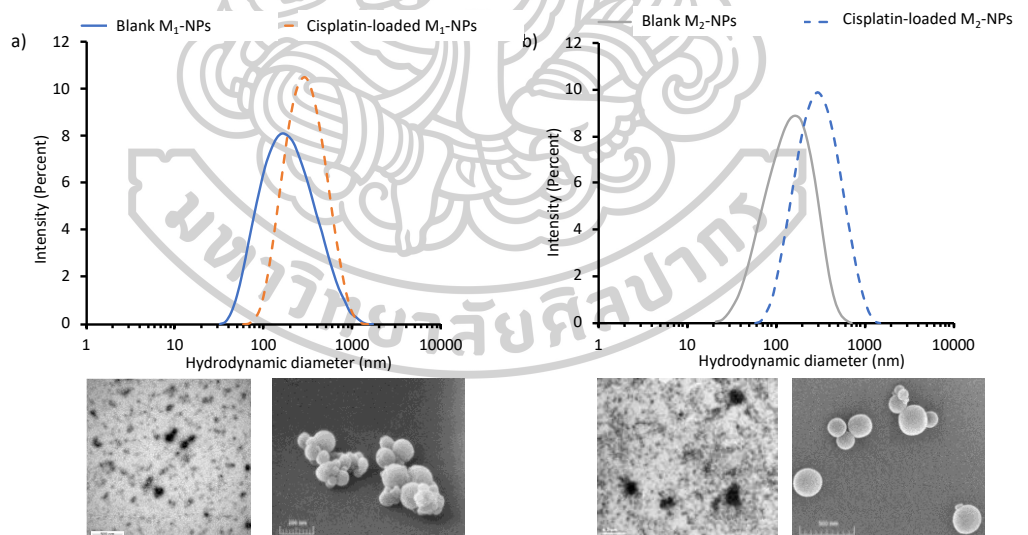
Figure 25 Size distribution and morphology observed under TEM (left) and SEM (right) of a) M_1-NPs and b) M_2-NPs.

4.1.2.3 Drug loading and drug content

CDDP was incorporated into the synthesized NPs through coordination bond via adsorption method. The platinum atom in the CDDP molecule coordinately binds to the carboxylic acid group on the NPs. At different ratio of CDDP to NPs, the resulted LC and %LE are shown in Table 4.3. It can be observed that the %LE was the highest at the NPs: CDDP ratio of 1:5 for both M_1-NPs and M_2-NPs. Thus, adding more CDDP to the system did not bring about a significant difference in %LE ($p > 0.05$). In contrast, once a greater amount of CDDP was added to the NPs, the LC significantly increased. The NPs:CDDP ratio that provided the highest LC was 1:10. The LC results were correlated to the carboxylic acid content on the NPs in which the amount of COOH contained in the NPs was roughly twice the LC value. This is due to the stoichiometry of the coordinate covalent bond of COOH:Pt is 2:1. All in all, the NPs:CDDP ratio of 1:10 was chosen for further investigations.

Table 5 %Loading efficiency and loading capacity of the synthesized NPs

NPs	Loading parameter	Ratio of NPs:CDDP			
		1:1	1:2.5	1:5	1:10
M_1-NPs	%LE	6.0 ± 1.5	9.0 ± 0.6	11.9 ± 0.6	11.7 ± 0.5
	LC (mmol/g)	2.1 ± 0.2	2.9 ± 0.2	3.1 ± 0.5	3.8 ± 0.1
M_2-NPs	%LE	6.1 ± 1.3	8.7 ± 1.2	17.6 ± 1.7	17.9 ± 0.9
	LC (mmol/g)	2.4 ± 0.1	2.8 ± 0.3	2.9 ± 0.3	3.9 ± 0.6

The drug loading into the NPs via coordinate covalent bond was confirmed by FT-IR. The CDDP-loaded M_1-NPs spectrum is pictured in Figure 4.3b. The finding assured the drug incorporation through a chemical aspect of coordination bond. The spectrum showed the bands that represent the CDDP loaded on the NPs including primary amine stretching (strong) at 3288 cm^{-1}, N–H bending at 1632 cm^{-1}, and N–H out of plane bending at 799 cm^{-1}. These representations are in accordance with the vibrations free CDDP as shown in Figure 4.3g; whereas, they cannot be found in the spectrum of the blank NPs (Figure 4.3a). CDDP was found to be successfully adsorbed into the NPs through a coordinate covalent bond as proven

by the FT-IR spectrum. The coordinate covalent bond created among the carboxylic acid group and the Pt atom of CDDP was illustrated by the significant band of the O–H stretching at 3419 cm^{-1}, the lowering of the carboxylate stretching intensity at 1451 cm^{-1}, and the presence of new metal complex vibration at 603 cm^{-1}. Thus, these presentations were not observed in the physical mixture of blank NPs and CDDP (Figure 4.3c). The described phenomena were similarly seen in the M_2-NPs spectra in Figure 4.3d-f. Considering the FT-IR spectra, the chemical interaction of coordination bond has the responsibility on CDDP loading into the synthesized NPs.

4.1.2.4 Drug release

The CDDP release from the synthesized NPs was investigated by the dialysis approach. It was found that the CDDP release was extended over 7 days as presented in Figure 4.5. At pH 7.4, representing the plasma environment, CDDP was released from both NPs for about 25% of the loaded drug in the initial period before being gradually released up to approximately 61% on day 7. The slow-release rate observed could be resulted from the strong interaction of coordinate covalent bond created among the platinum atoms of CDDP molecules and the carboxylic acid bearing on the synthesized NPs. The presence of chloride ions in the release medium has an effect on the CDDP release behavior. Notably, the acidic tumor environment was reported to have a significant role in diminishing the coordination bond between the platinum atom and the COOH of the NPs [12, 13, 205]. According to the previous reports, the drug loading mechanism and release profile could be beneficial for passive targeting delivery of the drug to the cancer cells. By that, the release of CDDP was also evaluated in an acidic release medium with pH of 5.0 and 6.5 to study the delivery potential at the tumor microenvironment. A significance increase in CDDP release was found at a lower pH since the coordination bond was weaken when the carboxylic acid was unionized. Around 80% of CDDP from both NPs was released on day 7 at the pH of 5.0. On the other hand, the CDDP release from M_2-NPs in the medium pH 5.0 was higher which was about 80% on day 7. The difference occurred in CDDP release from M_2-NPs at pH 6.5 may be due to the positioning of the drug incorporated in the NPs. The M_1-NPs retarded

the release of CDDP by the swelling of the hydrophilic components. On the contrary, CDDP was coated at the outer surface of the M_2-NPs which made the drug easily released from the NPs after breaking of the coordination bond. Overall, the findings indicated that the CDDP-loaded NPs could be advantageous for a prolonged delivery of CDDP with a passive targeting strategy.
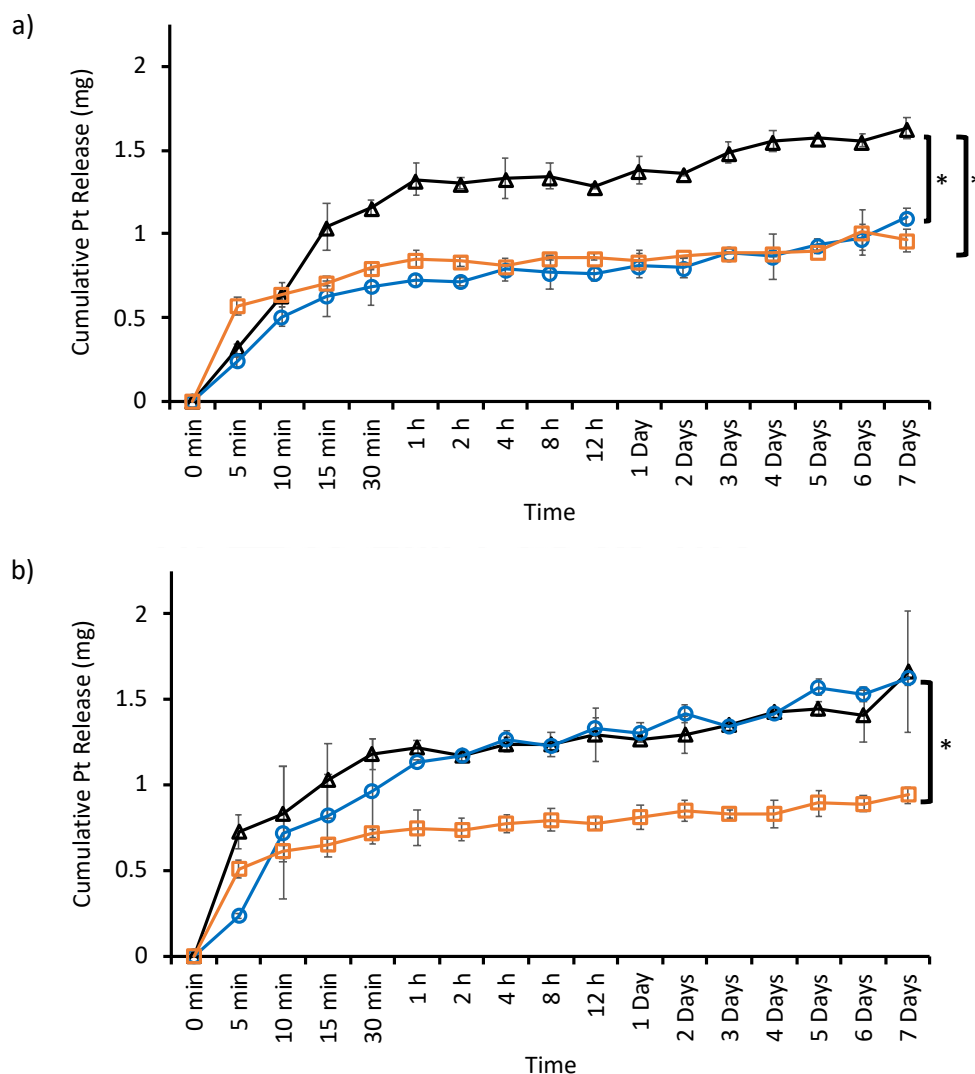
Figure 26 The release profile of CDDP from the a) M_1-NPs and b) M_2-NPs at ($\triangle$) pH 5.0, ($\bigcirc$) pH 6.5, and ($\square$) pH 7.4. *Statistically significant difference of accumulative drug release on day 7 ($p < 0.05$)

4.1.2.5 *In vitro* biocompatibility

The biocompatibility of the synthesized NPs was investigated on the HGF cells by the *in vitro* MTT assay. The percentage of relative cell viability is illustrated in Figure 4.6. The results presented that after a 24-h treatment with the synthesized NPs at a broad range of concentrations (0.01–5000 µg/mL), more than 80% of the normal HGF cells were still alive. This indicates that the blank NPs were non-toxic to the normal fibroblast cells at all the tested concentrations. Actually, the application of monomers used in the NPs synthesis was widely studied in different drug delivery systems and their safety has been previously reported [201, 206].
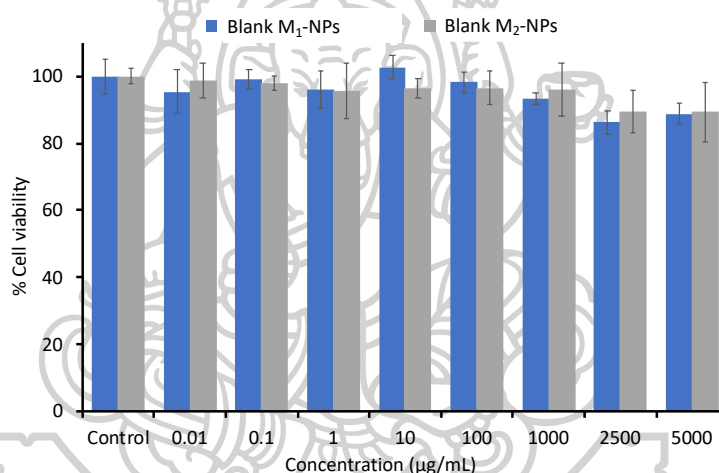
Figure 27 Percentage cell viability of HGF cells after being treated with the blank M1-NPs and M2-NPs.

4.1.2.6 *In vitro* cytotoxicity and cell death mechanism

The cytotoxic effect of the blank NPs, free CDDP, and CDDP-loaded NPs to the oral cancer cell (HN22) was examined using MTT assays. The samples were prepared in different concentrations and used to treat the HN22 cells for 24 h. The anticancer effect of each formulation is presented in Figure 4.7 and 4.8. The result showed that the blank M1-NPs and M2-NPs had no killing potential to the HN22 with at least 80% relative viable cells in every concentration tested. On the other hand, the CDDP-loaded NPs synthesized from the two methods showed a potent

HN22 killing effect with the IC50 values of 23.48 and 22.46 μg/mL for M_1-NPs and M_2-NPs, respectively. The results showed higher IC50 values compared to the free CDDP (11.77 μg/mL) because CDDP from the NPs was slowly released from the drug carrier and later performs its anticancer effect. Moreover, the cytotoxicity of the formulated CDDP-loaded NPs and free CDDP on the normal HGF cells was studied. As presented in Figure 4.9, free CDDP and CDDP-loaded NPs displayed similar cytotoxic effects with extensive cell viability reduction after the concentration was increased to over 50 μg/mL. The cytotoxic effect of free CDDP and CDDP-loaded NPs on HGF cells was lower than to the HN22 cells which could be because the proliferation rate of the normal cells is lower than the oral cancer cells [207].
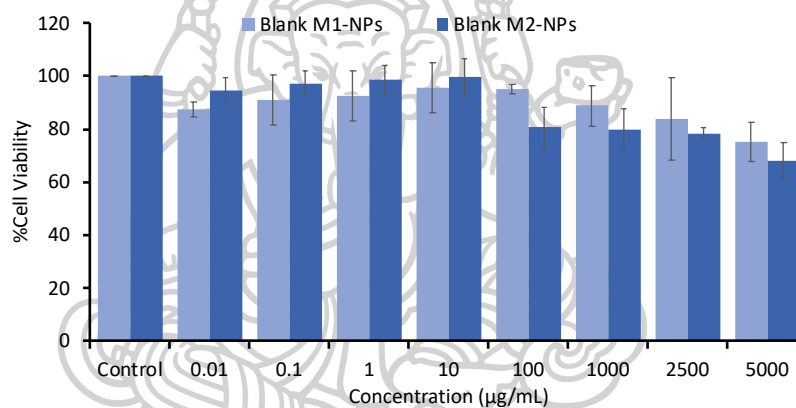
Figure 28 Percentage cell viability of HN22 cells after being treated with the blank M_1-NPs and M_2-NPs.
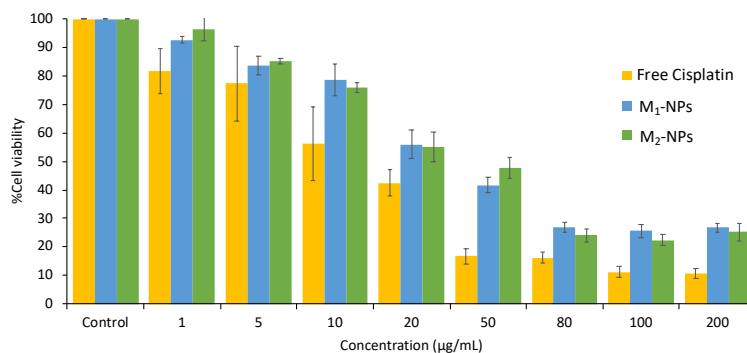
Figure 29 Cytotoxicity of free CDDP and CDDP-loaded NPs on HN22 cells.
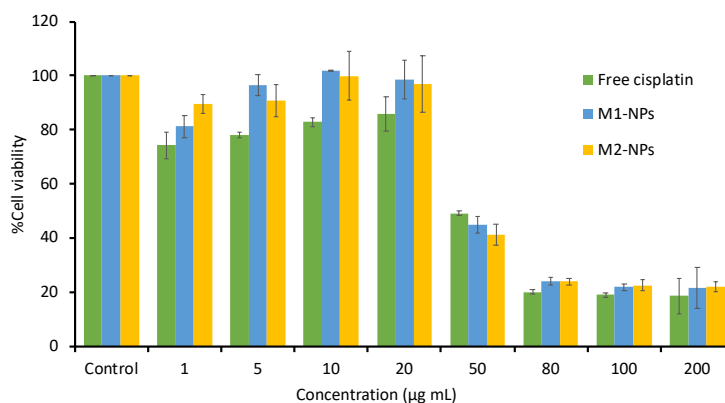
Figure 30 Cytotoxicity of free CDDP and CDDP-loaded NPs on HGF cells**.**

                    In vitro cell death mechanism of the formulated samples was evaluated using flow cytometry analysis. The results are displayed in Figure 4.10. Each quadrant represents a different cell death stage according to the fluorescent stains. The bottom-left quadrant indicates the live cells, the top-left quadrant refers to the dead cells, while the bottom-right and top-right quadrants belong to the early and late apoptosis death, respectively. The axes were slightly adjusted to correspond to the death of control experiments [208]. From the apoptotic induction analysis, free CDDP was found to mostly cause late apoptotic death (46.88%), followed by early apoptosis (16.36%). The result correlates to the death that occurred from the CDDP-loaded NPs that the majority of cell death was found in the late apoptosis stage. Above all, the cell death caused by the CDDP-loaded NPs showed lower late apoptotic death but higher in the early apoptosis pathway. Cell death pathway through early apoptosis programming was desirable since the cell membrane integrity was still maintained as the apoptotic bodies were created. In contrast, the late apoptotic death loses the integrity of the membrane leading to immunostimulatory molecule leakage and further causes inflammations subsequent to cell death [209, 210].
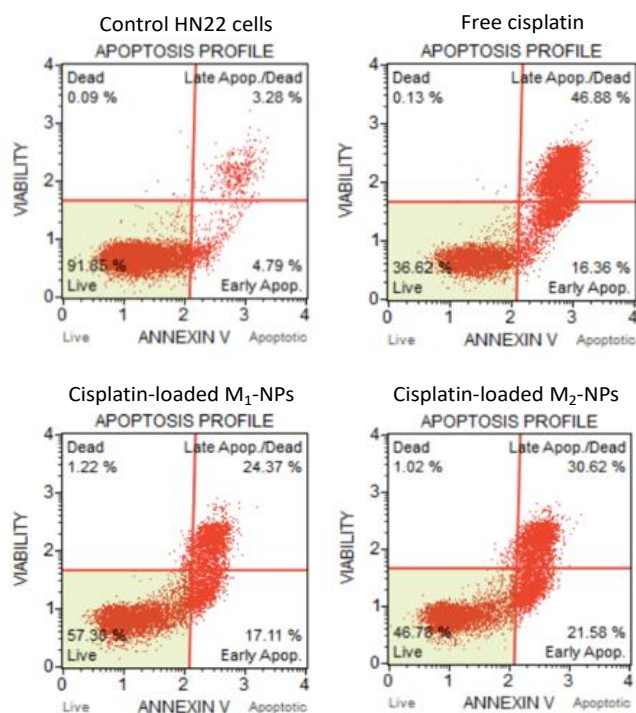
Figure 31 Apoptosis profile of control HN22 cells, free CDDP, and CDDP-bounded NPs

The cell death analysis was also performed using double staining technique and observed under an inverted microscope with fluorescence detection. Hoechst 33342 which is the membrane-permeable fluorescence dye was used to stain the nucleus. Hoechst 33342 permeates the cell membrane and presents a blue color. In addition to the non-apoptotic cells, the apoptosis mechanism processes nuclear condensation which can be detected with the significant bright blue color. On the other hand, PI which is a non-membrane permeable fluorescence dye intercalates the DNA base pair and illuminate the fluorescent red color at the nuclei of the cells that lost their membrane integrity [211]. The results are presented in Table 4.4. It can be observed that both apoptosis and necrosis cell death can be found in the cells that were treated with free CDDP and CDDP-loaded NPs. Nonetheless, necrosis death was not as dominant in that cells treated with CDDP-loaded NPs compared to the free CDDP. This is in accordance with the result from flow cytometry analysis. Therefore, the formulated CDDP-loaded

NPs could lead to a better anticancer effect in terms of cell death mechanism which induced less late apoptosis leading to lower inflammatory cell death while providing efficient anticancer effects.

Table 6 Fluorescence images (100×) of Hoechst 33342 and PI stained HN22 cells treated with free CDDP and CDDP-loaded NPs

	Hoechst 33342	Propidium Iodide	Overlay
Control			
Free CDDP			
CDDP-loaded M$_1$-NPs			
CDDP-loaded M$_2$-NPs			
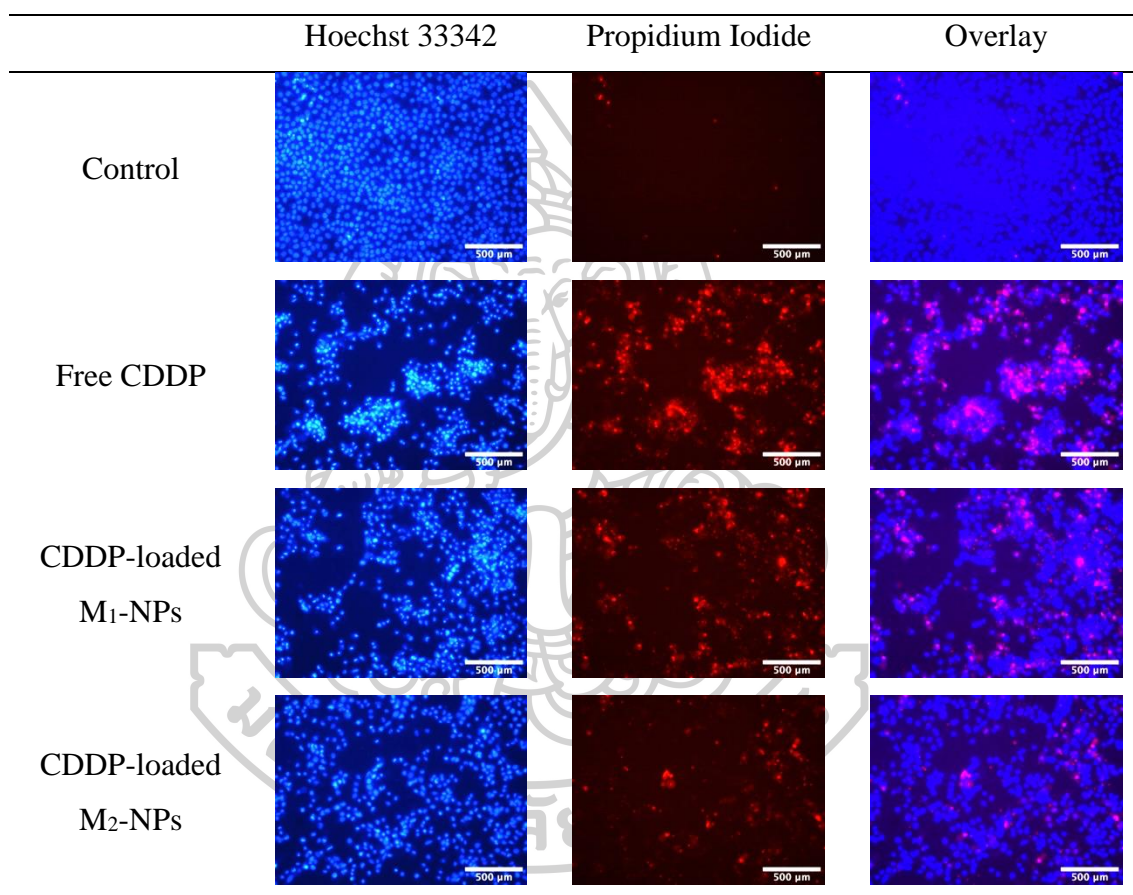
4.1.2.7 *In vitro* intracellular accumulation

The cellular uptake of CDDP-loaded NPs into the cancer cells compared to the free CDDP was evaluated by the determination of intracellular CDDP. The amount of CDDP in the treated cells at different treatment time determined the ability of the formulation to be accumulated in the cells. The higher amount of CDDP found in the cells specified the permeation and accumulation of the drug in the live cells; whereas, the lower value indicated rapid cell death after cellular inclusion or the drug did not permeate into the cells. The results disclosed that

the CDDP-loaded NPs could accumulate inside the cancer cells prior to a gradual release the drug to exhibit the cytotoxic effect at 24 h as presented in Figure 4.11. Besides, the platinum atom was found at a significantly lower extent in the cells treated with free CDDP compared to the CDDP-loaded NPs ($p < 0.05$). This may be due to the sudden death of the cancer cells after the taken up of CDDP or else the free drug was taken up at a lower amount than the NPs formulation. Nevertheless, the intracellular accumulation at 24 h did not show a significant difference ($p > 0.05$) which indicated the occurrence of CDDP killing effect for both free CDDP and CDDP-loaded NPs. In addition, the CDDP-loaded M_1-NPs were accumulated inside the cancer cells more than the M_2-NPs at the earlier time points. It is suggested that the aggregation of the M_2-NPs which showed a higher PDI value. There are many pathways of cellular internalization; however, particle size is an important factor affecting cellular uptake. CDDP can be taken up by the cells through passive diffusion mechanism, but limited due to the polar molecule. On the other hand, the cellular uptake of drug-loaded polymeric NPs was commonly found to be facilitated by endocytosis pathway which could enhance the entry of the polar drug through the lipid cell membrane [212, 213]. Researches had reported that an optimal size range is required to be taken up by the cells. Large particles are inconvenient to be internalized into the cells compared to the smaller particles in the appropriate range [212, 214]. The larger extent of CDDP accumulated in the cell also confirmed that the CDDP-loaded NPs would show a slower anticancer effect while leading to a less inflammatory cell death.
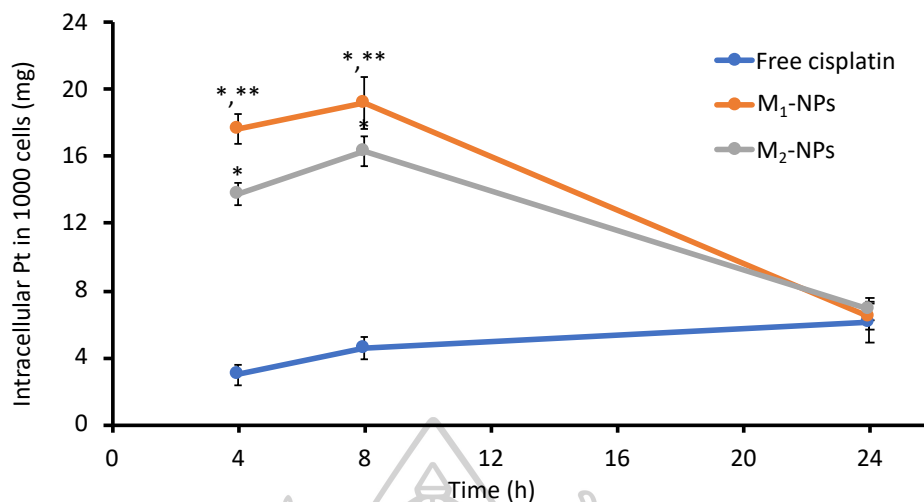
Figure 32 CDDP intracellular accumulation of free CDDP and CDDP-loaded NPs. *Statistically significant difference ($p < 0.05$) from free CDDP, **Statistically significant difference from M_2-NPs.

4.2 Development of mucoadhesive NPs for localized delivery of DOX

4.2.1 Synthesis of HAcat

HAcat was achieved after performing the carbodiimide coupling reaction as the synthesis scheme shown in Figure 4.12. The structure of the obtained polymer was verified by ^{1}H-NMR and ATR-FTIR. The ^{1}H-NMR spectra are presented in Figure 4.13a. The structure of the HA backbone displayed multiplet signals belonging to the pyranose-ring protons of the glycosaminoglycan core between 3.10–4.00 ppm. The protons of the acetamide methyl group at the side chain of *N*-acetyl glucosamine of HA are presented as a singlet peak at 2.03 ppm. Considering the spectrum of dopamine HCl, triplet representations at 3.26 and 2.88 ppm are attributed to the alpha and beta carbon atoms, respectively. Two doublet peaks located between 6.74 and 7.00 ppm were attributed to the catechol protons in the aromatic ring of dopamine structure. These peaks were not found in the HA spectrum but dominantly appeared in the spectrum of the synthesized HAcat at 3.24, 2.86, and 6.74–7.24 ppm. The other protons of the *N*-acetyl glucosamine and glucuronic acid core in the HAcat spectrum were in accordance with those presented in the HA spectrum indicating the successful synthesis of catechol grafted polymer.

The ATR-FTIR spectra of HA and HAcat are displayed in Figure 4.13b. From the spectrum of HA, the O–H stretching (broad), C–H asymmetric stretching, carboxylate (COO$^-$), and C–O–C stretching vibrations of the pyranose ring can be found at the wavenumber of 3273, 2886, 1406, and 1040 cm^{-1}, respectively. Also, the *N*-acetyl glucosamine amide bond (OC–NH) vibration was presented at 1618 cm^{-1}. The spectrum of HAcat correlates to the peak representations in the HA spectrum. In addition, the conjugation of catechol groups is shown by the inter-and intramolecular hydrogen bond presenting broader signals of O–H and N–H groups at 3273 cm^{-1} in the spectrum of HAcat compared to HA. Apart from that, the intensification of secondary amide bending at the wavenumber of 1562 cm^{-1} was also noticed after grafting of catechol moiety. The aromatic C–H stretching of the catechol group was found at about 3000 cm^{-1} with a broad band at 1650 cm^{-1} indicating the existence of aromatic C=C interaction. By that, the structure of HAcat was confirmed by these spectral characteristics.
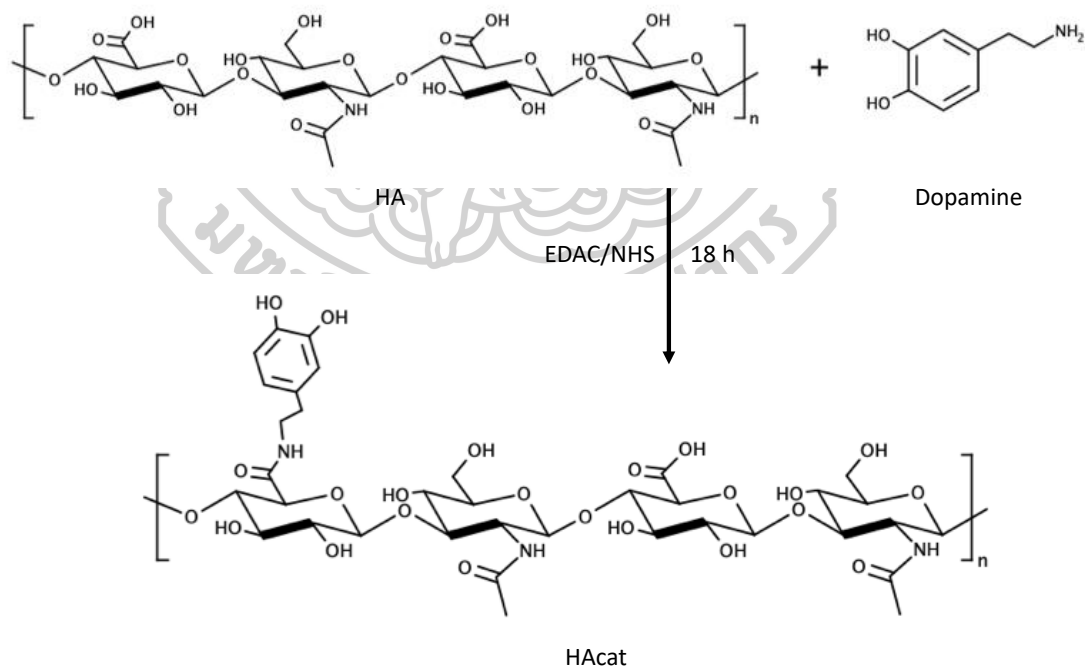
Figure 33 Synthesis scheme of HAcat
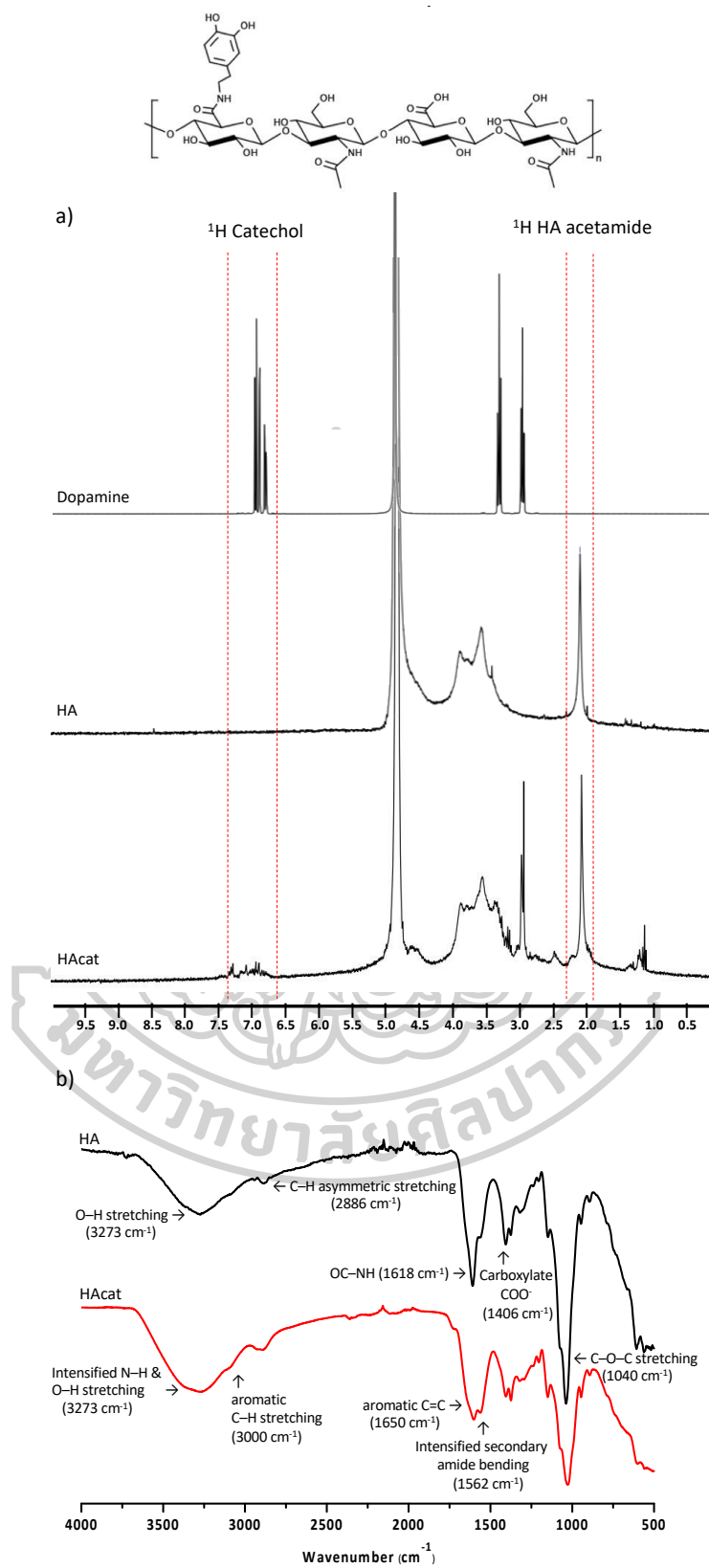
Figure 34 (a) ¹H-NMR spectra of HAcat, HA and dopamine HCl. (b) ATR-FTIR spectra of HAcat and HA

The integration of ^{1}H-NMR signals of the catechol group compared to the methyl protons of the HA acetamide in relative to their number of protons indicated the DS. The DS specified the content of catechol moiety attached to the core structure of HA. Table 4.5 showed that the DS increased as the amount of dopamine added to the reaction was increased. The results proved that the greater amounts of dopamine introduced to the reaction initiated more catechol group bearing on the polymer chain of HA. Owing to the highest %yield and catechol conjugation obtained after the synthesis, the HA:dopamine ratio of 1:3 was selected for the synthesis of the HAcat sample for further evaluations.

Table 7 The synthesis conditions and DS of HAcat

HA concentration (%w/v)	Molar ratio (HA:Dopamine)	%Yield	DS
0.5	1:1	71.81	0.46
0.5	1:2	67.36	0.71
0.5	1:3	71.74	0.95

4.2.2 NPs characterizations

4.2.2.1 Particle size, size distribution, zeta potential, and morphology

Mucoadhesive Cat-NPs were developed using ionotropic gelation method. SCScat was functioned as the cationic component to form interaction with an anionic HAcat polymer. The appropriate condition for formulating Cat-NP was searched by varying the weight ratios of SCScat:HAcat. The assessment of Cat-NPs on their particle size, PDI, surface charge, and morphology was conducted using DLS and TEM. As exhibited in Table 4.6, the proportion of SCScat and HAcat used to form the Cat-NPs affected the particle size and size distribution. All the developed Cat-NPs had negative zeta potential that may be caused by the succinate and carboxylate groups presented on the polymers. The Cat-NP samples were found

to have particle sizes between160–305 nm. The most suitable particle size with a narrowest size distribution was accomplished at the SCScat:HAcat ratio of 2:1. Herein, this composition was chosen as the particle-forming condition for further Cat-NP development. The morphology of the selected Cat-NPs was investigated by TEM examination. It was found that the Cat-NPs have a spherical morphology with a size in accordance with that determined by DLS (Figure 4.14).

Table 8 Particle size, size distribution, and zeta potential of the Cat-NPs

Ratio (SCScat:HAcat)	Particle size (nm)	PDI	Zeta potential (mV)
1:1	304.8 ± 6.29	0.3 ± 0.01	-21.6 ± 0.91
2:1	159.8 ± 3.82	0.2 ± 0.03	-19.8 ± 0.75
1:2	230.3 ± 20.15	0.5 ± 0.07	-8.64 ± 0.40
2:1 (DOX-loaded)	239.4 ± 5.28	0.3 ± 0.01	-12.7 ± 0.12
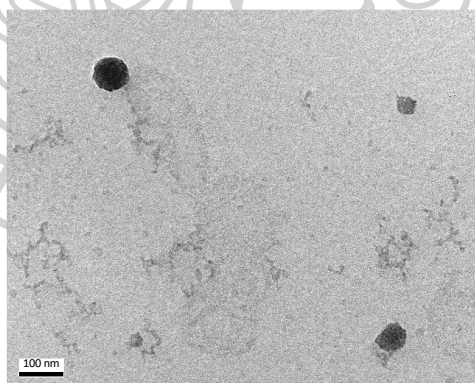
Figure 35 TEM micrograph of the Cat-NPs prepared from SCScat:HAcat at the ratio 2:1.

4.2.2.2 *Ex vivo* mucoadhesion

The mucoadhesive capability of the Cat-NPs was evaluated using a flow-through mucoadhesion study. Samples loaded with fluorescein

were rinsed off from the buccal mucous membrane by artificial saliva fluid. The remaining NPs at each time point were examined. The WO_{50} values, which indicated the volume of artificial saliva required to wash out 50% of the mucoadhesive material from the mucosal surface, was computed following the literature procedure to distinguish the difference among the samples. The quantity of the NPs remaining on the mucosal membrane in relative to the initial amount (% remaining) is illustrated in Figure 4.15a. The Cat-NPs showed superior mucoadhesive properties to the non-functionalized SCS/HA NPs and dextran. After rinsing with 60 mL of artificial saliva, a large extent of dextran was washed out and left only 10% remained on the buccal membrane. Meanwhile, around 50% of the SCS/HA NPs were left on the tissue. The calculated WO_{50} values from dextran and SCS/HA NPs wash-out profiles were 2 and 63 mL, respectively. An improvement in mucoadhesive properties were observed in the wash-out profile of the Cat-NPs, in which more than 60% of the NPs remained on the mucosal membrane after being washed with artificial saliva for 60 min (WO_{50} = 93 mL). The GFIs of each sample on the mucosal tissues after the washout at various time points are pictured in Figure 4.15b. The Cat-NPs presented the most intense fluorescent among the samples tested at the end of the experiment. Dextran has poor mucoadhesive properties since it is only capable to form weak interaction of hydrogen bonds with the mucous membrane [215]. By that, fluorescein-adsorbed dextran showed a very low WO_{50} value since it was rapidly wiped off the buccal membrane. On the other hand, the SCS/HA NPs and the Cat-NPs were able to be retained on the mucous membrane and mucin glycoprotein through hydrogen bonds and electrostatic interactions. Therefore, these NPs showed enhanced mucoadhesive properties. Furthermore, the information on WO_{50} values of SCS/HA NPs and Cat-NPs ascertained that functionalization of the NPs with the catechol groups provided higher mucoadhesive properties than the unmodified NPs. The catechol group grafted on the polymer chains may be responsible for the superior mucoadhesion of the prepared Cat-NPs with the ability to form permanent covalent bonds via various mechanisms [216, 217]. The catechol groups could bind to the thiols and amines of the mucin glycoprotein through Michael-type and Schiff-base reactions. Ionic interactions may also be important in the mucoadhesive mechanism especially in the initial stage prior

to the generation of covalent bond among the catechol moieties of the NPs and the thiol or amine groups of the glycoproteins [48].
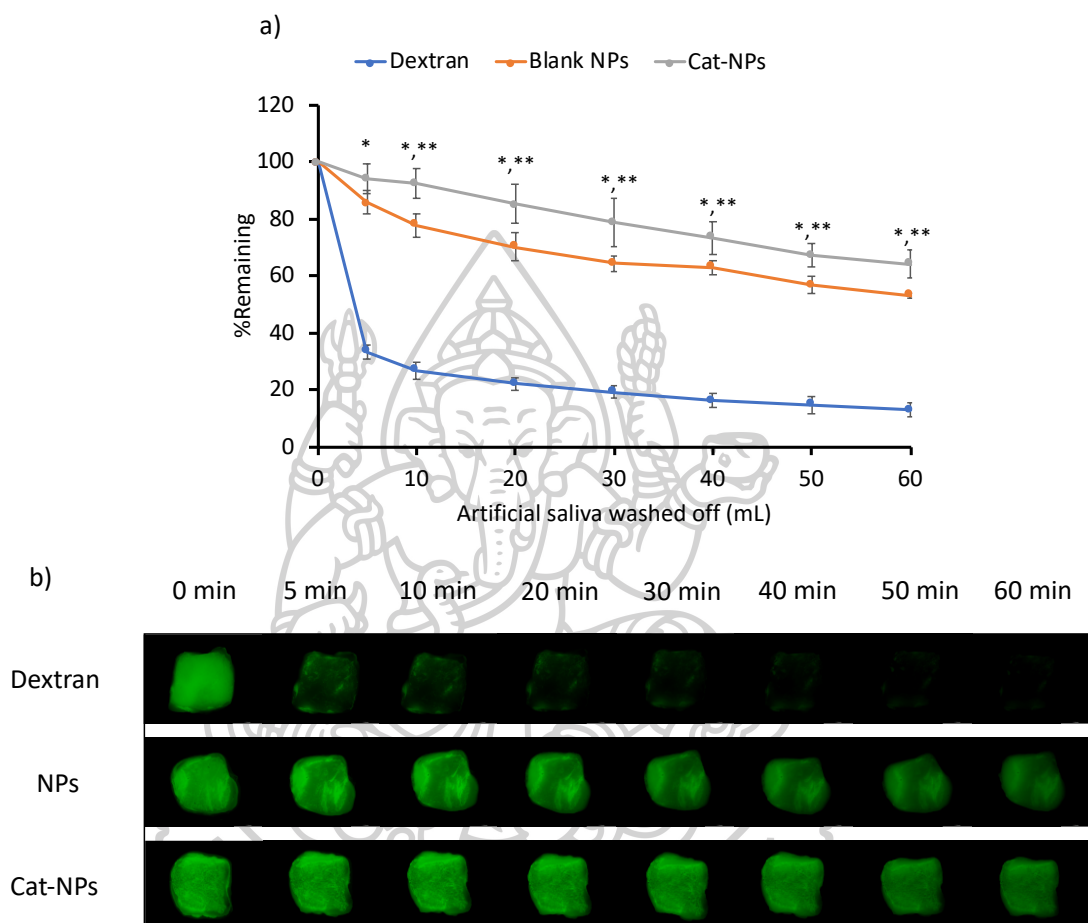
Figure 36 Comparison of the mucoadhesive properties of Cat-NPs, SCS/HA NPs, and dextran at different time points. (a) % Remaining after washing and (b) fluorescence intensities of fluorescein-loaded Cat-NPs, SCS/HA NPs, and dextran after washing for different time peroids (* Significant difference compared with dextran at 95%CI, ** significant difference compared with the SCS/HA NPs at 95%CI).

4.2.2.3 Drug loading

An anticancer drug, DOX, was loaded into the Cat-NPs using non-covalent interactions. Hydrogen bonding and electrostatic interaction may be created in the drug loading procedure. In the drug loading medium, protonation of

DOX is expected along with the ionization of carboxylic groups in SCScat and HAcat structures. Hence, the ionic interaction could be created among the drug and carriers. Also, both DOX and Cat-NPs contain hydrogen bond donors and acceptors in their molecules which enabled an binding interaction between DOX and Cat-NPs [218]. Figure 4.16 display the LC and %LE obtained from different ratios of Cat-NPs to DOX. The LC of DOX was approximately 250 µg/mg at all ratio of NPs:drug, as present in Figure 4.16a. Besides, the %LE declined significantly once the ratio of Cat-NPs to DOX increased. The maximum %LE was 70% which was obtained at the ratio of NPs:drug of 1:0.5, while the minimum %LE found was 30% at the ratio of NPs:drug of 1:2 and 1:5 (Figure 4.16b). Therefore, the Cat-NPs:DOX ratio of 1:0.5 was the most suitable condition for DOX loading.
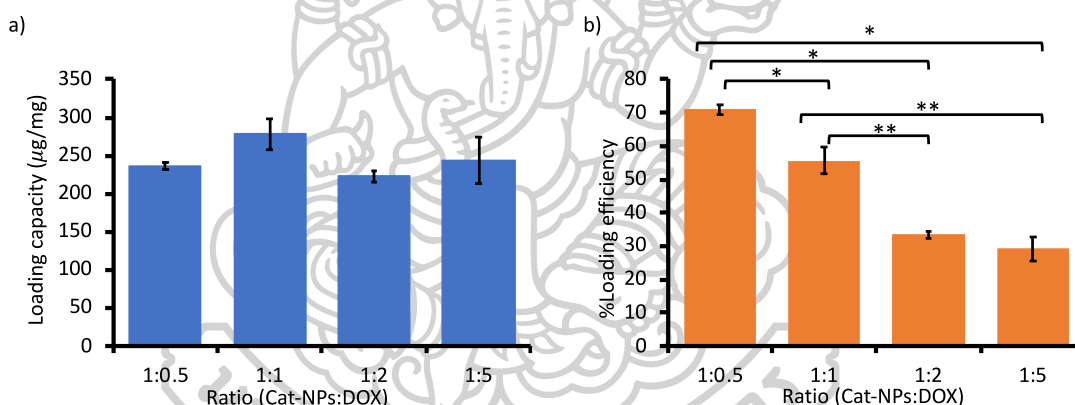
Figure 37 DOX loading on Cat-NPs calculated as (a) LC and (b) %LE. (*, ** Significant difference at 95%CI).

4.2.2.4   Drug release

The drug release in the artificial saliva was assessed to compare the release of DOX from DOX solution and the Cat-NPs. The release characteristics are presented in Figure 4.17. It was noticed that DOX from DOX solution freely permeate through the dialysis membrane and complete release was obtained within 3 h. On the contrary, the drug from the DOX-NPs was continuously released with a gradual release profile for over 24 h. Due to the hydrophilic property of DOX, immediate-release patterns were observed from both formulations at the

earlier stage. However, DOX from DOX solution release at a faster rate compared with that from DOX-NPs at every time point. The drug release from the DOX-NPs seems to be retarded by the swollen matrix created by the polymer components. In the first 3 h of the experiment, the release rate was found to be in a promptly release before a slower pace of drug release at the later stage. The drug which was adsorbed and located in the outer surface of the DOX-NPs could rapidly be released from the NPs. However, the release of the drug located in the polymer matrix was limited by the swollen matrix and showed a slower release rate. Above all, at 24 h, the cumulative amount of the DOX released from the DOX-NPs was equivalent to the final amount of DOX released from the DOX solution.
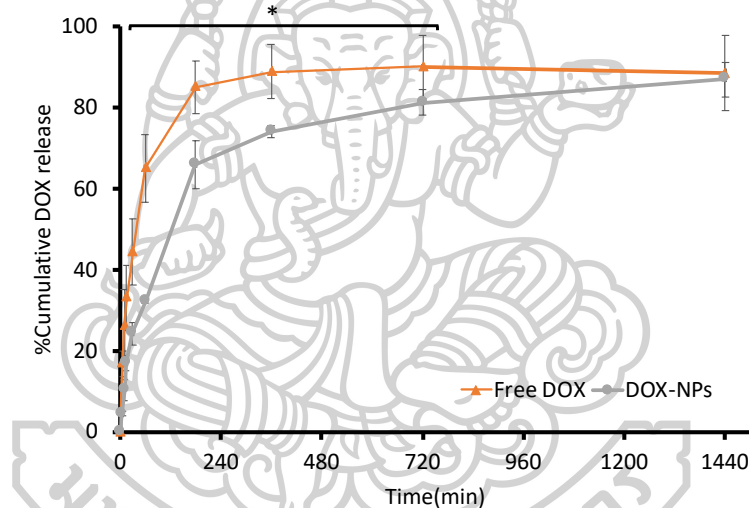
Figure 38 Release profiles of (–▲–) DOX solution and (–●–) DOX-NPs (*****
Significant difference at 95%CI).

4.2.2.5 *In vitro* biocompatibility and cytotoxicity

The biocompatibility and cytotoxicity of blank Cat-NPs were tested on the healthy HGF cells and HN22 cancer cells. The relative cell viability of more than 80% indicated that the NPs preparation is biocompatible and non-toxic to the cells. The findings showed that the cell viability of both HGF and HN22 cells was greater than 80% after being treated with 0.1–2500 µg/mL of Cat-NPs for 24 h, as shown in Figure 4.18. The results proved that the blank Cat-NPs were excellently biocompatible to the normal HGF and have no toxic effect on the

HN22 cancer cells. The findings suggested that the polymers employed to prepare the NPs (chitosan and HA) are not toxic to the human epithelial cells, which was also conveyed by the literature [219, 220]. Therefore, the polymer functionalization could maintain the safety of the polymers.
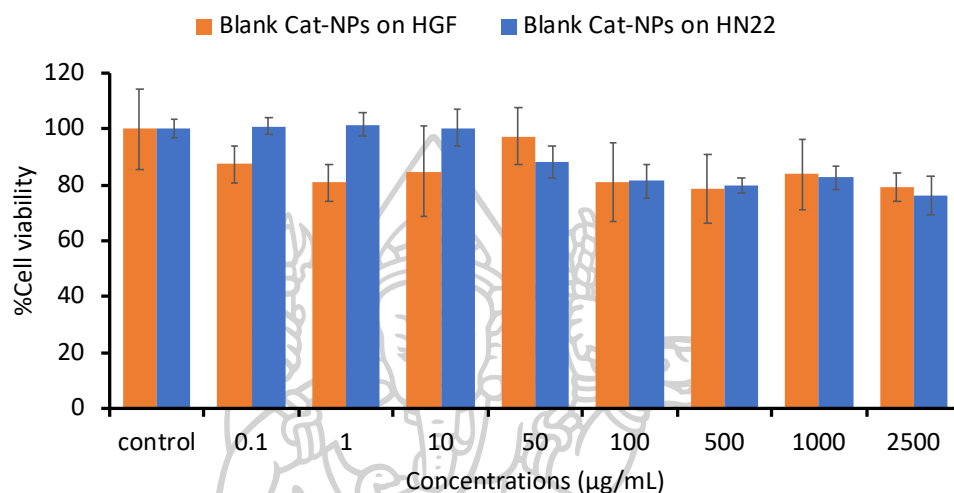
Figure 39 Twenty-four-hour cytotoxicity of the blank Cat-NPs on HGF and HN22 cell line.

The cytotoxic effect of DOX solution and DOX-NPs to the normal HGF cells is pictured in Figure 4.19a. At the concentrations of DOX above 20 µg/mL, the prepared samples showed a high toxic effect on the cells resulting in the percentage of cell viability being lower than 80%. The mechanism of DOX is related to the interference of macromolecule biosynthesis; therefore, it shows greater potency in killing the proliferating cells. Nonetheless, the healthy HGF cells proliferate at a slower rate compared with the cancer cells. Thus, a drastic death of HGF cells was not observed after the treatment with DOX and DOX-NPs for 24 h [221]. Besides, extensive cell death was evident after NH22 cancer cells were incubated with DOX and the DOX-NPs. The findings disclosed that the DOX solution was strongly effective to kill HN22 cells with an IC50 of 1.51 ± 0.18 µg/mL. Likewise, the DOX-NPs were profoundly toxic to the cancer cells with a slightly higher IC50 of 2.95 ± 0.49 µg/mL ($p < 0.05$) (Figure 4.19b). Despite the higher

inhibitory concentration of the DOX-NPs compared with the free DOX, the anticancer effects of the DOX-NPs were almost comparable to the free DOX at all the tested concentrations.
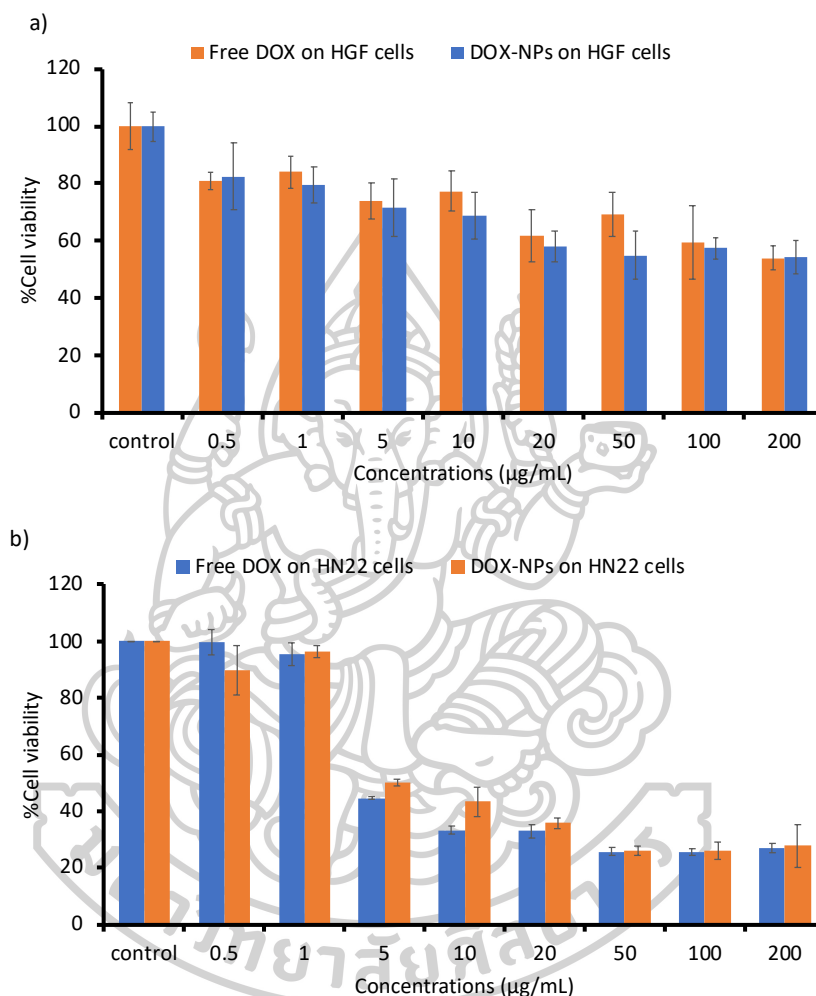
Figure 40 Percentage cell viability of DOX and DOX-NPs of HGF and HN22 cells after treated with DOX solution and DOX-NPs. ***** Significant difference at 95**%**CI.

4.2.2.6   *In vitro* cellular uptake

The ability of HN22 to take up DOX solution and DOX-NPs was evaluated by flow cytometry. The laser line of 488 nm was applied to detect the fluorescence intensity of DOX in each cell that was treated at different periods. MFI from 10,000-event analysis was reported. The instrument presented the average amount of DOX inside each cell and states the internalization ability of the

drug into the cancer cells. Also, the values can be inferred to the efficacy of DOX solution or DOX-NPs to kill the HN22 cells. Figure 4.20 displays the cellular uptake of DOX and DOX-NPs in the HN22 cells. The DOX-NPs were internalized and accumulated inside the HN22 cells at a much better rate than the DOX solution at every time periods ($p < 0.05$). From 4 to 8 h of incubation, free DOX was increasingly taken up by the cells but the uptake amount was not significantly increased after 8 h. However, the cellular uptake of DOX-NPs improved extensively up to 24 h. The reason for the limited uptake of free DOX could be the hydrophilicity of the drug. The polar structure of DOX could hardly penetrate the lipid cell membrane; by that, the drug could not be freely internalized. Nevertheless, the DOX-NPs could be effortlessly taken up by cancer cells because of their massive surface area that was advantageous for NPs and cell membrane communication. Considering the cytotoxic effect free DOX and DOX-NPs obtained from the MTT assay, we found that the IC50 values were very clos; hence, the cellular uptake is greatly higher for the DOX-NPs. This could also be due to the release of DOX was retarded and sustained from the Cat-NPs leading to the accumulation of drug after the cellular uptake. Therefore, the DOX-NPs could interact with the cells with a better affinity leading to DOX-NPs penetration to the cytosolic compartment [222]. Also, NPs constructed from polysaccharides have been shown to improve the cellular uptake and drug accumulation inside the cells through different endocytotic pathways, dominantly micropinocytosis [223].
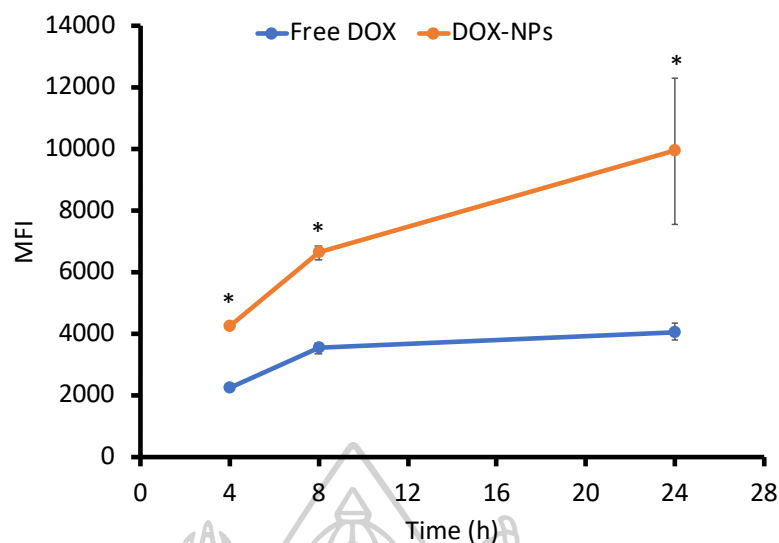
Figure 41 Cellular uptake and accumulation of DOX and DOX-NPs into HN22 cells (***** Significant difference at 95%CI).

4.2.2.7 Cell death mechanism

The HN22 cell death characteristics after a 24-h treatment with DOX solution or DOX-NPs was examined using double staining technique and detected with two different methods. Hoechst 33342 which is the membrane-permeable fluorescence dye and SYTOX^TM Green membrane impermeable dye were utilized for cell staining. Cells presenting DNA fragmentation and nuclear condensation were probed with Hoechst 33342 and presented a bright blue fluorescent illumination. The staining of necrotic cellular nucleic acids will, therefore, be made by the cell membrane non-penetrated green fluorescence dye [224]. The detection under an inverted microscope showed that after treating the cells with the blank NPs, the viable HN22 cells were comparable to that of the untreated control cells. On the contrary, cells that were incubated in DOX solution and DOX-NPs preparation exposed significant apoptotic and necrotic cells as shown in Table 4.7. Whereas, the DOX-NPs seemed to exhibit higher cytotoxic potency than the free DOX. The result was confirmed by the evaluation by flow cytometry. Annexin V conjugated with Alexa Fluor^TM 647 was acquired to stain the apoptosis cell death, and SYTOX^TM Green nucleic acid stain was employed to probe the necrotic cells. As revealed in Figure 4.21, DOX-NPs treated HN22 cells showed a greater number of

apoptotic cells (22%) than those treated with DOX solution (16%). Apoptosis induction is preferred because the programmed cell death creates apoptotic bodies and avoids the leakage of intracellular material leading to the deflation of inflammation-inducing cytokines and less inflammatory cell death. The cellular uptake characteristics of the DOX-NPs indicated that the anticancer agent was deposited within the cells before a gradual drug being released. Therefore, as compared with the free DOX, the DOX-NPs may provide a more potent cancer-killing effect preferably via apoptosis death mechanism [225, 226].

Table 9 Fluorescence images of Hoechst 33342 and SYTOX^{TM} Green staining on HN22 cell line treated with the blank Cat-NPs, free DOX, and the DOX-NPs (100× magnification)

	Control	Blank Cat-NPs	Free DOX	DOX-NPs
Hoechst 33342				
SYTOX^{TM} Green				
Merge				
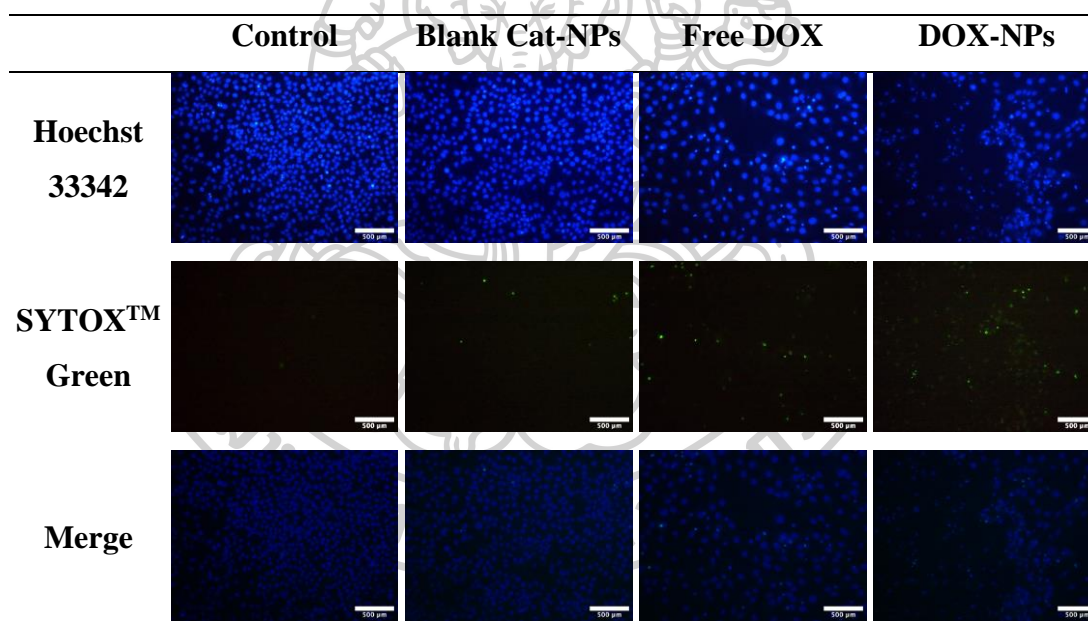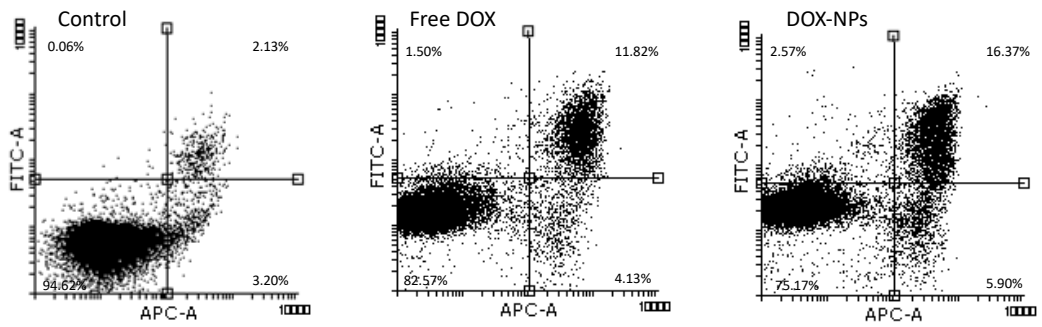
Figure 42 HN22 cell death analysis after being treated with free DOX and the DOX-NPs.

CHAPTER 5

CONCLUSIONS

5.1   Development of coordination bond-forming NVP/AA NPs for CDDP delivery

A new drug delivery avenue of NVP/AA NPs was synthesized through surfactant-free emulsion polymerization. The developed NPs were shown to have preferable structural, physicochemical, and biocompatible characteristics. The NVP/AA NPs synthesis by one- or two-step approach provided similar NPs characteristics although the arrangements of the components in the NPs was different. CDDP was bound onto the NPs through a coordinate covalent bond. A large number of drug loading was achieved with optimal %LE. A sustained release profile of CDDP from the NPs was obtained. The CDDP-loaded NPs exhibited excellent killing potency on an oral cancer cell line. Apart from that, the anticancer effect of CDDP-loaded NVP/AA NPs offered a higher potential to kill the cancer cells through a less inflammation pathway. CDDP-loaded NVP/AA NPs were able to be deposited inside the head and neck cancer cells leading to a gradual and continual release of the drug to perform its killing effect. Above all, the novel CDDP-loaded NVP/AA NPs could be a promising and potential drug carrier for the treatment of head and neck cancer. Nevertheless, further *in vivo* experiments should be carried out prior to the clinical applications.

5.2   Development of mucoadhesive NPs for localized delivery of DOX

The innovative functional Cat-NPs were produced from synthesized SCScat and HAcat polymers. The NPs were assembled by ionotropic gelation method and the size was reduced by ultrasonication. The particles were in nano-size and had a spherical shape with a negative surface charge. A great amount of DOX could be incorporated into the NPs. In addition, a prolonged-release characteristic of the drug was obtained. The Cat-NPs presented an enhance in mucoadhesive properties

compared to the non-functionalized NPs, which may be due to the different adhesion modes that could be created between the mucin and the Cat-NPs. The Cat-NPs could effectively deliver DOX and to the HN22 cells, where it preferably induces apoptosis of the cancer cells. The developed Cat-NPs may be a potential drug delivery platform for locally administered HNSCC treatment. However, to ascertain the safety and the clinical effectiveness of the proposed drug delivery system, further *in vivo* examinations are required.

All in all, the new polymeric NPs with specific functional groups for targeted delivery of anticancer drugs have been synthesized and prepared. The NVP/AA NPs and functionalized NPs of SCScat/HAcat exhibited promising characteristics as the nano-drug carriers. The investigations showed that the prepared NPs are equipped with desirable physicochemical properties, drug loading, and release characteristics. The evaluations on cancer-killing ability proved that anticancer agents (CDDP and DOX)-loaded NPs were delivered to the head and neck cancer cells through different targeting strategies and performed the efficient drug deposition and possessed potent anticancer effect against head and neck cancer cells.
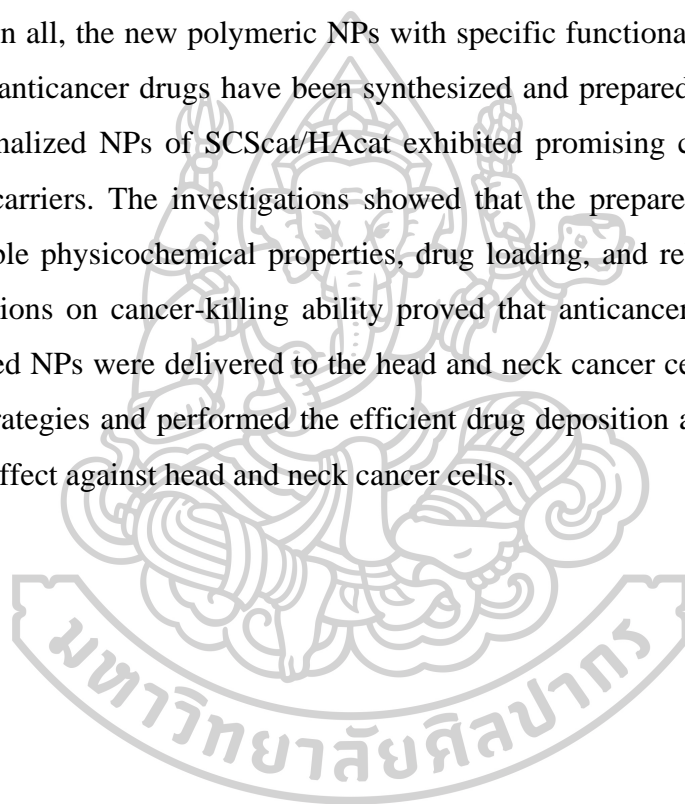
REFERENCES

[1] Global burden of disease cancer collaboration, global, regional, and national cancer incidence, mortality, years of life lost, years lived with disability, and disability-adjusted life-years for 32 cancer groups, 1990 to 2015: A Systematic Analysis for the Global Burden of Disease Study, JAMA Oncol, 3 (2017) 524-548.

[2] B.P. Cervenka, S. Rao, A.F. Bewley, Head and neck cancer and the elderly patient, Otolaryngol Clin North Am, 51 (2018) 741-751.

[3] N. Cohen, S. Fedewa, A.Y. Chen, Epidemiology and demographics of the head and neck cancer population, Oral Maxillofac Surg Clin North Am, 30 (2018) 381-395.

[4] W.M. Lydiatt, S.G. Patel, B. O'Sullivan, M.S. Brandwein, J.A. Ridge, J.C. Migliacci, A.M. Loomis, J.P. Shah, Head and Neck cancers-major changes in the American Joint Committee on cancer eighth edition cancer staging manual, CA Cancer J Clin, 67 (2017) 122-137.

[5] A.K. D'Cruz, R. Vaish, H. Dhar, Oral cancers: Current status, Oral Oncol, 87 (2018) 64-69.

[6] O. Kaidar-Person, Z. Gil, S. Billan, Precision medicine in head and neck cancer, Drug Resist Updat, 40 (2018) 13-16.

[7] J. de Lartigue, Rising to the therapeutic challenge of head and neck cancer, The Journal of Community and Supportive Oncology, 13 (2015) 73-80.

[8] L. Hartner, Chemotherapy for Oral Cancer, Dent Clin North Am, 62 (2018) 87-97.

[9] L.Q.M. Chow, Head and Neck Cancer, N Engl J Med, 382 (2020) 60-72.

[10] S. Dasari, P.B. Tchounwou, Cisplatin in cancer therapy: molecular mechanisms of action, Eur J Pharmacol, 740 (2014) 364-378.

[11] P. Huguenin, K.T. Beer, A. Allal, K. Rufibach, C. Friedli, J.B. Davis, B. Pestalozzi, S. Schmid, A. Thöni, M. Ozsahin, J. Bernier, M. Töpfer, R. Kann, U.R. Meier, P. Thum, S. Bieri, M. Notter, N. Lombriser, C. Glanzmann, Concomitant cisplatin significantly improves locoregional control in advanced head and neck cancers treated with hyperfractionated radiotherapy, Journal of Clinical Oncology, 22 (2004) 4665-4673.

[12] R. Trummer, W. Rangsimawong, W. Sajomsang, M. Kumpugdee-Vollrath, P. Opanasopit, P. Tonglairoum, Chitosan-based self-assembled nanocarriers

coordinated to cisplatin for cancer treatment, RSC Advances, 8 (2018) 22967-22973.

[13] D. Corinti, C. Coletti, N. Re, S. Piccirillo, M. Giampà, M.E. Crestoni, S. Fornarini, Hydrolysis of cis- and transplatin: structure and reactivity of the aqua complexes in a solvent free environment, RSC Advances, 7 (2017) 15877-15884.

[14] U. Ndagi, N. Mhlongo, M. Soliman, Metal complexes in cancer therapy &; an update from drug design perspective, Drug Design, Development and Therapy, Volume11 (2017) 599-616.

[15] C.F. Thorn, C. Oshiro, S. Marsh, T. Hernandez-Boussard, H. McLeod, T.E. Klein, R.B. Altman, Doxorubicin pathways: pharmacodynamics and adverse effects, Pharmacogenet Genomics, 21 (2011) 440-446.

[16] M. Moradzadeh Khiavi, A. Rostami, H. Hamishekar, M. Mesgari Abassi, A. Aghbali, R. Salehi, B. Abdollahi, S. Fotoohi, M. Sina, Therapeutic efficacy of orally delivered doxorubicin nanoparticles in rat tongue cancer induced by 4-nitroquinoline 1-oxide, Adv Pharm Bull, 5 (2015) 209-216.

[17] I. Khan, K. Saeed, I. Khan, Nanoparticles: Properties, applications and toxicities, Arabian Journal of Chemistry, (2017).

[18] Z. Tang, C. He, H. Tian, J. Ding, B.S. Hsiao, B. Chu, X. Chen, Polymeric nanostructured materials for biomedical applications, Progress in Polymer Science, 60 (2016) 86-128.

[19] A.R. Girija, 12 - Medical Applications of polymer/functionalized nanoparticle systems, in: K. Pielichowski, T.M. Majka (Eds.) Polymer Composites with Functionalized Nanoparticles, Elsevier2019, pp. 381-404.

[20] T. Ramasamy, H.B. Ruttala, P. Sundaramoorthy, B.K. Poudel, Y.S. Youn, S.K. Ku, H.-G. Choi, C.S. Yong, J.O. Kim, Multimodal selenium nanoshell-capped Au@mSiO2 nanoplatform for NIR-responsive chemo-photothermal therapy against metastatic breast cancer, NPG Asia Materials, 10 (2018) 197-216.

[21] T. Ramasamy, H.B. Ruttala, N. Chitrapriya, B.K. Poudal, J.Y. Choi, S.T. Kim, Y.S. Youn, S.K. Ku, H.G. Choi, C.S. Yong, J.O. Kim, Engineering of cell microenvironment-responsive polypeptide nanovehicle co-encapsulating a synergistic combination of small molecules for effective chemotherapy in solid

tumors, Acta Biomater, 48 (2017) 131-143.

[22] H.B. Ruttala, N. Chitrapriya, K. Kaliraj, T. Ramasamy, W.H. Shin, J.-H. Jeong, J.R. Kim, S.K. Ku, H.-G. Choi, C.S. Yong, J.O. Kim, Facile construction of bioreducible crosslinked polypeptide micelles for enhanced cancer combination therapy, Acta Biomaterialia, 63 (2017) 135-149.

[23] W.H. De Jong, P.J.A. Borm, Drug delivery and nanoparticles:applications and hazards, International journal of nanomedicine, 3 (2008) 133-149.

[24] M. Sharma, Chapter 18 - Transdermal and intravenous nano drug delivery systems: present and future, in: S.S. Mohapatra, S. Ranjan, N. Dasgupta, R.K. Mishra, S. Thomas (Eds.) Applications of Targeted Nano Drugs and Delivery Systems, Elsevier2019, pp. 499-550.

[25] K. Greish, Enhanced permeability and retention (EPR) Effect for anticancer nanomedicine drug targeting, in: S.R. Grobmyer, B.M. Moudgil (Eds.) Cancer Nanotechnology: Methods and Protocols, Humana Press, Totowa, NJ, 2010, pp. 25-37.

[26] n. nishiyama, y. kato, y. sugiyama, k. kataoka, cisplatin-loaded polymer-metal complex micelle with time-modulated decaying property as a novel drug delivery system, Pharmaceutical Research, 18 (2001) 1035-1041.

[27] M.L. Krieger, N. Eckstein, V. Schneider, M. Koch, H.D. Royer, U. Jaehde, G. Bendas, Overcoming cisplatin resistance of ovarian cancer cells by targeted liposomes in vitro, Int J Pharm, 389 (2010) 10-17.

[28] K. Avgoustakis, A. Beletsi, Z. Panagi, P. Klepetsanis, A.G. Karydas, D.S. Ithakissios, PLGA–mPEG nanoparticles of cisplatin: in vitro nanoparticle degradation, in vitro drug release and in vivo drug residence in blood properties, Journal of Controlled Release, 79 (2002) 123-135.

[29] X. Zhao, J. Pan, W. Li, W. Yang, L. Qin, Y. Pan, Gold nanoparticles enhance cisplatin delivery and potentiate chemotherapy by decompressing colorectal cancer vessels, International journal of nanomedicine, 13 (2018) 6207-6221.

[30] X. Lv, M. Zhao, Y. Wang, X. Hu, J. Wu, X. Jiang, S. Li, C. Cui, S. Peng, Loading cisplatin onto 6-mercaptopurine covalently modified MSNS: a nanomedicine strategy to improve the outcome of cisplatin therapy, Drug Des Devel Ther, 10

(2016) 3933-3946.

[31] A. Guven, G.J. Villares, S.G. Hilsenbeck, A. Lewis, J.D. Landua, L.E. Dobrolecki, L.J. Wilson, M.T. Lewis, Carbon nanotube capsules enhance the in vivo efficacy of cisplatin, Acta biomaterialia, 58 (2017) 466-478.

[32] N. Zhao, M.C. Woodle, A.J. Mixson, Advances in delivery systems for doxorubicin, J Nanomed Nanotechnol, 9 (2018).

[33] S. Sadaf, L. Walder, Doxorubicin Adsorbed on Carbon Nanotubes: Helical Structure and New Release Trigger, Advanced Materials Interfaces, 4 (2017) 1700649.

[34] D. Dhamecha, S. Jalalpure, K. Jadhav, S. Jagwani, R. Chavan, Doxorubicin loaded gold nanoparticles: Implication of passive targeting on anticancer efficacy, Pharmacological Research, 113 (2016) 547-556.

[35] F. Ketabat, M. Pundir, F. Mohabatpour, L. Lobanova, S. Koutsopoulos, L. Hadjiiski, X. Chen, P. Papagerakis, S. Papagerakis, Controlled Drug Delivery Systems for Oral Cancer Treatment-Current Status and Future Perspectives, Pharmaceutics, 11 (2019).

[36] A.K. Sah, A. Vyas, P.K. Suresh, B. Gidwani, Application of nanocarrier-based drug delivery system in treatment of oral cancer, Artif Cells Nanomed Biotechnol, 46 (2018) 650-657.

[37] V. Sankar, V. Hearnden, K. Hull, D.V. Juras, M.S. Greenberg, A.R. Kerr, P.B. Lockhart, L.L. Patton, S. Porter, M. Thornhill, Local drug delivery for oral mucosal diseases: challenges and opportunities, Oral Dis, 17 Suppl 1 (2011) 73-84.

[38] M.F. Attia, N. Anton, J. Wallyn, Z. Omran, T.F. Vandamme, An overview of active and passive targeting strategies to improve the nanocarriers efficiency to tumour sites, Journal of Pharmacy and Pharmacology, 71 (2019) 1185-1198.

[39] T. Ramasamy, H.B. Ruttala, B. Gupta, B.K. Poudel, H.G. Choi, C.S. Yong, J.O. Kim, Smart chemistry-based nanosized drug delivery systems for systemic applications: A comprehensive review, J Control Release, 258 (2017) 226-253.

[40] J.P. Rao, K.E. Geckeler, Polymer nanoparticles: Preparation techniques and size-control parameters, Progress in Polymer Science, 36 (2011) 887-913.

[41] T.K. Giri, 5 - Nanoarchitectured Polysaccharide-Based Drug Carrier for Ocular Therapeutics, in: A.M. Holban, A.M. Grumezescu (Eds.) Nanoarchitectonics for Smart Delivery and Drug Targeting, William Andrew Publishing2016, pp. 119-141.

[42] S. Mansuri, P. Kesharwani, K. Jain, R.K. Tekade, N.K. Jain, Mucoadhesion: A promising approach in drug delivery system, Reactive and Functional Polymers, 100 (2016) 151-172.

[43] P. Tonglairoum, R.P. Brannigan, P. Opanasopit, V.V. Khutoryanskiy, Maleimide-bearing nanogels as novel mucoadhesive materials for drug delivery, J Mater Chem B, 4 (2016) 6581-6587.

[44] L. Serra, J. Domenech, N.A. Peppas, Engineering design and molecular dynamics of mucoadhesive drug delivery systems as targeting agents, Eur J Pharm Biopharm, 71 (2009) 519-528.

[45] M. Davidovich-Pinhas, H. Bianco-Peled, Alginate-PEGAc: a new mucoadhesive polymer, Acta Biomater, 7 (2011) 625-633.

[46] C. Pornpitchanarong, K. Singpanna, T. Rojanarata, P. Opanasopit, T. Ngawhirunpat, P. Patrojanasophon, Catechol-Bearing Hyaluronic Acid Coated Polyvinyl Pyrrolidone/Hydroxyl Propyl-β-Cyclodextrin/Clotrimazole Nanofibers for Oral Candidiasis Treatment, Key Engineering Materials, 819 (2019) 163-168.

[47] N. Sahatsapan, T. Rojanarata, T. Ngawhirunpat, P. Opanasopit, P. Tonglairoum, 6-Maleimidohexanoic acid-grafted chitosan: A new generation mucoadhesive polymer, Carbohydr Polym, 202 (2018) 258-264.

[48] K. Kim, K. Kim, J.H. Ryu, H. Lee, Chitosan-catechol: a polymer with long-lasting mucoadhesive properties, Biomaterials, 52 (2015) 161-170.

[49] F. Du, Y. Wu, F. Du, L. Zhang, W. Feng, L. Zhao, R. Cai, L. Xu, G. Bian, J. Li, S. Zou, A. Gong, M. Zhang, Construction of catechol-grafted chitosan alginate/barium sulfate microcapsules for computed tomography real-time imaging and gastroretentive drug delivery, Int J Nanomedicine, 14 (2019) 6001-6018.

[50] J. Xu, S. Strandman, J.X. Zhu, J. Barralet, M. Cerruti, Genipin-crosslinked catechol-chitosan mucoadhesive hydrogels for buccal drug delivery, Biomaterials, 37 (2015) 395-404.

[51] G.M. Soliman, Y.L. Zhang, G. Merle, M. Cerruti, J. Barralet, Hydrocaffeic acid–chitosan nanoparticles with enhanced stability, mucoadhesion and permeation properties, European J Pharm Biopharm, 88 (2014) 1026-1037.

[52] D. Young, C.C. Xiao, B. Murphy, M. Moore, C. Fakhry, T.A. Day, Increase in head and neck cancer in younger patients due to human papillomavirus (HPV), Oral Oncol, 51 (2015) 727-730.

[53] C. Wittekindt, S. Wagner, S.J. Sharma, N. Wurdemann, J. Knuth, H. Reder, J.P. Klussmann, HPV - A different view on Head and Neck Cancer, Laryngorhinootologie, 97 (2018) S48-S113.

[54] D. Kawakita, K. Matsuo, Alcohol and head and neck cancer, Cancer Metastasis Rev, 36 (2017) 425-434.

[55] X. Liu, X.L. Gao, X.H. Liang, Y.L. Tang, The etiologic spectrum of head and neck squamous cell carcinoma in young patients, Oncotarget, 7 (2016) 66226-66238.

[56] S.H. Huang, B. O'Sullivan, Overview of the 8th Edition TNM Classification for Head and Neck Cancer, Curr Treat Options Oncol, 18 (2017) 40.

[57] A.D. Heroiu Cataloiu, C.E. Danciu, C.R. Popescu, Multiple cancers of the head and neck, Maedica (Bucur), 8 (2013) 80-85.

[58] P.H. Montero, S.G. Patel, Cancer of the oral cavity, Surg Oncol Clin N Am, 24 (2015) 491-508.

[59] A.K. D'Cruz, R. Vaish, H. Dhar, Oral cancers: Current status, Oral Oncol, 87 (2018) 64-69.

[60] G. Del Corso, A. Villa, A. Tarsitano, A. Gohel, Current trends in oral cancer: a systematic review, Cancer Cell & Microenvironment, (2016).

[61] M. Kumar, R. Nanavati, T. Modi, C. Dobariya, Oral cancer: Etiology and risk factors: A review, Journal of Cancer Research and Therapeutics, 12 (2016) 458.

[62] H.Y. Sroussi, M. Jessri, J. Epstein, Oral assessment and management of the patient with head and neck cancer, Oral Maxillofac Surg Clin North Am, 30 (2018) 445-458.

[63] J.A. Valdez, M.T. Brennan, Impact of Oral Cancer on Quality of Life, Dent Clin North Am, 62 (2018) 143-154.

[64] D.G. Pfister, S. Spencer, D. Adelstein, D. Adkins, Y. Anzai, D.M. Brizel, J.Y.

Bruce, P.M. Busse, J.J. Caudell, A.J. Cmelak, A.D. Colevas, D.W. Eisele, M. Fenton, R.L. Foote, T. Galloway, M.L. Gillison, R.I. Haddad, W.L. Hicks, Y.J. Hitchcock, A. Jimeno, D. Leizman, E. Maghami, L.K. Mell, B.B. Mittal, H.A. Pinto, J.A. Ridge, J.W. Rocco, C.P. Rodriguez, J.P. Shah, R.S. Weber, G. Weinstein, M. Witek, F. Worden, S.S. Yom, W. Zhen, J.L. Burns, S.D. Darlow, Head and Neck Cancers, Version 2.2020, NCCN Clinical Practice Guidelines in Oncology, J Natl Compr Canc Netw, 18 (2020) 873-898.

[65] E. Orlandi, S. Alfieri, C. Simon, A. Trama, L. Licitra, M. Hackl, E.V. Eycken, K. Henau, N. Dimitrova, et al, Treatment challenges in and outside a network setting: Head and neck cancers, European Journal of Surgical Oncology, 45 (2019) 40-45.

[66] S.B. Chinn, J.N. Myers, Oral Cavity Carcinoma: Current Management, Controversies, and Future Directions, J Clin Oncol, 33 (2015) 3269-3276.

[67] S.S. Baxi, D.J. Sher, D.G. Pfister, Value considerations in the treatment of head and neck cancer: radiation, chemotherapy, and supportive care, Am Soc Clin Oncol Educ Book, (2014) e296-303.

[68] A.L. Galbiatti, J.A. Padovani-Junior, J.V. Maniglia, C.D. Rodrigues, E.C. Pavarino, E.M. Goloni-Bertollo, Head and neck cancer: causes, prevention and treatment, Braz J Otorhinolaryngol, 79 (2013) 239-247.

[69] D.M. Cognetti, R.S. Weber, S.Y. Lai, Head and neck cancer: an evolving treatment paradigm, Cancer, 113 (2008) 1911-1932.

[70] A.E. Brown, J.D. Langdon, Management of oral cancer, Ann R Coll Surg Engl, 77 (1995) 404-408.

[71] J.J. Homer, M.J. Fardy, Surgery in head and neck cancer: United Kingdom National Multidisciplinary Guidelines, J Laryngol Otol, 130 (2016) S68-S70.

[72] T.S. Fu, A. Foreman, D.P. Goldstein, J.R. de Almeida, The role of transoral robotic surgery, transoral laser microsurgery, and lingual tonsillectomy in the identification of head and neck squamous cell carcinoma of unknown primary origin: a systematic review, J Otolaryngol Head Neck Surg, 45 (2016) 28.

[73] S.A. Yeh, Radiotherapy for head and neck cancer, Semin Plast Surg, 24 (2010) 127-136.

[74] S. Furness, A.M. Glenny, H.V. Worthington, S. Pavitt, R. Oliver, J.E. Clarkson, M.

Macluskey, K.K. Chan, D.I. Conway, C.E. Panel, Interventions for the treatment of oral cavity and oropharyngeal cancer: chemotherapy, Cochrane Database Syst Rev, (2010) CD006386.

[75] J.P. Pignon, A. le Maitre, E. Maillard, J. Bourhis, M.-N.C. Group, Meta-analysis of chemotherapy in head and neck cancer (MACH-NC): an update on 93 randomised trials and 17,346 patients, Radiother Oncol, 92 (2009) 4-14.

[76] G. Recondo, J.P. Armand, E. Tellez-Bernal, C. Domenge, M. Belehradek, F. De Vathaire, P. Wibault, J.M. Richard, E. Cvitkovic, Recurrent and/or metastatic head and neck squamous cell carcinoma: a clinical, univariate and multivariate analysis of response and survival with cisplatin-based chemotherapy, Laryngoscope, 101 (1991) 494-501.

[77] Bruce E Brockstein, Kerstin M Stenson, Shiyu Song, Overview of treatment for head and neck cancer, UpToDate, Post TW (Ed), UpToDate, Waltham, MA. (Accessed on August 26, 2021.)2021.

[78] L. Hartner, Chemotherapy for oral cancer, Dental Clinics of North America, 62 (2018) 87-97.

[79] A. Guidi, C. Codeca, D. Ferrari, Chemotherapy and immunotherapy for recurrent and metastatic head and neck cancer: a systematic review, Med Oncol, 35 (2018) 37.

[80] R.P.S. Banipal, M.K. Mahajan, Methotrexate revisited—in recurrent head and neck cancer, Palliative Care: Research and Treatment, 5 (2011).

[81] R.L. Woods, R.M. Fox, M.H. Tattersall, Methotrexate treatment of squamous-cell head and neck cancers: dose-response evaluation, Br Med J (Clin Res Ed), 282 (1981) 600-602.

[82] S. Dasari, P.B. Tchounwou, Cisplatin in cancer therapy: molecular mechanisms of action, Eur J Pharmacol, 740 (2014) 364-378.

[83] M.J. Ahn, A. D'Cruz, J.B. Vermorken, J.P. Chen, I. Chitapanarux, H.Q. Dang, A. Guminski, D. Kannarunimit, T.Y. Lin, W.T. Ng, K.U. Park, A.T. Chan, Clinical recommendations for defining platinum unsuitable head and neck cancer patient populations on chemoradiotherapy: A literature review.

[84] F. Petrelli, A. Coinu, V. Riboldi, K. Borgonovo, M. Ghilardi, M. Cabiddu, V.

Lonati, E. Sarti, S. Barni, Concomitant platinum-based chemotherapy or cetuximab with radiotherapy for locally advanced head and neck cancer: a systematic review and meta-analysis of published studies.

[85] P. Volling, W. Schröder M Fau - Rauschning, W. Rauschning W Fau - Achterrath, E. Achterrath W Fau - Stennert, E. Stennert, Carboplatin. The better platinum in head and neck cancer?

[86] H. Choy, C. Park, M. Yao, Current status and future prospects for satraplatin, an oral platinum analogue, Clin Cancer Res, 14 (2008) 1633-1638.

[87] R. Oun, Y.E. Moussa, N.J. Wheate, The side effects of platinum-based chemotherapy drugs: a review for chemists, Dalton Trans, 47 (2018) 6645-6653.

[88] N. Zhang, Y. Yin, S.J. Xu, W.S. Chen, 5-Fluorouracil: mechanisms of resistance and reversal strategies, Molecules, 13 (2008) 1551-1569.

[89] P.M. Wigmore, M. Mustafa S Fau - El-Beltagy, L. El-Beltagy M Fau - Lyons, J. Lyons L Fau - Umka, G. Umka J Fau - Bennett, G. Bennett, Effects of 5-FU.

[90] The Liverpool Head and Neck Oncology Group, A phase III randomised trial of cistplatinum, methotrextate, cisplatinum + methotrexate and cisplatinum + 5-FU in end stage squamous carcinoma of the head and neck. Liverpool Head and Neck Oncology Group, Br J Cancer, 61 (1990) 311-315.

[91] S.H. Hanemaaijer, I.C. Kok, R.S.N. Fehrmann, B. van der Vegt, J.A. Gietema, B.E.C. Plaat, M. van Vugt, M.R. Vergeer, C.R. Leemans, J.A. Langendijk, J. Voortman, J. Buter, S.F. Oosting, Comparison of carboplatin with 5-fluorouracil vs. cisplatin as concomitant chemoradiotherapy for locally advanced head and neck squamous cell carcinoma, Front Oncol, 10 (2020) 761.

[92] R. Rao, S. Ss, V. Shenoy, M.C. Hegde, V. Prasad, K. Prasad, Induction chemotherapy with cisplatin and 5-fluorouracil in advanced head and neck cancers: A Short Term Response Evaluation, J Clin Diagn Res, 9 (2015) XC08-XC12.

[93] D. Schrijvers, J.B. Vermorken, Taxanes in the treatment of head and neck cancer, Curr Opin Oncol, 17 (2005) 218-224.

[94] A. Stierle, G. Strobel, D. Stierle, P. Grothaus, G. Bignami, The search for a taxol-producing microorganism among the endophytic fungi of the Pacific yew, Taxus

brevifolia, J Nat Prod, 58 (1995) 1315-1324.

[95] K. Misiukiewicz, V. Gupta, R. Bakst, M. Posner, Taxanes in cancer of the head and neck, Anticancer Drugs, 25 (2014) 561-570.

[96] J. Guigay, M. Tahara, L. Licitra, U. Keilholz, S. Friesland, P. Witzler, R. Mesía, The evolving role of taxanes in combination with cetuximab for the treatment of recurrent and/or metastatic squamous cell carcinoma of the head and neck: evidence, Advantages, and Future Directions, Frontiers in Oncology, 9 (2019) 668.

[97] D. Cella, A. Peterman, S. Hudgens, K. Webster, M.A. Socinski, Measuring the side effects of taxane therapy in oncology: the functional assesment of cancer therapy-taxane (FACT-taxane), Cancer, 98 (2003) 822-831.

[98] A.I. Dreyfuss, J.R. Clark, B.G. Fallon, M.R. Posner, C.M. Norris, Jr., D. Miller, Cyclophosphamide, doxorubicin, and cisplatin combination chemotherapy for advanced carcinomas of salivary gland origin, Cancer, 60 (1987) 2869-2872.

[99] S.A. Saddoughi, E. Garrett-Mayer, U. Chaudhary, P.E. O'Brien, L.B. Afrin, T.A. Day, M.B. Gillespie, A.K. Sharma, C.S. Wilhoit, R. Bostick, C.E. Senkal, Y.A. Hannun, J. Bielawski, G.R. Simon, K. Shirai, B. Ogretmen, Results of a phase II trial of gemcitabine plus doxorubicin in patients with recurrent head and neck cancers: serum C(1)(8)-ceramide as a novel biomarker for monitoring response, Clin Cancer Res, 17 (2011) 6097-6105.

[100] P.G. Rose, F. Fu, L.M. Chambers, L. Mei, R. De Bernardo, B.L. Prendes, E. Lamarre, Incidence of squamous cell carcinomas of the head and neck following prolonged pegylated liposomal doxorubicin, Anticancer Drugs, 31 (2020) 747-750.

[101] H.H. Wang, Z.G. Fu, W. Li, Y.X. Li, L.S. Zhao, L. Wen, J.J. Zhang, N. Wen, The synthesis and application of nano doxorubicin- indocyanine green matrix metalloproteinase-responsive hydrogel in chemophototherapy for head and neck squamous cell carcinoma, Int J Nanomedicine, 14 (2019) 623-638.

[102] V. Damiani, E. Falvo, G. Fracasso, L. Federici, M. Pitea, V. De Laurenzi, G. Sala, P. Ceci, Therapeutic efficacy of the novel stimuli-sensitive nano-ferritins containing doxorubicin in a head and neck cancer model, Int J Mol Sci, 18 (2017).

[103] A. Galstyan, J. Cho, D.E. Johnson, J.R. Grandis, Chapter 5 - Modulation of the

PI3K/mTOR pathways, in: R.J. Kimple (Ed.) Improving the therapeutic ratio in head and neck cancer, Academic Press2020, pp. 89-105.

[104] D. Kong, Z. Zhang, Chapter 12 - PI3K/AKT Inhibitors as Sensitizing Agents for Cancer Chemotherapy, in: Z.-S. Chen, D.-H. Yang (Eds.) Protein Kinase Inhibitors as Sensitizing Agents for Chemotherapy, Academic Press2019, pp. 187-205.

[105] M. Fiedler, D. Schulz, G. Piendl, G. Brockhoff, J. Eichberger, A.N. Menevse, P. Beckhove, M. Hautmann, T.E. Reichert, T. Ettl, R.J. Bauer, Buparlisib modulates PD-L1 expression in head and neck squamous cell carcinoma cell lines, Exp Cell Res, 396 (2020) 112259.

[106] S. Li, K.R. Schmitz, P.D. Jeffrey, J.J. Wiltzius, P. Kussie, K.M. Ferguson, Structural basis for inhibition of the epidermal growth factor receptor by cetuximab, Cancer Cell, 7 (2005) 301-311.

[107] A. Lopez-Albaitero, R.L. Ferris, Immune activation by epidermal growth factor receptor specific monoclonal antibody therapy for head and neck cancer, Arch Otolaryngol Head Neck Surg, 133 (2007) 1277-1281.

[108] P. Specenier, J.B. Vermorken, Cetuximab: its unique place in head and neck cancer treatment, Biologics, 7 (2013) 77-90.

[109] T. Crombet Ramos, B. Mestre Fernandez, Z. Mazorra Herrera, N.E. Iznaga Escobar, Nimotuzumab for patients with inoperable cancer of the head and neck, Front Oncol, 10 (2020) 817.

[110] S.C. Lee, A. Lopez-Albaitero, R.L. Ferris, Immunotherapy of head and neck cancer using tumor antigen-specific monoclonal antibodies, Curr Oncol Rep, 11 (2009) 156-162.

[111] D.M. Pardoll, The blockade of immune checkpoints in cancer immunotherapy, Nat Rev Cancer, 12 (2012) 252-264.

[112] V.A. Boussiotis, Molecular and biochemical aspects of the PD-1 checkpoint pathway, N Engl J Med, 375 (2016) 1767-1778.

[113] S.I. Pai, D.P. Zandberg, S.E. Strome, The role of antagonists of the PD-1:PD-L1/PD-L2 axis in head and neck cancer treatment, Oral Oncol, 61 (2016) 152-158.

[114] R.L. Ferris, G. Blumenschein, Jr., J. Fayette, J. Guigay, A.D. Colevas, L. Licitra,

K. Harrington, S. Kasper, E.E. Vokes, C. Even, F. Worden, N.F. Saba, L.C. Iglesias Docampo, R. Haddad, T. Rordorf, N. Kiyota, M. Tahara, M. Monga, M. Lynch, W.J. Geese, J. Kopit, J.W. Shaw, M.L. Gillison, Nivolumab for Recurrent Squamous-Cell Carcinoma of the Head and Neck, N Engl J Med, 375 (2016) 1856-1867.

[115] W.H. De Jong, P.J. Borm, Drug delivery and nanoparticles:applications and hazards, Int J Nanomedicine, 3 (2008) 133-149.

[116] J.L. Arias, Drug targeting strategies in cancer treatment: an overview, Mini Rev Med Chem, 11 (2011) 1-17.

[117] R. Baghban, L. Roshangar, R. Jahanban-Esfahlan, K. Seidi, A. Ebrahimi-Kalan, M. Jaymand, S. Kolahian, T. Javaheri, P. Zare, Tumor microenvironment complexity and therapeutic implications at a glance, Cell Commun Signal, 18 (2020) 59.

[118] S. Nie, Understanding and overcoming major barriers in cancer nanomedicine, Nanomedicine (Lond), 5 (2010) 523-528.

[119] M.F. Attia, N. Anton, J. Wallyn, Z. Omran, T.F. Vandamme, An overview of active and passive targeting strategies to improve the nanocarriers efficiency to tumour sites, J Pharm Pharmacol, 71 (2019) 1185-1198.

[120] J. Yoo, C. Park, G. Yi, D. Lee, H. Koo, Active Targeting Strategies Using Biological Ligands for Nanoparticle Drug Delivery Systems, Cancers (Basel), 11 (2019).

[121] M.T. Manzari, Y. Shamay, H. Kiguchi, N. Rosen, M. Scaltriti, D.A. Heller, Targeted drug delivery strategies for precision medicines, Nature Reviews Materials, 6 (2021) 351-370.

[122] F. Roncato, F. Rruga, E. Porcu, E. Casarin, R. Ronca, F. Maccarinelli, N. Realdon, G. Basso, R. Alon, G. Viola, M. Morpurgo, Improvement and extension of anti-EGFR targeting in breast cancer therapy by integration with the Avidin-Nucleic-Acid-Nano-Assemblies, Nat Commun, 9 (2018) 4070.

[123] D. Li, X. Chen, H. Wang, J. Liu, M. Zheng, Y. Fu, Y. Yu, J. Zhi, Cetuximab-conjugated nanodiamonds drug delivery system for enhanced targeting therapy and 3D Raman imaging, J Biophotonics, 10 (2017) 1636-1646.

[124] Z. Jiang, J. Guan, J. Qian, C. Zhan, Peptide ligand-mediated targeted drug delivery of nanomedicines, Biomater Sci, 7 (2019) 461-471.

[125] P. Mi, Stimuli-responsive nanocarriers for drug delivery, tumor imaging, therapy and theranostics, Theranostics, 10 (2020) 4557-4588.

[126] J.B. Wolinsky, Y.L. Colson, M.W. Grinstaff, Local drug delivery strategies for cancer treatment: gels, nanoparticles, polymeric films, rods, and wafers, J Control Release, 159 (2012) 14-26.

[127] J.K. Patra, G. Das, L.F. Fraceto, E.V.R. Campos, M.D.P. Rodriguez-Torres, L.S. Acosta-Torres, L.A. Diaz-Torres, R. Grillo, M.K. Swamy, S. Sharma, S. Habtemariam, H.S. Shin, Nano based drug delivery systems: recent developments and future prospects, J Nanobiotechnology, 16 (2018) 71.

[128] Y. Yao, Y. Zhou, L. Liu, Y. Xu, Q. Chen, Y. Wang, S. Wu, Y. Deng, J. Zhang, A. Shao, Nanoparticle-Based Drug Delivery in Cancer Therapy and Its Role in Overcoming Drug Resistance, Front Mol Biosci, 7 (2020) 193.

[129] S. Senapati, A.K. Mahanta, S. Kumar, P. Maiti, Controlled drug delivery vehicles for cancer treatment and their performance, Signal Transduct Target Ther, 3 (2018) 7.

[130] S. Bhattacharyya, R.A. Kudgus, R. Bhattacharya, P. Mukherjee, Inorganic nanoparticles in cancer therapy, Pharm Res, 28 (2011) 237-259.

[131] T. Paunesku, T. Ke, R. Dharmakumar, N. Mascheri, A. Wu, B. Lai, S. Vogt, J. Maser, K. Thurn, B. Szolc-Kowalska, A. Larson, R.C. Bergan, R. Omary, D. Li, Z.R. Lu, G.E. Woloschak, Gadolinium-conjugated TiO2-DNA oligonucleotide nanoconjugates show prolonged intracellular retention period and T1-weighted contrast enhancement in magnetic resonance images, Nanomedicine, 4 (2008) 201-207.

[132] I.H. El-Sayed, X. Huang, M.A. El-Sayed, Surface plasmon resonance scattering and absorption of anti-EGFR antibody conjugated gold nanoparticles in cancer diagnostics: applications in oral cancer, Nano Lett, 5 (2005) 829-834.

[133] H.K.S. Yadav, A.A. Almokdad, S.I.M. shaluf, M.S. Debe, Polymer-based nanomaterials for drug-delivery carriers, Nanocarriers for Drug Delivery2019, pp. 531-556.

[134] Y. Herdiana, N. Wathoni, S. Shamsuddin, I.M. Joni, M. Muchtaridi, Chitosan-based nanoparticles of targeted drug delivery system in breast cancer treatment, Polymers (Basel), 13 (2021).

[135] J. Riestra-Ayora, C. Sánchez-Rodríguez, R. Palao-Suay, J. Yanes-Díaz, A. Martín-Hita, M.R. Aguilar, R. Sanz-Fernández, Paclitaxel-loaded polymeric nanoparticles based on α-tocopheryl succinate for the treatment of head and neck squamous cell carcinoma: in vivo murine model, Drug Delivery, 28 (2021) 1376-1388.

[136] B. Garcia-Pinel, C. Porras-Alcala, A. Ortega-Rodriguez, F. Sarabia, J. Prados, C. Melguizo, J.M. Lopez-Romero, Lipid-based nanoparticles: application and recent advances in cancer treatment, Nanomaterials (Basel), 9 (2019).

[137] L. Yan, S.H. Crayton, J.P. Thawani, A. Amirshaghaghi, A. Tsourkas, Z. Cheng, A pH-responsive drug-delivery platform based on glycol chitosan-coated liposomes, Small, 11 (2015) 4870-4874.

[138] S. Zalba, A.M. Contreras, A. Haeri, T.L. Ten Hagen, I. Navarro, G. Koning, M.J. Garrido, Cetuximab-oxaliplatin-liposomes for epidermal growth factor receptor targeted chemotherapy of colorectal cancer, J Control Release, 210 (2015) 26-38.

[139] M.C.O. da Rocha, P.B. da Silva, M.A. Radicchi, B.Y.G. Andrade, J.V. de Oliveira, T. Venus, C. Merker, I. Estrela-Lopis, J.P.F. Longo, S.N. Bao, Docetaxel-loaded solid lipid nanoparticles prevent tumor growth and lung metastasis of 4T1 murine mammary carcinoma cells, J Nanobiotechnology, 18 (2020) 43.

[140] J. Yang, Z. Ju, S. Dong, Cisplatin and paclitaxel co-delivered by folate-decorated lipid carriers for the treatment of head and neck cancer, Drug Deliv, 24 (2016) 792-799.

[141] S. Parveen, S.K. Sahoo, Polymeric nanoparticles for cancer therapy, J Drug Target, 16 (2008) 108-123.

[142] B.V.N. Nagavarma, H. Yadav, A. Ayaz, L. Vasudha, H. Shivakumar, Different techniques for preparation of polymeric nanoparticles- A review, Asian Journal of Pharmaceutical and Clinical Research, 5 (2012) 16-23.

[143] C.I.C. Crucho, M.T. Barros, Polymeric nanoparticles: A study on the preparation

variables and characterization methods, Mater Sci Eng C Mater Biol Appl, 80 (2017) 771-784.

[144] J. Han, D. Zhao, D. Li, X. Wang, Z. Jin, K. Zhao, Polymer-based nanomaterials and applications for vaccines and drugs, Polymers (Basel), 10 (2018).

[145] K. Krishnaswamy, V. Orsat, Sustainable Delivery Systems Through Green Nanotechnology, Nano- and Microscale Drug Delivery Systems2017, pp. 17-32.

[146] Y. Dong, S.S. Feng, Methoxy poly(ethylene glycol)-poly(lactide) (MPEG-PLA) nanoparticles for controlled delivery of anticancer drugs, Biomaterials, 25 (2004) 2843-2849.

[147] T. Akagi, T. Kaneko, T. Kida, M. Akashi, Preparation and characterization of biodegradable nanoparticles based on poly(gamma-glutamic acid) with l-phenylalanine as a protein carrier, J Control Release, 108 (2005) 226-236.

[148] R. Manchanda, A. Fernandez-Fernandez, A. Nagesetti, A.J. McGoron, Preparation and characterization of a polymeric (PLGA) nanoparticulate drug delivery system with simultaneous incorporation of chemotherapeutic and thermo-optical agents, Colloids Surf B Biointerfaces, 75 (2010) 260-267.

[149] A.K. Jain, N.K. Swarnakar, C. Godugu, R.P. Singh, S. Jain, The effect of the oral administration of polymeric nanoparticles on the efficacy and toxicity of tamoxifen, Biomaterials, 32 (2011) 503-515.

[150] K. Krishnamoorthy, M. Mahalingam, Selection of a suitable method for the preparation of polymeric nanoparticles: multi-criteria decision making approach, Adv Pharm Bull, 5 (2015) 57-67.

[151] E.M.A. Hejjaji, A.M. Smith, G.A. Morris, Evaluation of the mucoadhesive properties of chitosan nanoparticles prepared using different chitosan to tripolyphosphate (CS:TPP) ratios, Int J Biol Macromol, 120 (2018) 1610-1617.

[152] A.T. Jensen, W.S. Neto, G.R. Ferreira, A.F. Glenn, R. Gambetta, S.B. Gonçalves, L.F. Valadares, F. Machado, 8 - Synthesis of polymer/inorganic hybrids through heterophase polymerizations, in: P.M. Visakh, G. Markovic, D. Pasquini (Eds.) Recent Developments in Polymer Macro, Micro and Nano Blends, Woodhead Publishing2017, pp. 207-235.

[153] Z. Song, G.W. Poehlein, Kinetics of emulsifier-free emulsion polymerization of

styrene, Journal of Polymer Science Part A: Polymer Chemistry, 28 (1990) 2359-2392.

[154] S.-J. Yoon, H. Chun, M.-S. Lee, N. Kim, Preparation of poly(N-vinylcarbazole) (PVK) nanoparticles by emulsion polymerization and PVK hollow particles, Synthetic Metals, 159 (2009) 518-522.

[155] C. Colombo, L. Morosi, E. Bello, R. Ferrari, S.A. Licandro, M. Lupi, P. Ubezio, M. Morbidelli, M. Zucchetti, M. D'Incalci, D. Moscatelli, R. Frapolli, PEGylated Nanoparticles Obtained through Emulsion Polymerization as Paclitaxel Carriers, Mol Pharm, 13 (2016) 40-46.

[156] G. Shankar, Y. Agrawal, A review on nanoparticulate mucoadhesive system, 2017.

[157] A. Khan, R. Mahamana, E. Pal, Review on mucoadhesive drug delivery system: novel approaches in modern era, Rajiv Gandhi University of Health Sciences Journal of Pharmaceutical Sciences, 4 (2015) 128-141.

[158] P. Kurra, New generation mucoadhesive polymers - A review, Studies in the Novel, 2016 (2016) 1-6.

[159] J. Bagan, C. Paderni, N. Termine, G. Campisi, L. Lo Russo, D. Compilato, O. Di Fede, Mucoadhesive polymers for oral transmucosal drug delivery: a review, Curr Pharm Des, 18 (2012) 5497-5514.

[160] A. Popov, E. Enlow, J. Bourassa, H. Chen, Mucus-penetrating nanoparticles made with "mucoadhesive" poly(vinyl alcohol), Nanomedicine, 12 (2016) 1863-1871.

[161] S.K. Lai, D.E. O'Hanlon, S. Harrold, S.T. Man, Y.Y. Wang, R. Cone, J. Hanes, Rapid transport of large polymeric nanoparticles in fresh undiluted human mucus, Proc Natl Acad Sci U S A, 104 (2007) 1482-1487.

[162] S.K. Lai, Y.-Y. Wang, J. Hanes, Mucus-penetrating nanoparticles for drug and gene delivery to mucosal tissues, Advanced Drug Delivery Reviews, 61 (2009) 158-171.

[163] L.M. Ensign, R. Cone, J. Hanes, Oral drug delivery with polymeric nanoparticles: The gastrointestinal mucus barriers, Advanced Drug Delivery Reviews, 64 (2012) 557-570.

[164] J.R. Gum, J.W. Hicks, N.W. Toribara, E.M. Rothe, R.E. Lagace, Y.S. Kim, The

human MUC2 intestinal mucin has cysteine-rich subdomains located both upstream and downstream of its central repetitive region, Journal of Biological Chemistry, 267 (1992) 21375-21383.

[165] D.J. Thornton, From Mucins to Mucus: Toward a More Coherent Understanding of This Essential Barrier, Proceedings of the American Thoracic Society, 1 (2004) 54-61.

[166] V.M. Leitner, G.F. Walker, A. Bernkop-Schnürch, Thiolated polymers: evidence for the formation of disulphide bonds with mucus glycoproteins, European Journal of Pharmaceutics and Biopharmaceutics, 56 (2003) 207-214.

[167] K. Kesavan, G. Nath, J.K. Pandit, Sodium alginate based mucoadhesive system for gatifloxacin and its in vitro antibacterial activity, Sci Pharm, 78 (2010) 941-957.

[168] A.B. Nair, N. Sreeharsha, B.E. Al-Dhubiab, J.G. Hiremath, P. Shinu, M. Attimarad, K.N. Venugopala, M. Mutahar, HPMC- and PLGA-Based Nanoparticles for the Mucoadhesive Delivery of Sitagliptin: Optimization and In Vivo Evaluation in Rats, Materials (Basel), 12 (2019).

[169] R.P. Brannigan, V.V. Khutoryanskiy, Progress and current trends in the synthesis of novel polymers with enhanced mucoadhesive properties, Macromolecular Bioscience, 19 (2019) 1900194.

[170] F. Gabor, E. Bogner, A. Weissenboeck, M. Wirth, The lectin-cell interaction and its implications to intestinal lectin-mediated drug delivery, Adv Drug Deliv Rev, 56 (2004) 459-480.

[171] L. Lavín de Juan, V. García Recio, P. Jiménez López, T. Girbés Juan, M. Cordoba-Diaz, D. Cordoba-Diaz, Pharmaceutical applications of lectins, Journal of Drug Delivery Science and Technology, 42 (2017) 126-133.

[172] B. Moulari, A. Beduneau, Y. Pellequer, A. Lamprecht, Lectin-decorated nanoparticles enhance binding to the inflamed tissue in experimental colitis, J Control Release, 188 (2014) 9-17.

[173] A. Bernkop-Schnurch, V. Schwarz, S. Steininger, Polymers with thiol groups: a new generation of mucoadhesive polymers?, Pharm Res, 16 (1999) 876-881.

[174] M. Roldo, M. Hornof, P. Caliceti, A. Bernkop-Schnürch, Mucoadhesive thiolated

chitosans as platforms for oral controlled drug delivery: synthesis and in vitro evaluation, European Journal of Pharmaceutics and Biopharmaceutics, 57 (2004) 115-121.

[175] A. Mahmood, M. Lanthaler, F. Laffleur, C.W. Huck, A. Bernkop-Schnurch, Thiolated chitosan micelles: Highly mucoadhesive drug carriers, Carbohydr Polym, 167 (2017) 250-258.

[176] J. Nowak, F. Laffleur, A. Bernkop-Schnurch, Preactivated hyaluronic acid: A potential mucoadhesive polymer for vaginal delivery, Int J Pharm, 478 (2015) 383-389.

[177] M. Perrone, A. Lopalco, A. Lopedota, A. Cutrignelli, V. Laquintana, J. Douglas, M. Franco, E. Liberati, V. Russo, S. Tongiani, N. Denora, A. Bernkop-Schnurch, Preactivated thiolated glycogen as mucoadhesive polymer for drug delivery, Eur J Pharm Biopharm, 119 (2017) 161-169.

[178] T. Eshel-Green, H. Bianco-Peled, Mucoadhesive acrylated block copolymers micelles for the delivery of hydrophobic drugs, Colloids Surf B Biointerfaces, 139 (2016) 42-51.

[179] R.P. Brannigan, V.V. Khutoryanskiy, Synthesis and evaluation of mucoadhesive acryloyl-quaternized PDMAEMA nanogels for ocular drug delivery, Colloids and surfaces, B, Biointerfaces, 155 (2017) 538-543.

[180] C. Lee, J. Shin, J.S. Lee, E. Byun, J.H. Ryu, S.H. Um, D.I. Kim, H. Lee, S.W. Cho, Bioinspired, calcium-free alginate hydrogels with tunable physical and mechanical properties and improved biocompatibility, Biomacromolecules, 14 (2013) 2004-2013.

[181] Y. Yu, S. Xu, S. Li, H. Pan, Genipin-cross-linked hydrogels based on biomaterials for drug delivery: a review, Biomaterials Science, 9 (2021) 1583-1597.

[182] D.B. Kaldybekov, P. Tonglairoum, P. Opanasopit, V.V. Khutoryanskiy, Mucoadhesive maleimide-functionalised liposomes for drug delivery to urinary bladder, Eur J Pharm Sci, 111 (2018) 83-90.

[183] F. Haaf, A. Sanner, F. Straub, Polymers of N-Vinylpyrrolidone: Synthesis, Characterization and Uses, Polymer Journal, 17 (1985) 143-152.

[184] P.P. Kulikov, A.N. Kuskov, A.V. Goryachaya, A.N. Luss, M.I. Shtil'man,

Amphiphilic poly-n-vinyl-2-pyrrolidone: Synthesis, properties, nanoparticles, Polymer Science, Series D, 10 (2017) 263-268.

[185] A.N. Kuskov, A.A. Voskresenskaya, A.V. Goryachaya, M.I. Shtilman, D.A. Spandidos, A.K. Rizos, A.M. Tsatsakis, Amphiphilic poly-N-vinylpyrrolidone nanoparticles as carriers for non-steroidal anti-inflammatory drugs: characterization and in vitro controlled release of indomethacin, Int J Mol Med, 26 (2010) 85-94.

[186] B. Ray, M. Kotani, S. Yamago, Highly Controlled Synthesis of Poly(N-vinylpyrrolidone) and Its Block Copolymers by Organostibine-Mediated Living Radical Polymerization, Macromolecules, 39 (2006) 5259-5265.

[187] C. Xu, Y. Yan, J. Tan, D. Yang, X. Jia, L. Wang, Y. Xu, S. Cao, S. Sun, Biodegradable nanoparticles of polyacrylic acid–stabilized amorphous CaCO3 for Tunable pH-Responsive Drug Delivery and Enhanced Tumor Inhibition, Advanced Functional Materials, 29 (2019).

[188] D. Brown, Acrylic Acid, Encyclopedia of Toxicology2014, pp. 74-75.

[189] Y. Wang, J. Wang, Z. Yuan, H. Han, T. Li, L. Li, X. Guo, Chitosan cross-linked poly(acrylic acid) hydrogels: Drug release control and mechanism, Colloids and Surfaces B: Biointerfaces, 152 (2017) 252-259.

[190] U. Garg, S. Chauhan, U. Nagaich, N. Jain, Current Advances in Chitosan Nanoparticles Based Drug Delivery and Targeting, Adv Pharm Bull, 9 (2019) 195-204.

[191] T.K. Giri, Chapter 15 - Chitosan based nanoparticulate system for controlled delivery of biological macromolecules, in: A.M. Grumezescu (Ed.) Nanomaterials for Drug Delivery and Therapy, William Andrew Publishing2019, pp. 435-459.

[192] T.K. Giri, Chitosan based nanoparticulate system for controlled delivery of biological macromolecules, Nanomaterials for Drug Delivery and Therapy2019, pp. 435-459.

[193] M.W. TM, W.M. Lau, V.V. Khutoryanskiy, Chitosan and its derivatives for application in mucoadhesive drug delivery systems, Polymers (Basel), 10 (2018).

[194] D. Zhao, S. Yu, B. Sun, S. Gao, S. Guo, K. Zhao, Biomedical applications of chitosan and its derivative nanoparticles, Polymers (Basel), 10 (2018).

[195] A.S. Yadav, N.N.V. Radharani, M. Gorain, A. Bulbule, D. Shetti, G. Roy, T. Baby, G.C. Kundu, RGD functionalized chitosan nanoparticle mediated targeted delivery of raloxifene selectively suppresses angiogenesis and tumor growth in breast cancer, Nanoscale, 12 (2020) 10664-10684.

[196] K.N. How, W.H. Yap, C.L.H. Lim, B.H. Goh, Z.W. Lai, Hyaluronic acid-mediated drug delivery system targeting for inflammatory skin diseases: A mini review, Frontiers in Pharmacology, 11 (2020).

[197] H.-J. Cho, Recent progresses in the development of hyaluronic acid-based nanosystems for tumor-targeted drug delivery and cancer imaging, Journal of Pharmaceutical Investigation, 50 (2019) 115-129.

[198] G. Huang, H. Huang, Application of hyaluronic acid as carriers in drug delivery, Drug Deliv, 25 (2018) 766-772.

[199] M.Y. Hsiao, A.C. Lin, W.H. Liao, T.G. Wang, C.H. Hsu, W.S. Chen, F.H. Lin, Drug-loaded hyaluronic acid hydrogel as a sustained-release regimen with dual effects in early intervention of tendinopathy, Sci Rep, 9 (2019) 4784.

[200] J. Wang, N. Muhammad, T. Li, H. Wang, Y. Liu, B. Liu, H. Zhan, Hyaluronic Acid-Coated Camptothecin Nanocrystals for Targeted Drug Delivery to Enhance Anticancer Efficacy, Mol Pharm, 17 (2020) 2411-2425.

[201] K.M. Koczkur, S. Mourdikoudis, L. Polavarapu, S.E. Skrabalak, Polyvinylpyrrolidone (PVP) in nanoparticle synthesis, Dalton Trans, 44 (2015) 17883-17905.

[202] B. Gilbert, R.K. Ono, K.A. Ching, C.S. Kim, The effects of nanoparticle aggregation processes on aggregate structure and metal uptake, J Colloid Interface Sci, 339 (2009) 285-295.

[203] V. Raj, G. Prabha, Synthesis, characterization and in vitro drug release of cisplatin loaded Cassava starch acetate–PEG/gelatin nanocomposites, Journal of the Association of Arab Universities for Basic and Applied Sciences, 21 (2016) 10-16.

[204] B. Gupta, T. Ramasamy, B.K. Poudel, S. Pathak, S. Regmi, J.Y. Choi, Y. Son, R.K. Thapa, J.H. Jeong, J.R. Kim, H.G. Choi, C.S. Yong, J.O. Kim, Development of Bioactive PEGylated Nanostructured Platforms for Sequential Delivery of Doxorubicin and Imatinib to Overcome Drug Resistance in Metastatic Tumors,

ACS Appl Mater Interfaces, 9 (2017) 9280-9290.

[205] H. Zhao, J. Xu, J. Wan, S. Geng, H. Li, X. Peng, Q. Fu, M. He, Y. Zhao, X. Yang, Cisplatin-directed coordination-crosslinking nanogels with thermo/pH-sensitive triblock polymers: improvement on chemotherapic efficacy via sustained release and drug retention, Nanoscale, 9 (2017) 5859-5871.

[206] R. Melinda Molnar, M. Bodnar, J.F. Hartmann, J. Borbely, Preparation and characterization of poly(acrylic acid)-based nanoparticles, Colloid and Polymer Science, 287 (2009) 739-744.

[207] X. Ren, P. Ghassemi, H. Babahosseini, J. Strobl, M. Agah, Single-cell mechanical characteristics analyzed by multi-constriction microfluidic channels, ACS Sensors, 2 (2017).

[208] S.A. Kim, O.H. Kang, D.Y. Kwon, Cryptotanshinone induces cell cycle arrest and apoptosis of nsclc cells through the PI3K/Akt/GSK-3beta pathway, Int J Mol Sci, 19 (2018).

[209] V.A. Patel, A. Longacre, K. Hsiao, H. Fan, F. Meng, J.E. Mitchell, J. Rauch, D.S. Ucker, J.S. Levine, Apoptotic cells, at all stages of the death process, trigger characteristic signaling events that are divergent from and dominant over those triggered by necrotic cells: Implications for the delayed clearance model of autoimmunity, J Biol Chem, 281 (2006) 4663-4670.

[210] I.K.H. Poon, M.D. Hulett, C.R. Parish, Molecular mechanisms of late apoptotic/necrotic cell clearance, Cell Death & Differentiation, 17 (2009) 381-397.

[211] F. Belloc, P. Dumain, M.R. Boisseau, C. Jalloustre, J. Reiffers, P. Bernard, F. Lacombe, A flow cytometric method using Hoechst 33342 and propidium iodide for simultaneous cell cycle analysis and apoptosis determination in unfixed cells, Cytometry, 17 (1994) 59-65.

[212] P. Foroozandeh, A.A. Aziz, Insight into cellular uptake and intracellular trafficking of nanoparticles, Nanoscale Research Letters, 13 (2018).

[213] L. Galluzzi, L. Senovilla, I. Vitale, J. Michels, I. Martins, O. Kepp, M. Castedo, G. Kroemer, Molecular mechanisms of cisplatin resistance, Oncogene, 31 (2012) 1869-1883.

[214] S. Behzadi, V. Serpooshan, W. Tao, M.A. Hamaly, M.Y. Alkawareek, E.C.

Dreaden, D. Brown, A.M. Alkilany, O.C. Farokhzad, M. Mahmoudi, Cellular uptake of nanoparticles: journey inside the cell, Chem Soc Rev, 46 (2017) 4218-4244.

[215] S.L. Cook, S.P. Bull, L. Methven, J.K. Parker, V.V. Khutoryanskiy, Mucoadhesion: A food perspective, Food Hydrocolloids, 72 (2017) 281-296.

[216] P. Kord Forooshani, B.P. Lee, Recent approaches in designing bioadhesive materials inspired by mussel adhesive protein, J Polym Sci A Polym Chem, 55 (2017) 9-33.

[217] J.H. Ryu, S. Hong, H. Lee, Bio-inspired adhesive catechol-conjugated chitosan for biomedical applications: A mini review, Acta Biomaterialia, 27 (2015) 101-115.

[218] D.K. Rana, S. Dhar, A. Sarkar, S.C. Bhattacharya, Dual intramolecular hydrogen bond as a switch for inducing ground and excited state intramolecular double proton transfer in doxorubicin: an excitation wavelength dependence study, The Journal of Physical Chemistry A, 115 (2011) 9169-9179.

[219] B. Bellich, I. D'Agostino, S. Semeraro, A. Gamini, A. Cesaro, "The Good, the Bad and the Ugly" of Chitosans, Mar Drugs, 14 (2016).

[220] C. Suarez-Barrio, J. Etxebarria, R. Hernaez-Moya, M. Del Val-Alonso, M. Rodriguez-Astigarraga, A. Urkaregi, V. Freire, M.C. Morales, J.A. Duran, M. Vicario, I. Molina, R. Herrero-Vanrell, N. Andollo, Hyaluronic acid combined with serum rich in growth factors in corneal epithelial defects, Int J Mol Sci, 20 (2019).

[221] Y. Tsugeno, F. Sato, Y. Muragaki, Y. Kato, Cell culture of human gingival fibroblasts, oral cancer cells and mesothelioma cells with serum-free media, STK1 and STK2, Biomed Rep, 2 (2014) 644-648.

[222] J. Mosquera, I. Garcia, L.M. Liz-Marzan, Cellular uptake of nanoparticles versus small molecules: A matter of size, Acc Chem Res, 51 (2018) 2305-2313.

[223] S. Salatin, A. Yari Khosroushahi, Overviews on the cellular uptake mechanism of polysaccharide colloidal nanoparticles, J Cell Mol Med, 21 (2017) 1668-1686.

[224] C. Lema, A. Varela-Ramirez, R.J. Aguilera, Differential nuclear staining assay for high-throughput screening to identify cytotoxic compounds, Curr Cell Biochem, 1 (2011) 1-14.

[225] B.Z. Jin, X.Q. Dong, X. Xu, F.H. Zhang, Development and in vitro evaluation of mucoadhesive patches of methotrexate for targeted delivery in oral cancer, Oncol Lett, 15 (2018) 2541-2549.

[226] Y. Yang, G. Jiang, P. Zhang, J. Fan, Programmed cell death and its role in inflammation, Mil Med Res, 2 (2015) 12.

APPENDIX

APPENDIX A

Development of coordination bond-forming NVP/AA NPs for CDDP delivery

1. COOH Content

Table A.1 Quantification of COOH content on the NPs using salt-splitting titration

	Formulation	N1	N2	N3	$\overline{X}$	SD
F1	Method 1 NVP:AA (1:1)	4.28	3.76	4.89	4.31	0.56
F2	Method 1 NVP:AA (1:3)	6.75	7.44	7.58	7.26	0.44
F3	Method 1 NVP:AA (1:5)	5.00	5.03	5.28	5.10	0.16
F4	Method 2 NVP:AA (1:10)	7.81	7.80	7.46	7.69	0.20

2. Particle size and surface charge

Table A.2 Particle size, size distribution, and surface charge of the NPs

Formulation		N	Particle size			PDI			Zeta potential		
			$\overline{X}$	SD		$\overline{X}$	SD		$\overline{X}$	SD	
F1	Method 1 NVP:AA (1:1)	N1	181.4			0.401			-8.50		
		N2	152.6	173.6	18.4	0.382	0.397	0.014	-8.77	-8.6	0.2
		N3	186.7			0.409			-8.43		
F2	Method 1 NVP:AA (1:3)	N1	151.4			0.473			-19.60		
		N2	155.6	155.6	4.3	0.302	0.352	0.106	-19.20	-19.5	0.2
		N3	159.9			0.280			-19.60		
F3	Method 1 NVP:AA (1:5)	N1	185.9			0.228			-2.67		
		N2	184.1	183.7	2.4	0.225	0.242	0.027	-2.93	-2.7	0.2
		N3	181.2			0.274			-2.60		
F4	Method 2 NVP:AA (1:10)	N1	135.9			0.478			-26.40		
		N2	140.6	136.2	4.3	0.435	0.440	0.035	-25.60	-26.3	0.6
		N3	132.0			0.408			-26.80		
CDDP-loaded M1-NPs (1:3)		N1	223.4			0.337			-7.10		
		N2	205.6	212.4	9.6	0.355	0.377	0.054	-7.55	-7.4	0.2
		N3	208.1			0.439			-7.48		
CDDP-loaded M2-NPs (1:10)		N1	163.7			0.32			-7.58		
		N2	183.5	177.8	12.3	0.351	0.325	0.024	-7.60	-7.6	0.0
		N3	186.3			0.303			-7.61		

3. Particle size and surface charge in media

Table A.3 Particle size, size distribution, and surface charge of the NPs in different media on Day 0.

	Medium	N	Blank NPs (Day 0)								
			Particle size (nm)			PDI			Zeta potential (mV)		
				$\overline{X}$	SD		$\overline{X}$	SD		$\overline{X}$	SD
M_1-NPs	PBS	N1	150.9			0.357			-23.2		
		N2	151.6	152.2	1.7	0.371	0.365	0.007	-23.3	-25.2	3.3
		N3	154.1			0.368			-29.0		
	DMEM (without serum)	N1	127.5			0.263			-20.1		
		N2	126.9	127.5	0.6	0.239	0.252	0.012	-22.5	-21.3	1.2
		N3	128			0.254			-21.3		
	DMEM (with serum)	N1	115.7			0.454			-20.9		
		N2	116	115.2	1.1	0.456	0.454	0.002	-20.0	-20.3	0.5
		N3	113.9			0.453			-20.1		
M_2-NPs	PBS	N1	171.2			0.22			-17.2		
		N2	152.5	168.8	15.3	0.20	0.217	0.016	-17.3	-17.3	0.2
		N3	182.8			0.232			-17.5		
	DMEM (without serum)	N1	209.8			0.223			-11.9		
		N2	211.3	204.2	11.0	0.215	0.223	0.009	-12.5	-12.0	0.5
		N3	191.5			0.232			-11.6		
	DMEM (with serum)	N1	135.7			0.178			-17.7		
		N2	169.4	146.8	19.6	0.217	0.205	0.024	-18.7	-18.4	0.6
		N3	135.3			0.221			-18.9		

Table A.4 Particle size, size distribution, and surface charge of the NPs in different media on Day 14 in 37ºC.

	Medium	N	Blank NPs (Day 14)								
			Particle size (nm)			PDI			Zeta potential (mV)		
				$\overline{X}$	SD		$\overline{X}$	SD		$\overline{X}$	SD
M₁-NPs	PBS	N1	123.7			0.272			-15.8		
		N2	129.0	130.4	7.4	0.284	0.303	0.044	-14.5	-15.1	0.7
		N3	138.4			0.354			-15.1		
	DMEM (without serum)	N1	123.6			0.240			-20.0		
		N2	121.6	122.8	1.1	0.256	0.249	0.008	-21.7	-21.0	0.9
		N3	123.2			0.252			-21.3		
	DMEM (with serum)	N1	121.3			0.439			-16.0		
		N2	121.0	120.7	0.8	0.427	0.432	0.006	-17.4	-17.2	1.2
		N3	119.8			0.430			-18.3		
M₂-NPs	PBS	N1	134.5			0.222			-10.5		
		N2	136.8	131.9	6.6	0.273	0.234	0.035	-11.2	-11.1	0.6
		N3	124.4			0.207			-11.7		
	DMEM (without serum)	N1	138.2			0.230			-11.0		
		N2	130.5	130.6	7.6	0.218	0.218	0.012	-12.3	-11.3	0.9
		N3	123.1			0.207			-10.7		
	DMEM (with serum)	N1	145.5			0.237			-13.1		
		N2	152.1	147.4	4.1	0.245	0.238	0.006	-11.8	-12.1	0.9
		N3	144.6			0.233			-11.4		

4. CDDP standard curve for drug content
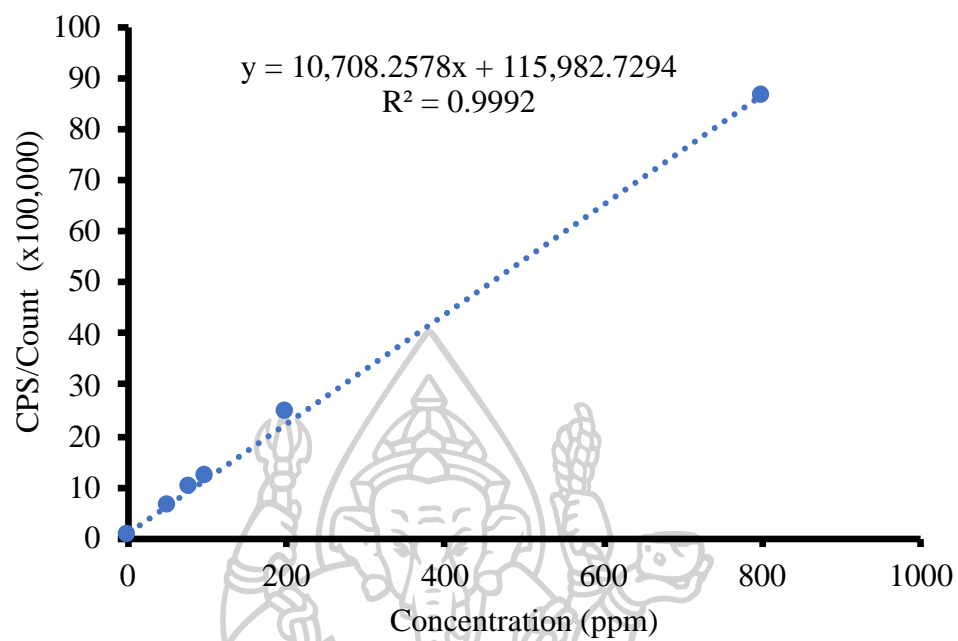
Figure A.1 Standard curve for CDP content quantification

5. Drug loading

Table A.5 %Loading efficiency and loading capacity of CDDP into the NPs

Formulation	Ratio (NPs:CDDP)	N	%Loading Efficiency			Loading capacity (mmol/g)		
				$\overline{X}$	SD		$\overline{X}$	SD
M$_1$-NPs	1:1	N1	7.66			2.28		
		N2	4.75	5.95	1.52	2.11	2.11	0.16
		N3	5.44			1.95		
	1:2.5	N1	9.36			3.07		
		N2	9.44	9.03	0.64	2.70	2.90	0.18
		N3	8.29			2.94		
	1:5	N1	12.58			2.91		
		N2	11.42	11.86	0.63	3.63	3.08	0.49
		N3	11.56			2.69		
	1:10	N1	12.28			3.76		
		N2	11.59	11.70	0.53	3.96	3.82	0.12
		N3	11.25			3.76		
M$_2$-NPs	1:1	N1	4.60			2.27		
		N2	7.00	6.11	1.32	2.54	2.38	0.14
		N3	6.74			2.34		
	1:2.5	N1	7.79			2.87		
		N2	8.28	8.69	1.16	2.59	2.84	0.25
		N3	10.01			3.07		
	1:5	N1	19.10			2.85		
		N2	17.96	17.61	1.68	3.24	2.93	0.29
		N3	15.79			2.69		
	1:10	N1	16.92			4.61		
		N2	18.29	17.91	0.86	3.87	3.93	0.65
		N3	18.51			3.31		

6. CDDP standard curve for drug release
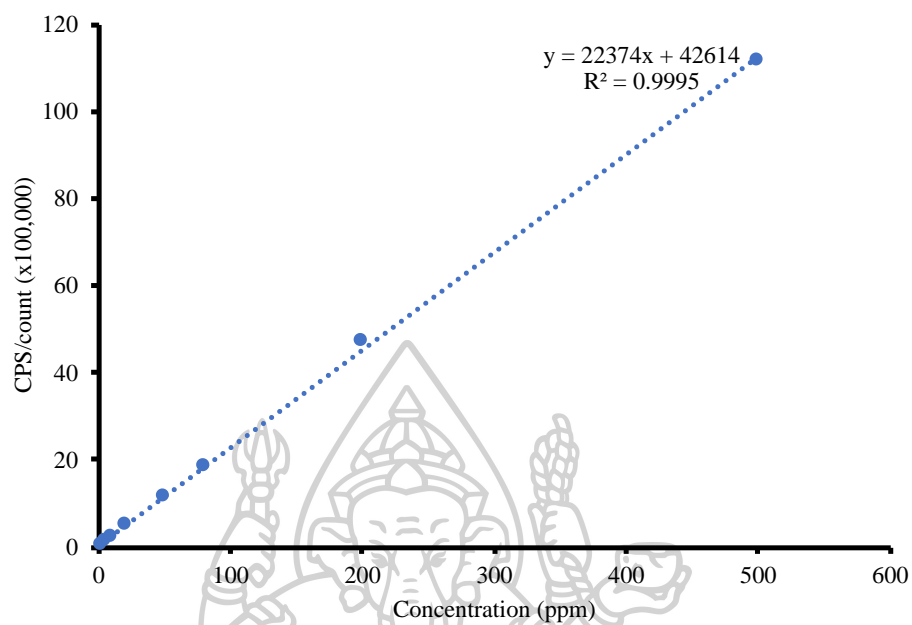
Figure A.2 Standard curve for CDDP release

7. Drug release

Table A.6 CDDP release from the NPs at various pH.

Time	pH 5.0				pH 6.5				pH 7.4			
	M_1-NPs		M_2-NPs		M_1-NPs		M_2-NPs		M_1-NPs		M_2-NPs	
	$\overline{X}$	SD	$\overline{X}$	SD	$\overline{X}$	SD	$\overline{X}$	SD	$\overline{X}$	SD	$\overline{X}$	SD
0 min	0	0	0	0	0	0	0	0	0	0	0	0
5 min	0.32	0.03	0.73	0.10	0.24	0.03	0.23	0.02	0.57	0.05	0.51	0.05
10 min	0.62	0.02	0.83	0.28	0.50	0.06	0.72	0.39	0.64	0.07	0.61	0.04
15 min	1.04	0.14	1.03	0.22	0.63	0.12	0.82	0.24	0.71	0.01	0.65	0.03
30 min	1.16	0.05	1.18	0.09	0.69	0.11	0.96	0.31	0.80	0.02	0.72	0.02
1 h	1.33	0.09	1.21	0.04	0.72	0.03	1.14	0.01	0.85	0.05	0.75	0.10
2 h	1.31	0.03	1.17	0.01	0.71	0.03	1.17	0.03	0.84	0.03	0.74	0.07
4 h	1.33	0.12	1.23	0.04	0.79	0.07	1.26	0.05	0.81	0.00	0.77	0.05
8 h	1.34	0.08	1.24	0.07	0.78	0.10	1.23	0.03	0.86	0.01	0.80	0.07
12 h	1.28	0.01	1.29	0.16	0.76	0.04	1.33	0.06	0.86	0.02	0.77	0.04
1 Day	1.38	0.08	1.26	0.01	0.81	0.07	1.30	0.06	0.84	0.06	0.81	0.07
2 Days	1.36	0.01	1.30	0.11	0.80	0.06	1.41	0.05	0.87	0.00	0.85	0.06
3 Days	1.49	0.06	1.35	0.00	0.89	0.00	1.34	0.03	0.89	0.00	0.83	0.03
4 Days	1.55	0.06	1.42	0.00	0.87	0.13	1.42	0.03	0.89	0.02	0.83	0.08
5 Days	1.58	0.01	1.44	0.04	0.94	0.03	1.57	0.05	0.90	0.02	0.89	0.07
6 Days	1.56	0.04	1.40	0.15	0.98	0.08	1.53	0.04	1.01	0.13	0.89	0.05
7 Days	1.63	0.06	1.66	0.35	1.11	0.05	1.62	0.04	0.96	0.07	0.94	0.05

8. Intracellular accumulation

Table A.7 Amount of CDDP accumulated in the HN22 cells at different time points.

	Time (h)	Pt (mg/1000 cell)				
		N1	N2	N3	$\overline{X}$	SD
Free drug	4	2.65	2.68	3.80	3.04	0.66
	8	4.18	4.27	5.54	4.66	0.76
	24	5.22	5.49	7.88	6.20	1.46
M_1-NPs	4	16.89	17.24	18.97	17.70	1.11
	8	17.53	18.50	21.21	19.08	1.91
	24	5.93	6.04	7.64	6.54	0.95
M_2-NPs	4	12.31	12.59	13.77	12.89	0.78
	8	14.21	14.85	16.31	15.12	1.08
	24	5.42	5.50	6.87	5.93	0.81

APPENDIX B

Development of mucoadhesive NPs for localized delivery of DOX

1. Particle size and surface charge

Table B.1 Particle size, size distribution, and zeta potential of the Cat-NPs.

| Ratio (SCScat:HAcat)	N	Particle size (nm)			PDI			Zeta potential (mV)		
			$\overline{X}$	SD		$\overline{X}$	SD		$\overline{X}$	SD
1:1	N1	306.0			0.27			-21.2		
	N2	310.4	304.8	6.29	0.26	0.3	0.01	-22.6	-21.6	0.91
	N3	298.0			0.28			-20.9		
2:1	N1	155.5			0.23			-8.51		
	N2	161.3	159.8	3.82	0.18	0.2	0.03	-9.09	-19.8	0.75
	N3	162.7			0.20			-8.33		
1:2	N1	253.5			0.50			-8.51		
	N2	220.2	230.3	20.15	0.52	0.5	0.07	-9.09	-8.64	0.40
	N3	217.2			0.62			-8.33		
2:1 (loaded DOX)	N1	233.5			0.29			-12.8		
	N2	241.2	239.4	5.28	0.29	0.3	0.01	-12.6	-12.7	0.12
	N3	243.6			0.28			-12.6		

2. *Ex vivo* mucoadhesion

Table B.2 %Remaining of the mucoadhesive material on porcine buccal tissue at various time.

Dextran

Time	%Remaining				
	N1	N2	N3	$\overline{\overline{X}}$	SD
0	100.00	100.00	100.00	100.00	0.00
5	36.36	31.49	31.92	33.26	2.70
10	29.62	27.23	23.57	26.80	3.04
20	24.66	21.41	20.12	22.06	2.34
30	21.52	18.16	18.06	19.25	1.97
40	19.19	14.27	15.19	16.22	2.62
50	17.95	11.62	14.50	14.69	3.17
60	14.76	10.12	13.87	12.92	2.46

CS/HA NPs

Time	%Remaining				
	N1	N2	N3	$\overline{\overline{X}}$	SD
0	100.00	100.00	100.00	100.00	0.00
5	83.95	82.78	90.37	85.70	4.09
10	76.96	74.32	82.15	77.81	3.99
20	68.72	66.06	75.52	70.10	4.88
30	62.47	62.89	67.54	64.30	2.81
40	61.12	62.01	65.68	62.94	2.42
50	54.14	59.74	56.62	56.83	2.81
60	53.76	52.32	53.05	53.04	0.72

Cat-NPs

Time	%Remaining				
	N1	N2	N3	$\overline{\overline{X}}$	SD
0	100.00	100.00	100.00	100.00	0.00
5	88.45	96.23	97.85	94.18	5.02
10	86.59	95.39	95.87	92.62	5.22
20	77.54	88.98	89.55	85.36	6.78
30	69.23	83.96	83.36	78.85	8.34
40	66.87	75.36	77.95	73.40	5.79
50	62.71	68.13	70.55	67.13	4.02
60	58.37	66.45	67.67	64.17	5.05

3. DOX standard curve for drug content

y = 0.554x + 0.1518
R² = 0.9888
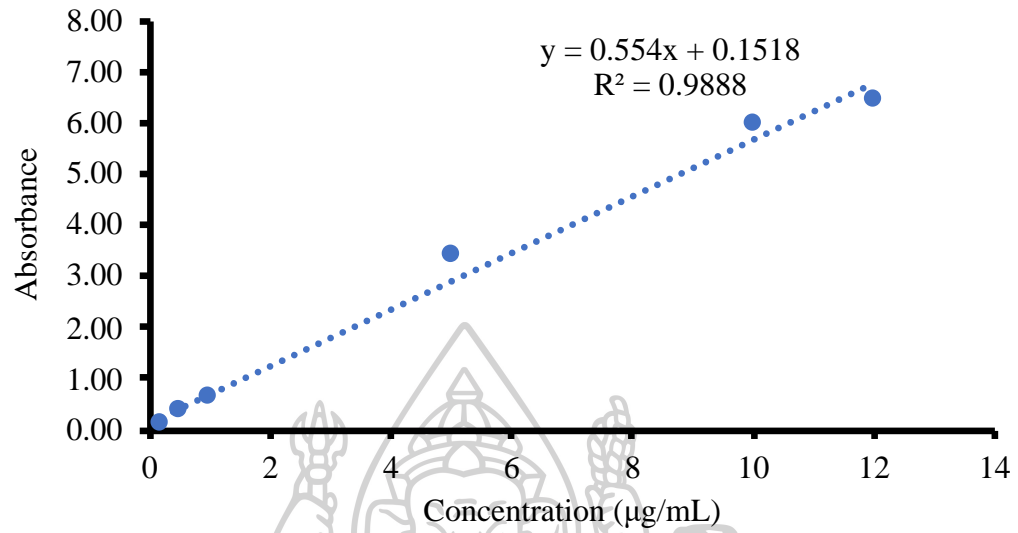
Figure B.1 Standard curve for DOX content quantification
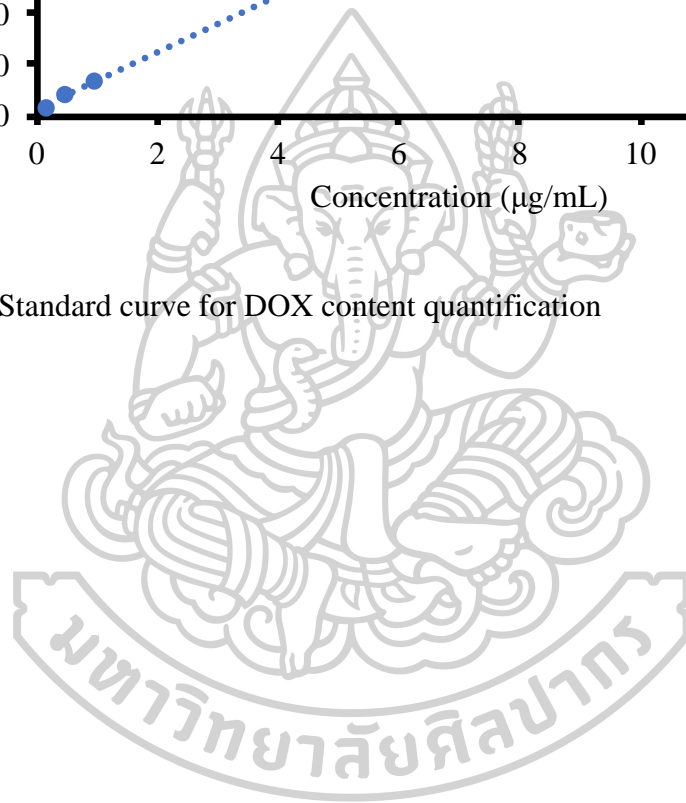
4. Drug loading

Table B.3 DOX content in the Cat-NPs.

NPs:DOX	N	%Loading efficiency			Loading capacity (μg/mg)		
			$\overline{X}$	SD		$\overline{X}$	SD
1:0.5	N1	69.76			232.54		
	N2	72.46	70.9	1.37	241.54	236.55	4.58
	N3	70.67			235.57		
1:1	N1	51.31			256.55		
	N2	56.72	5.71	3.99	283.62	278.54	19.94
	N3	59.09			295.46		
1:2	N1	33.86			225.76		
	N2	34.34	33.47	1.13	228.96	223.13	7.50
	N3	32.20			214.66		
1:5	N1	33.20			276.70		
	N2	25.94	29.24	6.68	216.13	243.68	30.65
	N3	28.58			238.19		

5. DOX standard curve for drug release

$$y = 0.5951x + 0.1140$$
$$R^2 = 0.9958$$
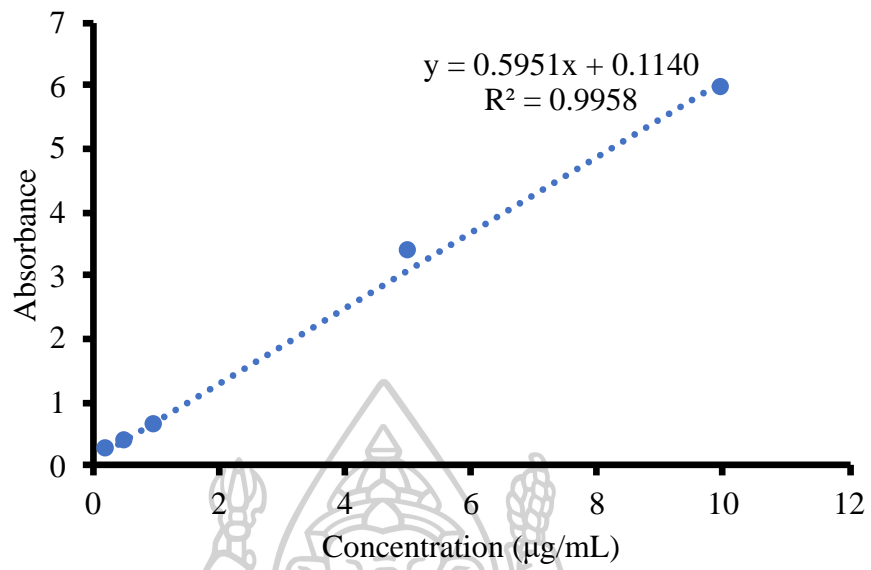
Figure B.2 Standard curve for DOX release quantification

6. Drug release

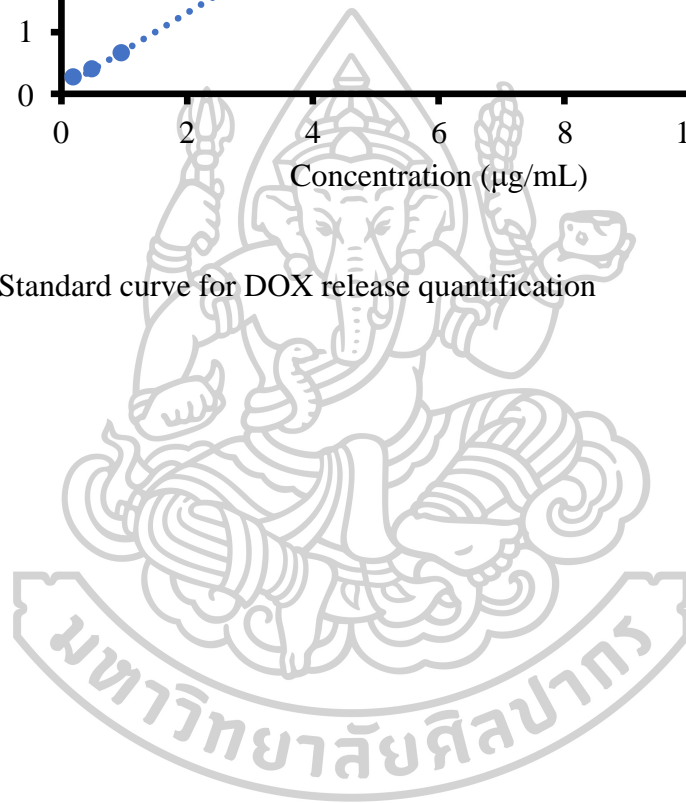**Table B.4** DOX release from the Cat-NPs at different time point.

Free DOX	%Release				
Time (min)	N1	N2	N3	$\overline{X}$	SD
0	0	0	0	0	0
5	19.70	13.49	17.10	16.76	3.12
10	34.63	16.94	26.62	26.06	8.86
15	41.09	25.28	32.75	33.04	7.91
30	49.59	34.95	48.35	44.30	8.11
60	62.16	58.55	74.40	65.04	8.31
180	79.36	83.41	92.22	85.00	6.57
360	82.68	87.63	96.07	88.79	6.77
720	83.86	87.10	98.89	89.95	7.91
1440	80.92	85.97	98.80	88.56	9.21
DOX-NPs	**%Release**				
Time (min)	N1	N2	N3	$\overline{X}$	SD
0	0	0	0	0	0
5	3.90	4.95	4.35	4.40	0.53
10	7.38	11.38	11.98	10.25	2.50
15	15.11	16.94	18.74	16.93	1.81
30	21.40	26.89	24.46	24.25	2.75
60	32.27	32.26	31.65	32.06	0.36
180	66.35	59.77	71.60	65.91	5.93
360	75.62	72.44	74.08	74.05	1.59
720	81.39	77.91	84.13	81.14	3.12
1440	89.38	81.94	89.41	86.91	4.30

7. *In vitro* cellular uptake

Table B.5 The amount of DOX taken up by the HN22 cells at different time point determined by mean fluorescence intensity of 10,000 events by flow cytometer.

Free dox	Mean fluorescence intensity				
Time (h)	N1	N2	N3	$\overline{X}$	SD
4	2269	2298	2219	2262.00	39.96
8	3567	3705	3347	3539.67	180.56
24	4299	3754	4162	4071.67	283.51
DOX-NPs	Mean fluorescence intensity				
Time (h)	N1	N2	N3	$\overline{X}$	SD
4	4383	4218	4227	4276.00	92.77
8	6920	6514	6496	6643.33	239.77
24	8533	12693	8602	9942.67	2382.11

VITA

NAME   MR. CHAIYAKARN PORNPITCHANARONG

DATE OF BIRTH   04 July 1992

PLACE OF BIRTH   Bangkok, Thailand

INSTITUTIONS
ATTENDED   2017 – Present   Pharmaceutical Technology Ph.D. Program, Faculty of Pharmacy, Silpakorn University, Thailand.
2021   Visiting Research Student, School of Chemistry, University of Edinburgh, Edinburgh, Scotland, United Kingdom
2010 – 2015   Bachelor Degree, Doctor of Pharmacy (2nd Class Honors), Pharmaceutical Chemistry, Faculty of Pharmacy, Silpakorn University, Thailand.

HOME ADDRESS   Samutprakarn, Thailand

PUBLICATION   International journal

1. Kwanputtha Arunprasert, Chaiyakarn Pornpitchanarong, Theerasak Rojanarata, Tanasait Ngawhirunpat, Praneet Opanasopit, Porawan Aumklad, Prasopchai Patrojanasophon. Development and valuation of novel water-based drug-in-adhesive patches for the transdermal delivery of ketoprofen. Pharmaceutics. 2021; 13: 789.

2. Kwanputtha Arunprasert, Chaiyakarn Pornpitchanarong, Nitjawan Sahatsapan, Praneet Opanasopit, Prasopchai Patrojanasophon. Synthesis and evaluation of poly(Ethylene glycol) diacrylate-modified chitosan as a mucoadhesive polymer. Thai J Pharm Sci, 2021; 45(3):202–7.

3. Chaiyakarn Pornpitchanarong, Suwannee Panomsuk, Theerada Taesotikul. Effect of cisplatin/curcumin-loaded polycaprolactone nanoparticles on oral carcinoma cells. Key Eng Mater. 2021;901:123-8

4. Chaiyakarn Pornpitchanarong, Theerasak Rojanarata, Praneet Opanasopit, Tanasait Ngawhirunpat, Prasopchai Patrojanasophon. Catechol-modified chitosan/hyaluronic acid nanoparticles as a new avenue for local delivery of doxorubicin to oral cancer cells. Colloids Surf B Biointerfaces, 2020;196:111279.

5. Chaiyakarn Pornpitchanarong, Theerasak Rojanarata, Praneet Opanasopit, Tanasait Ngawhirunpat, Prasopchai Patrojanasophon. Preactivated-thiolated polyacrylic acid/1-vinyl pyrrolidone nanoparticles as

nicotine carriers for smoking cessation. RSC Advances. 2020;10: 33517.

6. Chaiyakarn Pornpitchanarong, Theerasak Rojanarata, Praneet Opanasopit, Tanasait Ngawhirunpat, Prasopchai Patrojanasophon. Clotrimazole nanosuspensions-loaded hyaluronic acid-catechol/polyvinyl alcohol mucoadhesive films for oral candidiasis treatment. J Drug Deliv Sci Technol. 2020;60: 101927.

7. Chaiyakarn Pornpitchanarong, Theerasak Rojanarata, Praneet Opanasopit, Tanasait Ngawhirunpat, Prasopchai Patrojanasophon. Development and Evaluation of thermally-crosslinked mucoadhesive GantrezTM S-97/polyvinyl alcohol/ hyaluronic acid-catechol nanofibers. Key Eng Mater. 2020;859:208-13.

8. Chaiyakarn Pornpitchanarong, Theerasak Rojanarata, Praneet Opanasopit, Tanasait Ngawhirunpat, Prasopchai Patrojanasophon. Synthesis of novel N-vinylpyrrolidone/acrylic acid nanoparticles as drug delivery carriers of cisplatin to cancer cells. Colloids Surf B Biointerfaces, 2020;185:110566.

9. Chaiyakarn Pornpitchanarong, Nitjawan Sahatsapan, Theerasak Rojanarata, Praneet Opanasopit, Tanasait Ngawhirunpat, Prasopchai Patrojanasophon. Curcumin-incorporated Thiolated Chitosan/alginate Nanocarriers: Physicochemical Properties and Release Mechanism. Indian J Pharm Sci 2020;82(1):97-103.

10. Chaiyakarn Pornpitchanarong, Kanokwan Singpanna, Theerasak Rojanarata, Praneet Opanasopit, Tanasait Ngawhirunpat, Prasopchai Patrojanasophon. Catechol-Bearing Hyaluronic Acid Coated Polyvinyl Pyrrolidone/Hydroxyl Propyl-β-Cyclodextrin/Clotrimazole Nanofibers for Oral Candidiasis Treatment. Key Eng Mater. 2019;819:613-8.

11. Chaiyakarn Pornpitchanarong, Theerasak Rojanarata, Praneet Opanasopit, Prasopchai Patrojanasophon, Tanasait Ngawhirunpat. Synthesis of N-vinylpyrrolidone/Acrylic acid nanoparticles for drug delivery: Method optimization MATEC Web Conf. 2018;192:01020.

Thai academic article
1. Chaiyakarn Pornpitchanarong, Tanasait Ngawhirunpat, Prasopchai Patrojanasophon. Novel mucoadhesive polymers and their application in transmucosal drug delivery. Center for continuing Pharmaceutical Education. ISSD: 1006-1-000-003-12-

2561.

AWARD RECEIVED   2017 – Present   Scholarship: Thailand Research Funds
through the Golden Jubilee Ph.D Program (Grant No.
PHD/0021/2560)
August 2019   "First Place" – ISPE Hackathon.
Singapore ISPE Conference and Exhibition 2019
July 2019   "The highest award in ISPE Thailand
Student Poster Competition" ISPE Thailand Student Poster
Competition, ISPE Thailand annual meeting 2019
June 2019   "Best oral presentation award" The
International Conference and Exhibition on
Pharmaceutical Sciences and Technology 2019 (PST
2019)
March 2019   "Outstanding award" – Oral presentation.
The 6th International Conference on Advanced
Pharmaceutical Research (ICAPH 2019)
May 2020   "Bronze Medal" – Oral presentation. The
International Conference and Exhibition on
Pharmaceutical Sciences and Technology 2020 (PST
2020)